Development of an active SONAR platform for AUV applications in a closed environment

by

Konrad Jens Friedrich

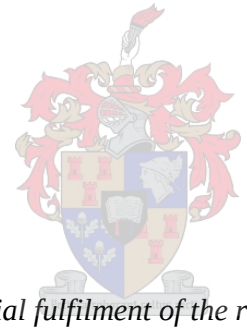

Thesis presented in partial fulfilment of the requirements for the degree
Master of Science in Engineering
at the
University of Stellenbosch

Department of Electrical and Electronic Engineering
University of Stellenbosch
Private Bag X1, 7602, Matieland, South Africa

Supervisor: Mr. J. Treurnicht

March 2012

DECLARATION

By submitting this thesis electronically, I declare that the entirety of the work contained therein is my own, original work, that I am the sole author thereof (save to the extent explicitly otherwise stated), that reproduction and publication thereof by Stellenbosch University will not infringe any third party rights and that I have not previously in its entirety or in part submitted it for obtaining any qualification.

March 2012

ABSTRACT

In recent years Autonomous Underwater Vehicles (AUVs) have become interesting for harbor mapping and protection. AUVs require a SONAR sensor for observing their surroundings, thus enabling them to perform collision avoidance manoeuvres and scanning their operating environment for intruders or foreign objects, e.g. mines.

To perform such actions the SONAR sensor is required to supply very fine range resolution for target imaging, as well as providing information about possible target velocity.

Basic SONAR theory is discussed, as well as different approaches to signal design and processing techniques, for achieving the required resolution in range and target velocity. Two of the discussed approaches are selected for processing range and target velocity, respectively.

Both approaches are simulated for their validity before being tested by using a custom-built platform. The platform is highly configurable and designed for capacity of testing a variety of SONAR signals and set ups. Furthermore, the platform is built by using off-the-shelf components to minimize development costs.

The results of simulations and practical tests are presented. A high correlation between theory and practice is achieved.

The knowledge and the platform presented form the stepping stone for further SONAR sensor developments.

OPSOMMING

In die laaste jare het outonome onderwater voertuie (OOV) toenemend belangrik geword vir die kartografie en beskerming van hawens. OOV's vereis SONAR sensore wat hulle in staat stel, om hulle omgewing waar te neem en sodoende botsing vermydings take te verrig en ook om hul werksomgewing noukeurig te skandeer om indringers of vreemde voorwerpe, bv. myne, op te spoor.

Om sulke werk te verrig, word van die SONAR sensor vereis, om baie fyn afstand oplossings vir teiken te verskaf, insluitend die moontlike snelheid van die teiken.

Basiese SONAR teorie word bespreek, en dan verskeie benaderings van sein ontwerp en verwerkings tegnieke. Twee van die bespreekte benaderings word gekies om afstand en teiken snelheid onderskeidelik te verwerk.

Altwee benaderings word gesimuleer om hul geldigheid vas te stel, voor dat hulle getoets word op 'n pasmaat vervaardigde platform. Die platform is hoogs aanpasbaar en is ontwerp vir sy vermoë om 'n verskeidenheid SONAR seine en verwerkings te hanteer. Verder is die platform vervaardig met standard rakonderdele om ontwikkelingskoste so laag as moontlik te hou.

Die uitslae van die simulerings en praktiese toetse word voorgestel. 'n Hoë mate aan korrelasie is bereik tussen teorie en praktyk.

Die kennis en die platvorm, wat hier voorgestel word, vorm die eerste trappie vir toekomstige SONAR sensor ontwikkeling.

TABLE OF CONTENTS

Page left blank intentionally

LIST OF FIGURES

NOMENCLATURE

SONAR	Sound Navigation and Ranging
RADAR	Radio Navigation and Ranging
AUV	Autonomous Underwater Vehicle
UAV	Unmanned Aerial Vehicle
ESL	Electronic Systems Laboratory
IMT	Institute for Marine Technology
FMCW	Frequency Modulated Continuous Wave
CW	Constant Wave
LFM	Linear Frequency Modulated
HFM	Hyperbolic Frequency Modulated
SFM	Sinusoidal Frequency Modulated
PL	Propagation Loss
SL	Source Level
TS	Target Strength
DI	Directivity Index
RL	Reverberation Level
SNR	Signal to Noise Ratio
MF	Matched Filter
IF	Inverse Filter
PRN	Pseudo-Random Number
DDS	Direct Digital Synthesiser
FIFO	First In First Out
DAC	Digital to Analogue Converter
ADC	Analogue to Digital Converter
PIR	Phase Increment Register
LPF	Low Pass Filter
SPI	Serial I/O Port Interface
PLL	Phase Lock Loop
LNA	Ultralow Noise Amplifier
VGA	Variable Gain Amplifier

CU	Control Unit
M&M	University of Stellenbosch Mechanical & Mechatronic Engineering
EMC	Electro Magnetic Coupling

ACKNOWLEDGEMENTS

I would like to express my gratitude to the following people and institutions:

- IMT for giving me the opportunity for a challenging Masters.
- Mr. Treurnicht as my study leader.
- TUCSIN for helping me finance my studies.
- CSIR Pretoria for their transducers, as well as expert advice on SONAR from Mr. Van Jaarsveld and Mr. Nicolaides.
- CSIR Stellenbosch for giving me access to their towing tank facilities.
- My parents for their support, advice and encouragement throughout my university career. Special thanks to my father for proofreading my thesis numerous times.
- Sampie my super annoying officemate, for keeping me in a good mood throughout the two years and helping me with my measurements.
- Grit von Flotow for proofreading my thesis.
- Last but not least AK, for your support, smiles and all the good times we shared, making work feel like a breeze.

Page left blank intentionally

Chapter 1

INTRODUCTION

1.1 Overview

Sound Navigation And Ranging systems, better known in its abbreviated form as SONAR [1], utilize acoustic waves (sound waves) in an underwater environment to detect, locate and potentially identify objects (targets).

By definition RADAR (Radio Detection And Ranging) [2] closely resembles SONAR, but differs by the environment's medium and the type of operating signal each system utilizes. Acoustic waves, being mechanical vibrations, are the preferred signal for exploring the underwater environment, as they travel nearly unimpeded in water, due to the high density of the medium, and are therefore able to penetrate a channel for many kilometres, depending upon the frequency of the signal as well as the dissolved ion content of the water. By comparison, electromagnetic waves are highly impeded by water, due to the high dissolved ion content in water, and are capable of penetrating a water channel to the order of several centimetres up to a few meters, again depending upon the frequency of the signal and the dissolved ion content of the water.

In contrast to detection limited to only listening to sound waves emitted from targets, as is done with passive SONAR systems, SONAR in its active form seeks targets within its volume of coverage by emitting acoustic waves and monitoring echoes from reflective targets. Knowing the speed at which sound travels in water and the time it takes for a signal to travel to and from a target, it is possible to calculate the range of the target in relation to the SONAR. Additionally, in the case of a target travelling relative to the SONAR platform, information regarding the radial velocity of the target towards the platform may be determined by detecting the Doppler frequency shift of the echo.

The ability to detect, classify and form an image of targets and their surroundings is generally of extreme importance to the field of underwater engineering, both for the commercial and military sectors. The commercial sector is interested in the sea floor profile for pipeline and communication link routing, as well as deep sea mining exploration purposes. Furthermore, monitoring of submerged structures such as the ones previously mentioned, as well as deep

sea platforms and similar structures, is of great importance to the commercial sector. The military interest, by contrast, lies in detecting submarines, mines and the like, and in underwater weapon guidance. Both sectors have a major interest in harbour monitoring and mapping for logistical as well as security reasons. Harbours need to be constantly monitored for depth, as ships are ever growing in size, and for obstacles and threats on the harbour floor. These could be objects such as mines, and possibly hostile intruders, which need to be detected in order to guarantee a safe passage and docking period for ships. Another interest common to the commercial and military sectors is the inspection of ship hulls for damage and biological build-up which reduces efficiency of ships and creates unwanted noise in the water which may interfere with the stealth of military vessels.

Deploying humans to perform the above mentioned tasks with SONAR equipment would result in huge capital as well as human resource expenditure. Thus AUVs (Autonomous Underwater Vehicle) [3] have evolved in recent years as a technology that could perform all of the previously mentioned tasks, both for the commercial and military sectors. Utilizing different types of SONAR technologies, an AUV could be able to find its way through and map a confined space such as a harbour. Needless to say, an AUV has to cope with a much harsher environment than its aerial counterpart, the UAV (Unmanned Aerial Vehicle). Besides water being a general threat to an AUV's electronics, it is capable of crushing the vehicle at sufficient depths. Furthermore, confinement of the operating envelope is a much bigger problem in an underwater environment, as an AUV is not only restricted by the sea floor but also by the sea surface, making it impossible for an AUV to simply pass over obstacles, as some of these could protrude beyond the surface of the water.

Confined underwater environments also pose an additional challenge for producing accurate SONAR sensor data. A SONAR signal sent out to detect a target in a confined underwater space may be reflected repeatedly from the confining walls, bubbles and biologics, moving water masses as well as the floor and ceiling of the environment. These multi-path reflections, called reverberation, may lead to the detection of ghost images of targets or even prevent targets from being detected at all.

1.2 Scope of the Thesis

During recent years, extensive research and development has been accomplished in the field of UAVs at the University of Stellenbosch's Department of Electrical and Electronic Engineering research laboratory, the Electronic Systems Laboratory (ESL). After successfully completing many airborne projects it was decided to extend research efforts of the ESL to autonomous land and underwater vehicles. At the same time, the Institute for Marine Technology (IMT) was looking into obtaining more insight into collision avoidance SONAR technology for their own in-house developed AUV. Combining forces in the investigation of collision avoidance SONAR suitable for AUV applications, a testing unit was required in order to confirm theory and simulations about different SONAR types and implementations. Although complete SONAR solutions are readily available on the market, none of the solutions provide the user with the option of altering hardware and software configurations for specific testing purposes. Moreover, such complete SONAR solutions tend to be very expensive.

The objectives of this thesis are threefold:

Firstly, to research and understand the most prominent forms of SONAR signals currently utilised and the processing thereof. Signals and processing methods applicable for collision avoidance SONAR in a confined space had to be selected accordingly for further investigation.

Secondly, the performance of theory selected to be suitable for AUV collision avoidance SONAR should be verified by computer simulation for its ability to accurately detect range and radial speed of targets.

Thirdly, SONAR implementations with a satisfactory computer simulation outcome should be verified in hardware. It was therefore necessary to develop a highly configurable, though low cost SONAR platform upon which different SONAR implementations could be studied both for their range and speed accuracy.

The requirements for the AUV collision avoidance SONAR were determined as follows:

- Maximum range of 50 m
- Maximum detectable target velocity of $3\ \mathrm{m/s}$

- High accuracy in range resolution ΔR, ideally to the nearest 1 cm
- Accuracy in velocity resolution Δv no worse than $0.1\ \mathrm{m/s}$
- Reverberation resistant

As will become clear by reading this text, in order to achieve the above constraints a relatively high operating frequency is required, as compared to general SONAR equipment. The intended operating frequency of the platform will be centred about $280\ \mathrm{kHz}$, with a total bandwidth of $100\ \mathrm{kHz}$.
The focus of the thesis is concentrated upon the development of a multifunctional SONAR platform, which should ultimately form the basis for further research and development. The platform is designed for fresh water environment. Testing of the platform will be performed in a closed fresh water environment with the characteristics of a "dead" sea. Little attention is thus paid to problems of sound mechanics arising due to varying water temperature, salinity, currents and similar ocean related phenomena.

The similarities and differences between RADAR and SONAR will be highlighted, as applicable, due to the faculty's future ambitions to use RADAR in an underwater environment.

1.3 Outline of the Thesis

Basic theory regarding the propagation, absorption and reflection of sound in water is discussed in Chapter 2. Noise and reverberation are examined for their influence to this project. Furthermore, the concept of range resolution and Doppler frequency shift is introduced. The discussion is extended on how to accurately determine both range resolution and Doppler frequency shift, by making use of various processing techniques. Lastly various waveforms are discussed for their ability to resolve for range and Doppler, and chosen accordingly for further investigation.

A detailed pulse design process, of waveforms discussed in Chapter 2, is further studied for its applicability in Chapter 3. The design is done in order to meet all range and Doppler requirements for the respective pulse, as stated in scope of this thesis. The two pulse designs are simulated in software to confirm their ability to resolve range and Doppler frequency. System performance is discussed regarding the simulation results.

Chapter 4 gives an in-depth description of the required hardware. The hardware is divided into blocks according to the sub-system components. Each block is discussed as a single entity. The sub-system components which are defining other components are discussed first. To conclude the chapter a description of the interaction of all sub-system components, thus forming a SONAR system, is given.

The test results for the hardware in Chapter 4 are discussed in Chapter 5. The system is tested for its performance in both range resolution and Doppler frequency resolution. As in Chapter 3 the results and shortcomings are discussed and evaluated.

In Chapter 6 the conclusion and recommendations for future work are outlined.

Chapter 2

LITERATURE STUDY

The reason for choosing sound waves as a preferred signal for investigating the underwater environment is pointed out by Heinz G. Urban in Handbook of Underwater Acoustic Engineering, where he states:

"Sound waves are mechanical vibrations. Compared to all other kinds of waveforms they travel easily through the ocean. Sound waves represent pressure changes in the medium and constitute wave fields in space and time. Wave fields of different frequency and intensity can superimpose in the medium." [1]

2.1 Active Sonar Basics

Active SONAR transmits a sound pulse into the water volume to be explored for potential targets, and waits for the return of possible reflections of the pulse from various potential targets present inside the water volume of interest, as depicted in Figure 2.1. Sending out an acoustic pressure wave is accomplished by using piezoelectric transducers, which convert an applied voltage signal to mechanical pressure waves. The echo is received and converted back to an electrical signal by a similar but inverse mechanism.

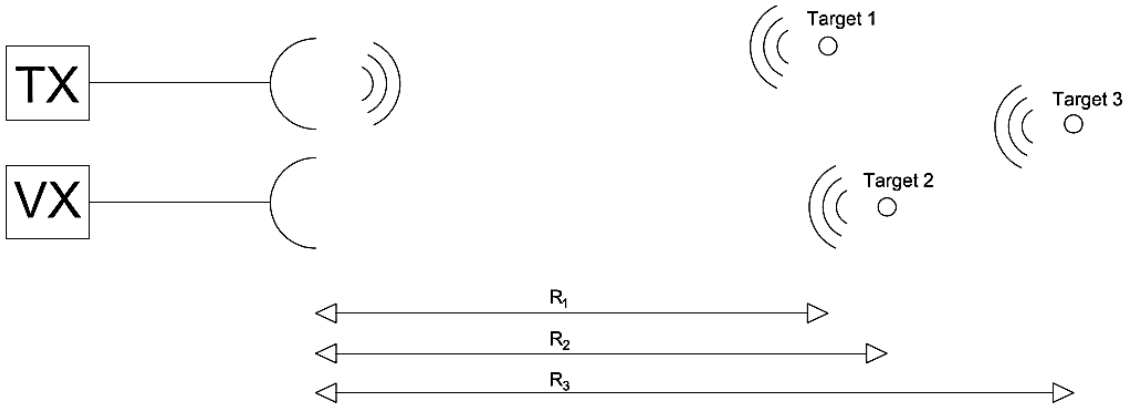

Figure 2.1- Simple SONAR model

Each of the reflections received will have a distinct time delay of τ_i corresponding to the range R_i of the reflective objects. Furthermore, each reflection received will be scaled by a

certain constant a_i which accounts for various system gains and propagation losses. Assuming a linear system, the total signal received, v_{RX} may thus be expressed as being the sum of all the reflections received of the original signal v_{TX}.

$$v_{RX}(t) = \sum_{i=1}^{N} a_i v_{TX}(t - \tau_i) \tag{2.1}$$

For the i'th target the respective time delay τ_i is defined by Equation (2.2), where R_i represents the range to the reflecting object in metres and c depicts the velocity of sound in water in metres per second:

$$\tau_i = \frac{2R_i}{c} \tag{2.2}$$

The amplitude scaling factor a_i for each respective target depends upon a number of factors, such as transmitting power, transducer gains, size of the targets, as well as transmission and absorption losses, which in turn are highly dependent on the medium the wave is travelling in. In a RADAR environment the amplitude scaling is determined by using the radar equation [4, p. 3], a simplified form of which is shown below,

$$a_i \propto \sqrt{\frac{G^2 \sigma \lambda^2}{(4\pi)^3 R_i^4}}, \tag{2.3}$$

where G represents combined antenna gains, σ is the radar cross section of a target, and λ represents the wave length of the signal. An extended version of Equation (2.3) in a logarithmic form, called the SONAR equation, applies to the underwater environment. The SONAR equation stated by Equation (2.4) will be discussed in more detail in Section 2.1.15.

$$DT = SL - 2PL + TS - (NL + RL - DI) \tag{2.4}$$

2.1.1 Range

Range computations for both SONAR and RADAR applications are generally accomplished by measuring the time delay between a transmitted pulse and an echo received. Knowing the speed, designated as c, at which the signal travels in its respective medium, the range may easily be computed by using the following equation:

$$R = \frac{c\tau}{2} \tag{2.5}$$

The factor of $\frac{1}{2}$ compensates for the return path time delay of the signal travelling to the target and back to the transducer.

The above approach is suitable for cases where a Matched Filter or Inverse Filter is used as a signal processing technique. Both types of filters will be evaluated at a later stage. A slightly different approach in finding the range R to a target is demonstrated in Section 2.4.3, but was deemed unsuitable for the scope of this thesis. The technique described as De-Ramping Technique is used for Frequency Modulated Constant Wave (FMCW) RADAR, where a constant signal is transmitted.

The maximum and minimum range detectable by SONAR is determined by a number of factors ranging from the selection of signal type and the processing of it, to the type of hardware used, and how it is set up.
However, the most salient factors determining the absolute range limits of detectable targets due to sound mechanics in water are cavitation and the near-field of an array.

The phenomenon of cavitation limits the maximum power transmittable by a projector into a respective medium. The limitations in range of SONAR due to cavitation will be investigated in Section 2.1.8.

The near-field of a projector, or an array of projectors, also known as the Fresnel field, determines the minimum distance required for a target in order to be detectable. A single projector is understood to have a near field, because the pressure waves originate from a number of points on the projector face. Inside the Fresnel zone the sound beam is affected by constructive and destructive interferences. Detection of targets within the field may thus not be reliable. Outside the Fresnel field, pressure waves combine to form a relatively uniform

wave front, called the far field. The near field of a projector may be calculated by using the following formula, which was obtained from the technical notes of Olympus piezoelectric ultrasonic transducers [5] ,

$$N = \frac{D^2}{4\lambda}\left[1 - \left(\frac{\lambda}{D}\right)^2\right] \qquad (2.6)$$

where

- $N =$ Near field distance in meter
- $D =$ Projector diameter in meter
- $\lambda =$ Wave length of signal

2.1.2 Range Resolution

The Range resolution of SONAR, commonly denoted as ΔR describes the ability of the SONAR to resolve targets that are in close proximity to each other. Illustrated in Figure 2.2, SONAR setup a) is unable to detect two separate targets, as compared to SONAR setup b) which clearly detects two distinct targets.

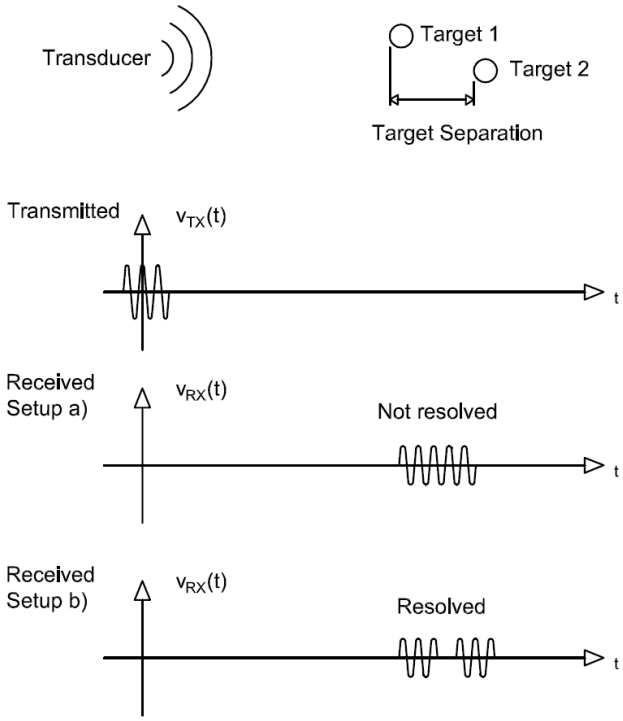

Figure 2.2 - Range resolution

The formula to calculating ΔR is again applicable to both SONAR and RADAR, as the basic mechanics are the same. As illustrated in Figure 2.3, which was adapted from the book of Bassem R. Mahafz, *MATLAB Simulations for Radar Systems Design* [6]**,** an incident pulse of length T hitting two targets may be resolved separately if the reflecting targets are separated by at least $cT/2$. With $1/T$ being the bandwidth B of the pulse, the range resolution may be expressed by the following equation:

$$\frac{\Delta R}{m} = \frac{c}{2B} = \frac{cT}{2} \tag{2.7}$$

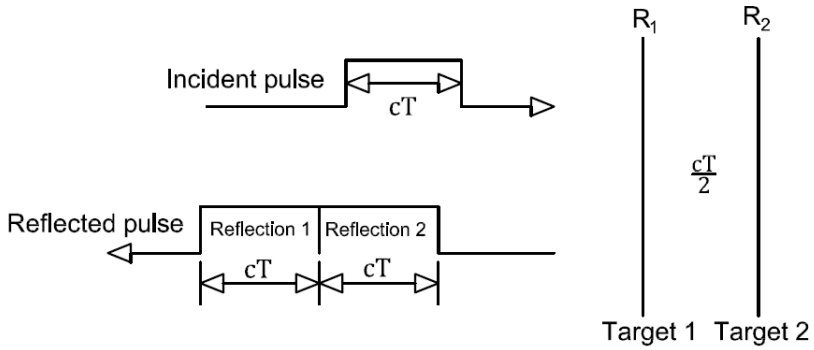

Figure 2.3 - Minimum target separation

2.1.3 Doppler

The Doppler phenomenon describes the change in frequency of a signal due to the motion of a target in relation to the source of the signal. Both RADAR and SONAR use Doppler frequency shifts to extract information from a signal regarding a target's radial velocity, and the platform's own velocity, as well as to suppress clutter. In case of a stationary platform and a moving target, the frequency of the incident signal is either shifted lower or higher, depending on, whether the target is retreating from, or approaching the signal source. According to R. Bassam, *MATLAB Simulations for Radar Systems Design* [6], the change in frequency f_d relative to the centre frequency f_0 of the signal may be expressed as,

$$f_d = \frac{2v}{c - v} f_0 \approx \frac{2v}{c} f_0 \tag{2.8}$$

where v denotes the radial speed of the target in relation to the signal source in metres per second. Given the specification of a maximum target speed of one meter per second, the

denominator of the above equation is simplified to being the signal speed c in the medium, since $v \ll c$. Thus the shift in frequency depends solely upon the radial speed of the target with respect to the signal source.

When comparing SONAR and RADAR it should be noted that the only difference between the two, regarding Doppler calculations, is the speed c at which the signal travels in its medium. This, however, has a significant effect, as the ratio of object velocity to sound velocity for SONAR, where $c \approx 1500\ \mathrm{m/s}$, becomes 10000 times larger as compared to RADAR, where $c \approx 3 * 10^8\ \mathrm{m/s}$. Doppler shifts may thus be detected at a higher accuracy with SONAR than with RADAR.

2.1.4 Sound Propagation

Whereas great similarities have been observed between RADAR and SONAR in the previous sections, the current section elucidates some of most radical differences between SONAR and RADAR. The basis of these differences is formed by the medium in which the investigating signal propagates. Compared to RADAR, where its electromagnetic waves are capable of travelling nearly unattenuated in air and are generally affected to a relatively minor degree by variations in the medium in which they are travelling, SONAR experiences great difficulties in the oceans. The waters of the oceans are anything but homogeneous. Apart from containing reflecting biological as well as non-biological suspended particles, the oceans consist of layers and flumes of water of different temperatures and salinity. At the boundary of each of such layer or flume, changes in temperature and salinity occur, causing sound waves to become reflected and refracted, as the impedance of the water varies. These changes in water temperature and salinity are due to a number of factors. Besides depth, geology, seismic activity, freshwater inflow or the influence of seasons, there are a number of unpredictable elements such as underwater currents and storms that may influence a water column, and consequently the way sound propagates through it. The result is that it is always possible for SONAR to fail in acquiring targets in so-called shadow zones. An example of such an event is shown in Figure 2.4, taken from the book of A.D Waite, *Sonar for Practicing Engineers* [7], where a sound pulse travels in a so-called surface duct, without penetrating into a lower water layer.

For the scope of this project, shadow zones and similar problems caused by refraction, are assumed to be of little importance due to the short range specified, as well as to the fact that

this project is limited to an almost ideal environment. This assumption is nevertheless valid for an ocean-going SONAR as well, due to the intention for this SONAR to specifically function as a very short range horizontally forward-looking collision avoidance sensor. Acoustic path problems arising from different surface layers are thus of no concern.

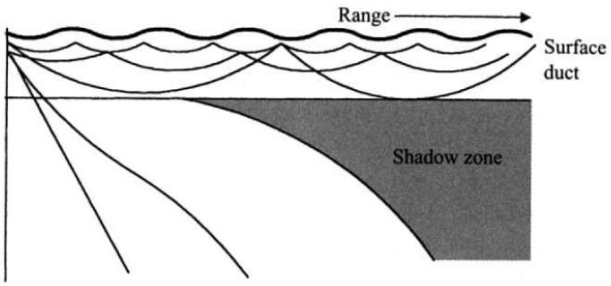

Figure 2.4 - Surface duct propagation [7, p. 55]

However, an effect that needs to be taken into account is reverberation. As already mentioned in the introduction, SONAR is far more susceptible to the effects of reverberation than RADAR. One of the main reasons for this is the fact that the SONAR environment is enclosed both by the seafloor at the bottom, as well as by the water surface from above, both causing interfering reflections. These reflections really become problematic in a shallow water enclosed environment, as is envisaged for this project. Signals are not only fully reflected by the walls of a harbour, but are then bounced repeatedly between the surface and the bottom of the enclosed environment. The other reason for the more significant effect of underwater reverberation is the relatively slow velocity of a sound wave in water as compared to the velocity of an electromagnetic wave. After a SONAR pulse has been sent out, the waiting period for the pulse to decay due to propagation and absorption losses, becomes quite significant in comparison to RADAR. Consequently, the scanning rate of SONAR is much lower than that of RADAR in order to avoid excessive reverberation.

Special precaution is required during the selection of wave forms and processing techniques to accommodate and minimize the effects of reverberation.

2.1.5 Sound Velocity

One of the challenges for SONAR is to accurately determine and predict the speed c at which sound travels under water. The speed of sound and the factors influencing it play a vital role in underwater acoustics. Complications in calculating basic Doppler and Range equations may already be expected by examining Equation (2.7) and Equation (2.8), should the sound velocity

not be constant. The three main natural factors influencing the speed of sound in water are temperature, depth and salinity of the water. An illustration of the effects of depth and temperature on sound velocity is shown in Figure 2.5, which was obtained from the book of A.D. Waite, *Sonar for Practicing Engineers* [1].

Again we may ignore nearly all of the problems arising from fluctuating sound velocity. The reasons for this are as before, the assumptions of very short range and a horizontal type of operation. Therefore the velocity of sound in water may be regarded as being constant for the purposes of this project, which applies to both a harsh ocean environment and an ideal fresh water tank type of environment.
Determining the correct underwater sound velocity c is accomplished by using an equation from L.E. Kinsler, *Fundamentals of Acoustics* [8].

$$c = 1448.6 + t(4.618 - 0.0523t) + 1.25(s - 35) + 0.017d \qquad (2.9)$$

where,

- $c =$ Velocity of sound $(\mathrm{m/s})$
- $t =$ Temperature $(℃)$
- $s =$ Salinity (ppt)
- $d =$ Depth (m)

The same result is obtained by using a logarithmic equation from A.D. Waite's book, *Sonar for Practicing Engineers* [7].

$$c = 1492.9 + 3(t - 10) - 6x10^{-3}(t - 10)^2 - 4x10^{-2}(t - 18)^2 + 1.2(s - 35) - 10^{-2}(t - 18)(s - 35) + d/61 \qquad (2.10)$$

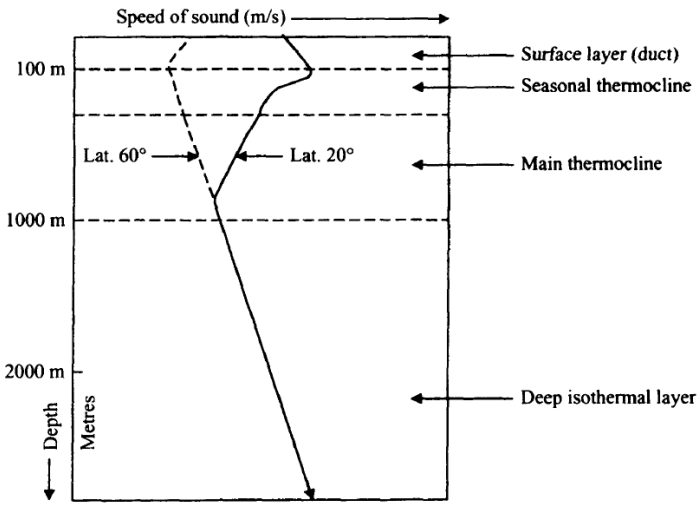

Figure 2.5 - Sound velocity profile [7, p. 52]

2.1.6 Acoustical Reference Units

It is customary to specify reference units for sound pressure and sound intensity in underwater acoustics. Using the books of Heinz G. Urban, *Handbook of Underwater Acoustics Engineering* [1] and A.D. Waite, *Sonar for Practicing Engineers* [7], as a standard, the reference unit for sound pressure is defined as $p_0 = 1\ \mu\text{Pa}$. The reference for sound intensity I_0, which is related to pressure, is calculated as shown below. The calculations are done assuming standard conditions for fresh water $c = 1480\ \text{m/s}$ and $\rho_0 = 1000\ \text{kg/m}^3$.

$$I_0 = \frac{p_0^2}{\rho_0 c} = 0.67568 * 10^{-18}\ \text{W/m}^2 \tag{2.11}$$

The formal definition of sound intensity is the energy per second crossing a unit area.
Intensities from calculations are thus often stated as,
're the intensity due to a pressure of 1 µPa' or more loosely as, '$re\ 1\mu\text{Pa}$'.

2.1.7 Source Level

The Source Level is defined in the book of Heinz G. Urban, *Handbook of Underwater Acoustics Engineering* [1], as

$$\frac{SL}{dB_{re\ 1\mu Pa\ at\ 1\ m}} = 10\ log\left(\frac{intensity\ of\ source\ at\ standard\ range}{reference\ intensity}\right) = 10log(\frac{I}{I_0}) \tag{2.12}$$

The standard range using the metric system is defined as $r_0 = 1$ meter. It is introduced to overcome difficulties in making practical measurements. Assuming an omni-directional source, the surface area of an emitted pulse may be described as that of a sphere being $4\pi r^2$. At standard range the surface area equates to 12.6 m^2. Equation (2.11) is thus rewritten below into logarithmic form by applying standard range r_0 and standard intensity I_0.

$$\frac{SL}{dB_{re\ 1\mu Pa}} = 10logP + 170.7\ dB \qquad (2.13)$$

It should be noted that P represents the total *acoustic* power radiated, which is a certain percentage of the *electrical* power applied to the projector, depending upon the transducer efficiency.

Equation (2.13) assumes an omnidirectional signal transmission, which is generally unpractical. Most projectors are directional, which needs to be incorporated in the SL equation as the transmission Directivity Index DI_t.

$$\frac{SL}{dB_{re\ 1\mu Pa}} = 10logP + 170.7dB + DI_t \qquad (2.14)$$

2.1.8 Cavitation

The limitation concerning the ability of transmitting power into water is defined firstly by the amount of power the transmitting projector is designed for, and secondly the phenomenon of cavitation. At the threshold of cavitation bubbles start to form on the surface of the projector. Bubbles occur on the surface of the projector because the negative acoustic pressure is below the pressure of the medium surrounding the projector. The formation of bubbles results in a radical loss in radiated acoustic power. Instead of being transferred into the medium, the acoustic power is absorbed and scattered within the bubbles. Besides negatively affecting the beam pattern, cavitation also erodes the surface of the transmitting projector.

Heinz G. Urban, *Handbook of Underwater Acoustics Engineering* [1], states that cavitation is mainly a function of depth. The higher the pressure surrounding the projector, the higher the cavitation limit shifts. Frequency and pulse length also affect the onset of cavitation, but are less dominant than pressure. Nevertheless, higher frequencies increase the cavitation limit. Furthermore, it is stated that cavitation starts at a point on the projector and spreads across

the surface of the projector with time. Therefore, short pulses are possible at much higher power levels compared to long pulses.

A conservative approach to calculating the cavitation limit $\mathrm{I_c(z)}$ may be expressed by the following equation for pulses longer than $5\ \mathrm{ms}$. The equation is converted into the metric system from the book of Robert J. Urick, *Principles of Underwater Sound for Engineers* [9, p. 74].

$$\frac{I_c(z)}{W/m^2} = \gamma \cdot 0.33 \cdot 10^4 \left(1 + 0.1\frac{z}{m}\right)^2 \qquad (2.15)$$

In the above equation z represents the operating depth of the projector in meters. Furthermore, Urick assumes $\gamma = 0.5$ as a constant, to compensate for the non-linear distribution of pressure.

For the practical evaluation of maximum allowable power, the intensity I_c at which cavitation commences must be calculated in terms of SL. For purposes of practical testing, the depth z of Equation (2.15) is assumed to be at least one meter. The intensity I_c resulting in cavitation may be converted into pressure p_c using Equation (2.11). The SL of a projector at a depth of one meter at which cavitation commences is thus:

$$SL = 20\ log\left(\frac{p_c}{1\mu Pa}\right) = 217\ dB_{re\ 1\mu Pa} \qquad (2.16)$$

The above result is confirmed in the book of Heinz G. Urban, *Handbook of Underwater Acoustics Engineering* [1, p. 162].

2.1.9 Propagation Losses

Propagation Loss (PL) in SONAR, which is the decrease in acoustic intensity between a source and a receiver, is the sum of spreading loss and absorption loss. The general spherical spreading loss experienced in SONAR is the same as experienced in RADAR, where power is radiated equally in all directions. Given that intensity is a quantity of power divided by area, with area being the surface area of a sphere due to equal spreading, power is equal to intensity multiplied by area.

$$\frac{P}{W} = 4\pi r^2 I \qquad (2.17)$$

With power being constant in the above equation, the intensity has to decrease with increasing radii. Following the standard notation of A.D. Waite, *Sonar for Practicing Engineers* [7], the PL at standard due to spreading loss at range $r_1 = 1$ m may be expressed as follows.

$$\frac{P}{W} = 4\pi r_1^2 I_1 = 4\pi r_2^2 I_2$$

$$\frac{PL}{dB} = 10\,log\left(\frac{I_1}{I_r}\right) = 10log\,r^2$$

$$\frac{PL}{dB} = 20\,log\ r \qquad (2.18)$$

PL is calculated in meters.

Following the notes of A.D. Waite, *Sonar for Practicing Engineers* [7], a special case of spreading loss is examined. Contrary to the spherical spreading law, where power is spreading evenly, the cylindrical spreading law describes a case where the source is enclosed by parallel planes that are h meters apart. Again, by increasing cylindrical surfaces, a decrease in intensity can be observed. Waite follows the same path as before to derive the PL for the cylindrical spreading law.

$$P = 4\pi r_1 h_1 I_1 = 4\pi r_2 h_2 I_2$$

$$\frac{PL}{dB} = 10\,log\left(\frac{I_1}{I_r}\right)$$

$$\frac{PL}{dB} = 10\,log\ r \qquad (2.19)$$

Although the spherical spreading law is generally valid in most cases, the cylindrical spreading law is mentioned as it is applicable to very confined water scenarios. Such a scenario is valid for the practical testing of this project, which is conducted in a towing tank of dimensions 3x3x86 meters (depth, width, length).

The second phenomenon leading to the attenuation of the intensity of a signal is the absorption loss α. In his book *Handbook of Underwater Acoustics Engineering* [1], Heinz G. Urban, describes the process of absorption as one that converts acoustic energy into heat. Furthermore, he states that the absorption process in fluids may be grouped into the following three categories: internal friction, internal heat dissipation, and the effects of relaxation. The

elements influencing these three processes are again the same as already discussed in Section 2.1.5, with the exception, that frequency is the dominant influence for absorption. In order to get a better estimate of the PL, Equation (2.18) needs to be adapted to accommodate absorption loss as well. Again following the book by Heinz G. Urban, *Handbook of Underwater Acoustics Engineering* [1], the PL equation is adapted as shown below.

$$\frac{PL}{dB} = 20\,log\ r + \alpha r \cdot 10^{-3} \qquad (2.20)$$

The algorithm for calculating absorption loss α has been revised several times in past years, with many different variations being available today. For purposes of this project the absorption loss in fresh water at a maximum frequency of $330\ \mathrm{kHz}$ needs to be calculated. Choosing the latest and most conservative algorithm from the journal article of M. A. Ainslie and J.G. McColm, *A simplified formula for viscous and chemical absorption in sea water* [10], the following absorption loss factor may be determined.

$$\alpha = 0.0285\ dB/m \qquad (2.21)$$

with,

- Frequency equal to $330\ \mathrm{kHz}$
- Temperature equal to $18\ ℃$
- Depth equal to 1 meter
- Salinity equal to 0.5 ppt
- Acidity (ph) equal to 8

At the proposed maximum range of this project the attenuation due to absorption is only $1.425\ \mathrm{dB}$, compared to the spherical spreading loss of $34\ \mathrm{dB}$ and the cylindrical spreading loss of $17\ \mathrm{dB}$. Attenuation due to absorption is therefore negligible and is thus omitted from simulations estimating SONAR performance in Chapter 3.

2.1.10 Directivity

The two identical projectors used for this project have a non-omni-directional beam pattern resulting in an improvement in SNR. This gain in SNR is commonly referred to as the directivity index (DI) of a projector or projector array. The DI of a projector in SONAR is the equivalent to the gain of an antenna in respect of RADAR. The projectors used for this project, and which are discussed in more detail in Section 4.2, have a round face with a diameter of $D = 5\ \mathrm{cm}$. In case of the diameter of the projector face being considerably greater than the wavelength of the transmitted signal, the following equation from the book of Robert J. Urick, *Principles of Underwater Sound for Engineers* [9], theoretically describes the DI of a circular piston source.

$$\frac{DI}{dB} = 10\,log\left(\frac{\pi D}{\lambda}\right)^2 \qquad (2.22)$$

for $2D \gg \lambda$

An average DI of $29.4\ \mathrm{dB}$ is assumed throughout this project for calculation purposes. The DI is calculated for the anticipated centre frequency of $280\ \mathrm{kHz}$.

2.1.11 Target Strength

The echo returned from an underwater target is denoted as Target Strength (TS). The target strength in SONAR is stated as a separate entity in logarithmic form, in comparison to RADAR, where the reflectivity of the target is incorporated in the radar equation as the radar cross section σ of the target. Except for incorporation of the ability of a target to reflect a signal differently into computations concerning predictions of target detection and system performance, the basic concept of targets and their ability to reflect a signal is the same. The radar cross section according to Solnik, *Introduction to Radar Systems* [4], is the following,

$$\sigma = \pi r^2$$

where r is the radius of a sphere in meters. Following the book of the of A.D. Waite, *Sonar for Practicing Engineers* [7], we find that the reflected acoustic intensity I_r of a sphere in water is,

$$I_r = \pi r_s^2 I_i \qquad (2.23)$$

where r_s is the radius of the sphere in meters, and I_i is the incident wave. The factor πr_s^2 is the scattering cross-section, which is the same as in RADAR.

In order to keep to the standard notation already established in the previous sections, the reflected intensity I_r is referred to as the intensity of a reflected wave from the centre of a sphere at standard distance $r = 1\ \mathrm{m}$. The result is then converted into logarithmic form.

$$\frac{I_r}{W/m^2} = \frac{\pi r_s^2 I_i}{4\pi r^2} \tag{2.24}$$

$$\frac{TS}{dB} = 10\,log\left(\frac{I_r}{I_i}\right) = 10log(\frac{r_s^2}{4}) \tag{2.25}$$

Although targets have various shapes, which all result in different TS, no further targets are investigated. All calculations and practical tests are conducted for the case of spherical targets only. Spheres distribute the reflected echo uniformly and omni-directionally, which make them suitable as reference targets, as their TS is independent of orientation.

2.1.12 Noise

As with RADAR, the factor limiting the ability of SONAR to detect or resolve targets is noise. According to Solnik, *Introduction to Radar Systems* [4], noise in RADAR is unwanted electromagnetic energy, as well as thermal noise. The electromagnetic energy according to Solnik, either originates from within the receiver itself, or it enters through the receiving antenna along with the signal received. The noise energy entering through the receiving antenna is known as environmental noise, which in turn is known as background radiation or cosmic noise, arriving from outer space. Other noise energy that may enter the receiving antenna may come from various manmade radiating entities. The degree of the influence of ambient noise depends on the operating frequency of the RADAR.

The thermal noise EMF (electromotive force) in RADAR is due to the thermal motion of electrons in the receiver input. It is modelled as a voltage across a resistive receiver input, and may be expressed by the following equation from the book of David M. Pozar, *Microwave and RF Design of Wireless Systems* [11],

$$V_n = \sqrt{4RkTB}, \tag{2.26}$$

where

- V_n is the RMS noise voltage of a resistor
- k is Boltzmann's constant $= 1.380 \cdot 10^{-23}$ J/K
- T is the temperature, in degrees Kelvin (K)
- B is the bandwidth, in Hz
- R is the antenna impedance, in Ω

With SONAR the noise experienced arises from similar principles to those of noise occurring in RADAR. For SONAR specifically A.D. Waite, *Sonar for Practicing Engineers* [7], distinguishes between three sources of noise:

- Thermal noise
- Ambient noise (Noises from the ocean)
- Vessel noise

The approximate thermal noise for SONAR systems may be computed by using the same equation as for RADAR. Equation (2.38) is thus true for SONAR as well, except for the radiation resistance R of an antenna, which must be replaced by the sum of the motional resistance R_m and the resistance R_p of the projector. For an underwater application the thermal noise does not arise only from the thermal agitation of electrons, but is rather also due to the thermal agitation of water molecules, applying a fluctuating pressure on the projector surface. These agitated water molecules are modelled as the motional resistance R_m. For a perfect receiver ($R_p = 0$) A.D. Waite, *Sonar for Practicing Engineers* [7], quantizes typical thermal noise as,

$$\frac{N_{thermal}}{dB_{re\ 1\mu Pa}} = -15 + 20\,log\ f, \qquad (2.27)$$

where f is expressed in kilohertz.

For the purpose of this project it may be assumed that of the three noise entities mentioned, none but the thermal noise is relevant. This assumption is true, because firstly the platform is being designed for and tested in an enclosed freshwater tank, free of any sources of sound and water agitation, secondly, because of the intended high centre frequency of 280 kHz of the platform, this assumption is generally valid for an ocean-going prototype as well. At high frequencies the thermal noise becomes dominant over other noise sources. The spectrum level of shipping and self-noise, as well as all other ambient noise forms decreases dramatically

beyond 100 kHz. Figure 2.6, which was obtained from the book of A.D. Waite, *Sonar for Practicing Engineers* [7], illustrates the noise spectrum levels of different noise sources across a frequency band spanning 100 Hz to 100 kHz. The different spectra of noise sources plotted in the figure are shipping, rain, thermal noise and sea state, which is indicated as DDS. The different sea states depicted are categorized from 1 to 6, where 6 resembles a sea state with wind speeds of 28 knots and wave heights of 3 m from crest to trough. The straight line with positive slope at the bottom right corner of Figure 2.6 indicates the spectrum level of thermal noise due to frequency. Biological noise is omitted from the figure. However, Heinz G. Urban in his book, *Handbook of Underwater Acoustics Engineering* [1], states that the highest frequency produced by biological organisms is around 20 kHz. Thus biological noise may be ignored for the purposes this project.

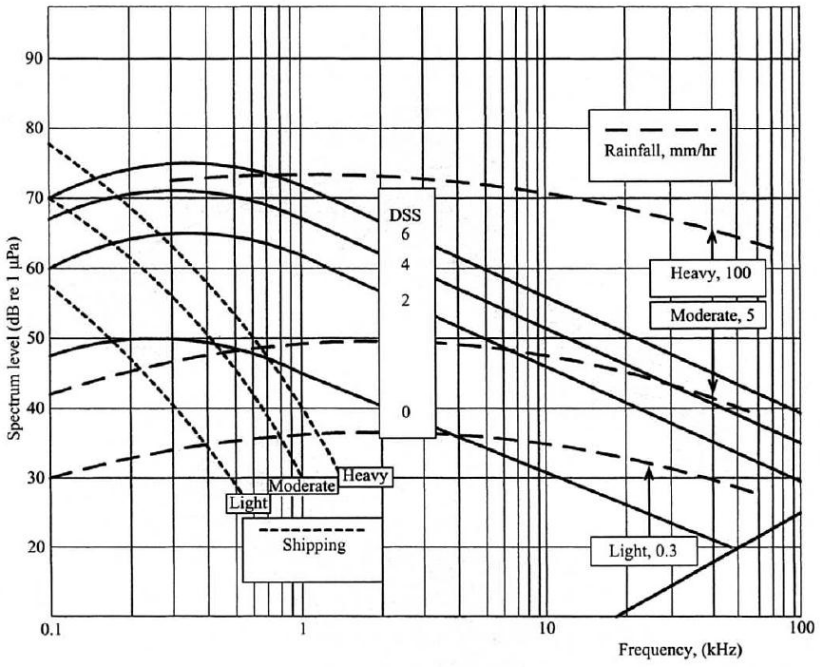

Figure 2.6 - Ambient noise of the sea [7, p. 88]

From the above figure it may be concluded that for a sea-going SONAR platform, with an operating frequency above 100 kHz, only heavy rainfall and strongly agitated sea conditions could contribute significantly to the overall noise level experienced by the platform.

Noise introduced by the receiver itself is assumed to be negligible. The receiver amplifier is chosen for a special low noise application with a noise figure of 2.5 dB [12] at the anticipated operating conditions. Furthermore, quantization noise of the 14 bit A/D converter is also

deemed to be negligible. The dynamic range requirements are easily met by the 14 bit resolution of the converter.

The total noise to the system for the worst case scenario at $330\ \mathrm{kHz}$ is thus assumed to be:

$$N_{thermal} = 35\ dB_{re\ 1\mu Pa} \qquad (2.28)$$

2.1.13 Reverberation Level

Reverberation is described as the received acoustic intensity at the receiver due to the back-scattering of a transmitted signal from in-homogeneities in the isonified water volume, and boundaries of the water volume.

Generally, reverberation is classified into three main categories according to their source:

- Volume reverberation
- Sea surface reverberation
- Sea bottom reverberation

For this project, volume reverberation is considered to be the main source of reverberation. Volume reverberation describes scattering due to in-homogeneities in the scanned water volume, such as suspended particles, changes in temperature or air bubbles in the water. The SONAR is intended to function as a collision avoidance unit. Therefore it will have a horizontal and forward looking characteristic and will thus only scan the bottom or the surface in extreme cases. Bottom and surface reverberations are therefore considered to be negligible.

As in RADAR, the basic parameter for reverberation calculations is constituted by the backscattering capacity of the area or volume which is being investigated. The backscattering cross section of a unit area or volume used for RADAR calculations was adapted for SONAR applications. For SONAR, the backscattering coefficient $S_{A,V}$ is defined as the ratio of the scattered intensity, referred to one meter from the acoustic centre, to the intensity of the incident plane wave. The value of $S_{A,V}$ is hard to predict. In his book, *Principles of Underwater Sound for Engineers* [9], Robert J. Urick states various figures for different environments, from which $S_{A,V}$ can be read.

$$\frac{S_{A,V}}{dB} = 10\,log\frac{I_{scat}}{I_{incident}} \tag{2.29}$$

Applying the above equation, the reverberation level at the receiver caused by volume reverberation, is expressed in the book of Robert J. Urick, *Principles of Underwater Sound for Engineers* [9], as:

$$\frac{RL}{dB} = SL - 40\,log\,r + S_V + 10logV, \tag{2.30}$$

where

- SL is the source level in dB
- r is the range between the transmitter and isonified volume in meter
- V is the isonified volume in m^3

For the case of the distance r being large in comparison to the cross-section of the isonified volume, which is true for this project, the following volume equality is true:

$$V = \frac{cT}{2}\frac{\pi r^2 \theta_h \theta_v}{4}, \tag{2.31}$$

where

- c is the speed of sound in m/s
- T is the pulse length of a CW pulse in seconds,
- or the reciprocal bandwidth of an FM pulse
- θ_h and θ_v are the respective horizontal and vertical beamwidths in radians

2.1.14 Detection Threshold and Detection Index

The detection threshold is defined by Heinz G. Urban, *Handbook of Underwater Acoustics Engineering* [1], as follows: "The detection threshold is the signal-to-noise ratio at the input of the receiver that results in a signal-to-noise ratio at the output of the receiver, with defined probabilities of detection and false alarm."

$$\frac{DT}{dB_{re\ 1\mu Pa}} = 10\,log\,\left(\frac{S}{N_o}\right)_{in}, \qquad (2.32)$$

where

- S is the signal power in the receiver input frequency band
- N_0 is the noise power in 1 Hz bandwidth

The detection threshold relates a pre-assigned level of correctness to a required signal to noise ratio at the receiver input which leads to a signal to noise ratio at the output of the receiver. At the selected level the detection threshold would satisfy the SONAR equation in such a way that a signal is only just detected. Should the selected threshold be too low, many "false alarms" will be detected, thus noise would be detected as a target. On the other hand, if the selected threshold is too high, only very strong targets will be recognised. In simple words, if the set detection threshold is exceeded, a target is assumed to have been detected.

Determination for the threshold is subject to the conditions of a given probability of detection $p(D)$ and probability of false alarm $p(FA)$. The probability $p(D)$ is the probability of a signal being present and detected. The probability $p(FA)$ describes the event of a target being detected due to noise, with no signal being present. The statistical detection process may thus be modelled with the aid of two distribution functions. One of the functions consists of pure noise N and the other consists of noise and signal $S + N$. Figure 2.7 shows the two distribution functions. Assuming a selected threshold level as shown, the hatched area below the signal plus noise distribution function envelope, to the right of the threshold level indicates the probability of the detection of a signal plus noise $p(D)$. The dark area below the noise distribution function to the right of the threshold level indicates the probability of false detection due to noise, in other words the probability of a false alarm $p(FA)$.

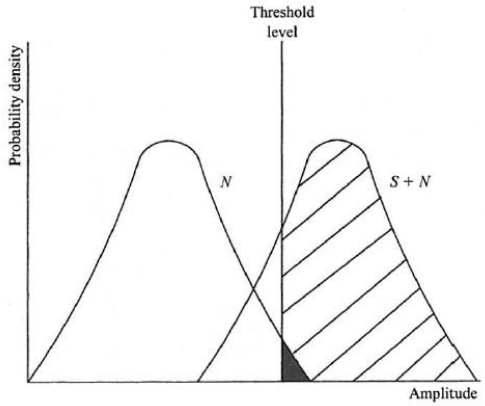

Figure 2.7 - Probability density distribution [7, p. 122]

The detection index d represents the SNR at the output of the SONAR receiver. It is described in the book of Heinz G. Urban, *Handbook of Underwater Acoustics Engineering* [1], as the distance between two statistical distribution functions. Thus the two probabilities of detection and false alarm are directly related via the detection index d. The detection index d therefore indicates how easily a signal may be found in noise. More details regarding the derivation of the detection index may be found in the book of Robert J. Urick, *Principles of Underwater Sound for Engineers* [9]. According to Urick the detection index for Gaussian distribution is represented as shown below.

$$d = \frac{[\,E\{(s_{out}+n_{out})\}-E\{n_{out}\}]^2}{\sigma_{out}^2} = \left(\frac{S}{N}\right)_{out}^2, \qquad (2.33)$$

where

- $E\{s\}$ is the expected value of the signal s
- σ is the standard deviation of both distribution functions

The detection index may be found as a function of $p(D)$ and $p(FA)$ using receiver operating plots. Assuming Gaussian noise for both distribution functions of Figure 2.7, the detection index d may be found for specific $p(D)$ and $p(FA)$ using the graphs shown in Figure 2.8, as obtained from the book of Robert J. Urick, *Principles of Underwater Sound for Engineers* [9]. According to the report by Ross L. Dave, *Detection Threshold Modelling Explained* [13], a common combination of the two probabilities for system evaluation is $p(D) = 0.5$ and $p(FA) = 10^{-4}$, resulting in $d = 25$.

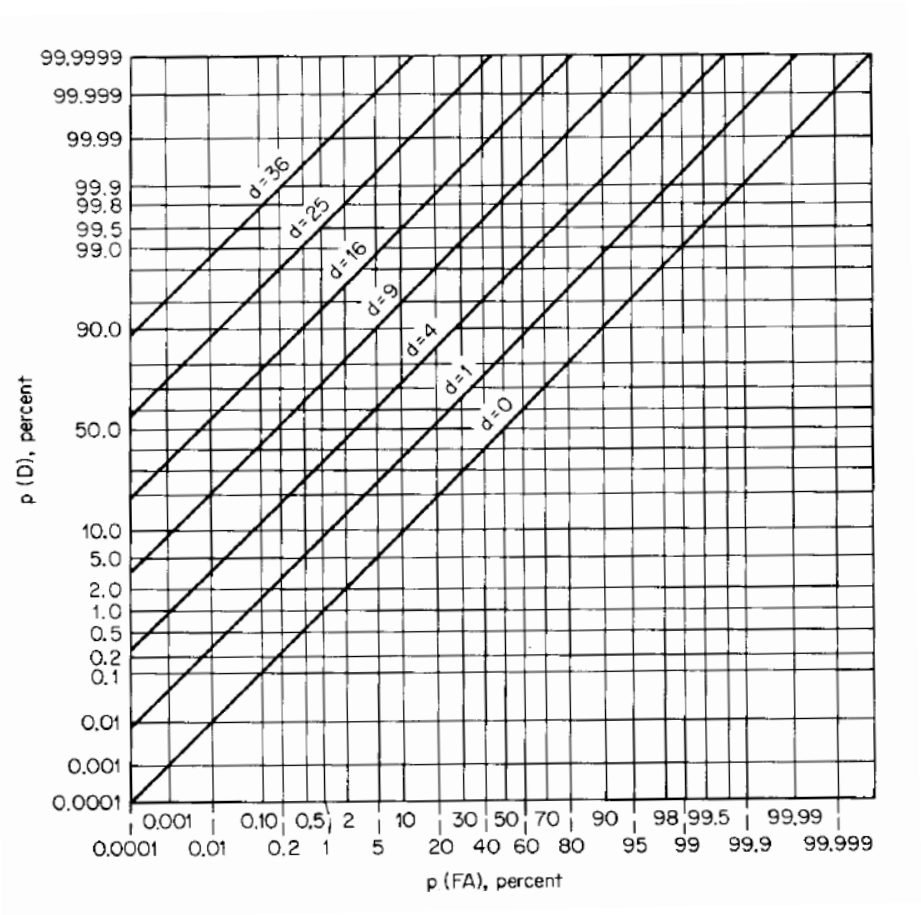

Figure 2.8 - Receiver operating characteristic [9]

Having determined a suitable detection index d, it needs to be related to the input signal-to-noise ratio of a specific receiver setup. For this project a known signal which is corrupted with noise will be correlated against its noise free replica.

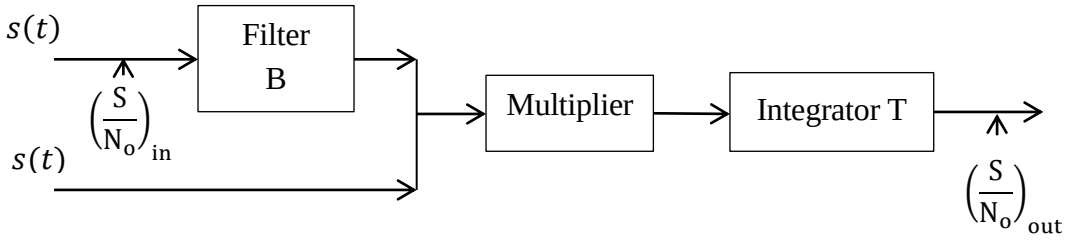

Figure 2.9 - Correlation receiver

For the above case of a correlation receiver the detection index, according to Heinz G. Urban, *Handbook of Underwater Acoustics Engineering* [1], may be expressed by:

$$d = 2BT\left(\frac{S}{N}\right)_{in} \tag{2.34}$$

Solving Equation (2.34) for $(\frac{S}{N})$ and inserting the answer into Equation (2.32), the following detection threshold is obtained:

$$DT = 10log\frac{d}{2T}, \tag{2.35}$$

where

- $N_o = \frac{N}{B}$ (Equation (2.32))
- B is the bandwidth of the input filter
- T is the duration of the pulse

For the specific case of reverberation limited detection for a LFM pulse, where reverberation fills the whole input band, the detection threshold is adjusted as follows:

$$DT_R = DT - 10logB \tag{2.36}$$

2.1.15 The SONAR equation

The SONAR equation is a valuable tool when approximating the performance of and comparing different systems. This equation forms the absolute basis for preliminary performance estimation. More accurate performance predictions regarding range and Doppler resolution are determined at later stages. The equation itself is closely related to the RADAR equation, which is stated in its simplified form as Equation (2.3). One of the main differences between the RADAR and SONAR equations is that only dimensionless elements are used for the SONAR equation, which is expressed in logarithmic notation.

The SONAR equation in its simplest form, which is specifically of interest to this project, is given in the book by Heinz G. Urban, *Handbook of Underwater Acoustics Engineering* [1], as follows:

$$DT = SL - 2PL + TS - (NL + RL - DI), \quad (2.37)$$

where

- PL represents the propagation loss in dB
- SL represents the projector source level in dB
- TS represents the target strength in dB
- DI represents the directivity index of the transducers in dB – calculated for transducers
- NL represents the noise level in dB
- RL represents the reverberation level in dB
- DT represents the detection threshold in dB

The detection threshold may be thought of as the signal-to-noise ratio (SNR) at the receiver input, which ultimately indicates the effectiveness of a SONAR system design.

2.2 Target Scene Model

According to the lecture notes of A.J. Wilkinson, *Notes on Radar/Sonar Signal Processing: Fundamentals,* [14], scenes resulting in more complex return signals, such as multi-path propagation and similar, may be described completely by their impulse response $\zeta(t)$ as illustrated in Figure 2.10, which was adapted from Wilkinson's notes. Thus, if a Dirac delta impulse is transmitted, the received response $v_{RX}(t)$ according to Wilkinson, is the impulse response $\zeta(t)$ of the system.

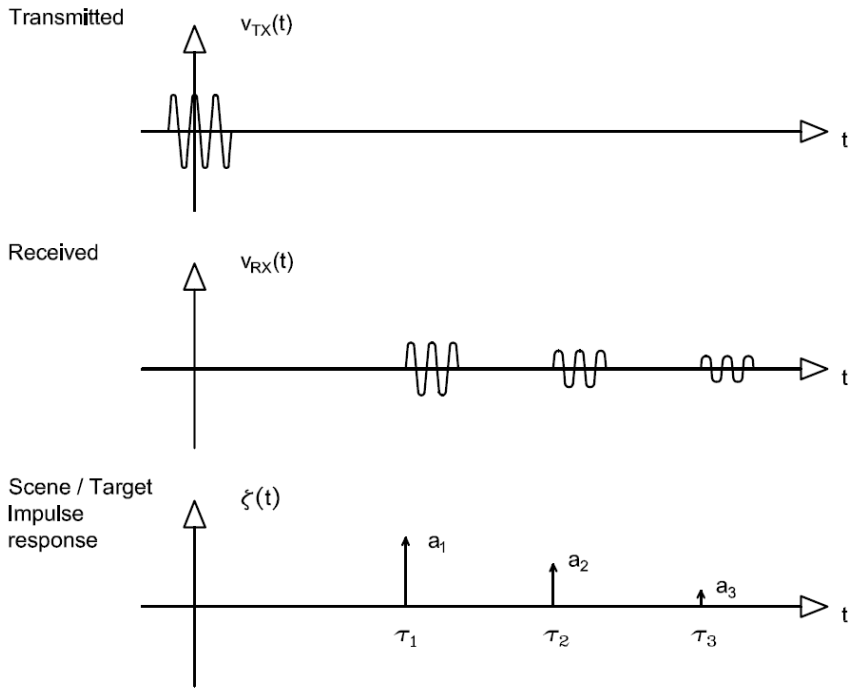

Figure 2.10- Response from several point targets

Furthermore, Wilkinson states that if an arbitrary waveform $v_{TX}(t)$ is transmitted, the received signal is simply the convolution of the scene's impulse response $\zeta(t)$ and the transmitted pulse $v_{TX}(t)$.

$$v_{RX}(t) = \zeta(t) \circledast v_{TX}(t) = \int_{-\infty}^{\infty} \zeta(\tau) v_{TX}(t-\tau) d\tau \qquad (2.38)$$

Extending the above equation for the case of the reflecting scene being a number of point targets, the impulse response of the scene may be thought of as the sum of weighted impulses.

$$\zeta(t) = \sum_{i=1}^{N} a_i \delta(t - \tau_i) \tag{2.39}$$

Applying the above the solution of $\zeta(t)$ to the convolution of Equation (2.38),(2.39) results in the received signal having the following form:

$$v_{RX}(t) = \left[\sum_{i=1}^{N} a_i \delta(t - \tau_i)\right] \circledast v_{TX}(t)$$

$$v_{RX}(t) = \left[\sum_{i=1}^{N} a_i \delta(t - \tau_i) \circledast v_{TX}(t)\right]$$

$$v_{RX}(t) = \sum_{i=1}^{N} a_i v_{TX}(t - \tau_i) \tag{2.40}$$

It may thus be concluded that all the information pertaining to the scene may be found in the scene's impulse response $\zeta(t)$ which, in turn, is contained within the received signal $v_{RX}(t)$.

2.3 Received Signal Description and Processing

Unlike in to RADAR, where I-Q channels are commonly used to significantly reduce the required sampling processing requirements in order to achieve Nyquist requirements, no I-Q channels are utilized for this project. Although I-Q channel processing would reduce processing power requirements, the desired operating frequency and bandwidth for this project are well within the processing capabilities of off-the-shelve components. Thus for reasons of simplicity, quadrature sampling is not applied in this project.

In the previous section it was shown that all information regarding the inspected scenery is contained as the scene's impulse response within the received signal. The aim is thus to extract the scene's impulse response $\zeta(t)$ from the received signal $v_{RX}(t)$. Besides containing information regarding targets of the scanned scenery, the received signal will also be

corrupted with broadband noise, and by the nonlinear characteristics of the transmit-and-receive hardware of the SONAR system.

In order to limit receiving noise, the received signal will be filtered by a suitable analogue Band Pass (BP) filter before sampling. After sampling the digital signal may be passed through a software defined filter, to further reduce noise, should the analogue filter be insufficient. Unlike analogue filters digital filters can be designed for exact cut-off frequencies and theoretically unlimited sharp cut-offs.

After filtering, the digital signal is processed for range and Doppler frequency shift applying the techniques discussed in the following section.

In RADAR, the received signal is usually base-banded after being received by an IQ down-converter. Base-banding a signal shifts the spectral components of the signal around zero hertz. This allows for the signal to be low-pass filtered instead of band-pass filtered. Furthermore, base-banding reduces the memory requirements of a system, as only the positive frequency components of a received signal are recorded. The negative frequency components contain no additional information and are thus discarded. Although for this project no IQ channel processing is realized, base-banding may still be implemented in software, by post-processing the received signal. Base-banding the received signal revealed a reduction in signal quality during simulations. Given that ample memory and post-processing power is available, it was decided not to implement base-banding on the received signal for this project.

2.4 Range and Doppler Processing Techniques

In order to extract information regarding range and Doppler frequency shifts of potential targets from the received signal, the received signal is usually correlated in a certain way against the transmitted signal. The two most well-known and widely used correlation techniques are matched filtering (MF) and inverse filtering (IF). Both techniques have advantages and disadvantages. Literature is available on the blending of the output of the two filters to achieve the best results according to each situation, by adjusting the percentage each filter contributes[1]. For purposes of this project the filters are only discussed in isolation.

A different approach to correlation for obtaining range and Doppler measurements is discussed in Section 2.4.3.

2.4.1 Matched Filter (MF)

By definition the MF is a correlator, which compares two known signals to generate an output, indicating how well the two signals match. The feature which makes the MF unique is its ability to produce a maximum achievable instantaneous SNR at its output, in case of a signal plus additive white noise being present at its input. To determine the impulse response $h(t)$, which maximises the SNR at a predetermined time t_o, the model of the MF shown below is examined. White Gaussian noise is added to the input signal $s(t)$, with a two-sided power spectral density of $N_0/2$.

Figure 2.11 – General Receiver

Following the derivation of B. Levanon, *Radar Signals* [15], it may be proven that the optimum impulse response as expressed by Equation (2.41) will maximise the output SNR.

[1] N. Sharma, *Trading detection for resolution in active sonar receivers* [17]

$$h(t) = Ks^*(t_0 - t) =_{K=1,t_0=0}= s^*(t), \quad (2.41)$$

where

- K is an arbitrary constant
- s^* is the complex conjugate of s
- t_0 is a predetermined delay, equal to the time of an echo

The same holds true for the frequency response:

$$H(f) = KS^*(f)\,exp(-j2\pi f t_0) =_{K=1,t_0=0}= S^*(f) \quad (2.42)$$

It should be noted that the processing of the MF receiver is performed in the frequency domain, as convolution in the time domain becomes multiplication in the frequency domain.

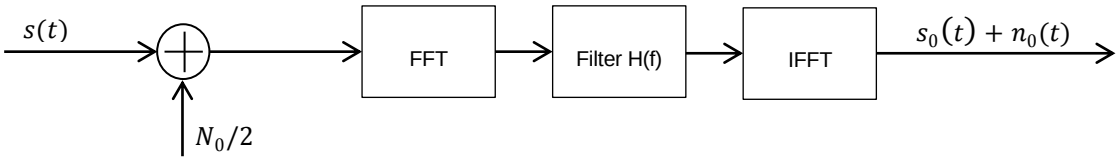

Figure 2.12 - Matched Filter Receiver

According to Levanon the peak instantaneous SNR achievable by the MF at t_0 is defined by:

$$SNR(t_0) = \frac{2E}{N_0}, \quad (2.43)$$

where E is the energy of the finite-time signal:

$$E = \int_{-\infty}^{\infty} s^2(t)dt \quad (2.44)$$

It should be noted that the peak SNR only depends on the energy of the signal and the input noise power. Signal waveform has no influence.

To ensure causality of the filter a time delay term τ_0 needs to be incorporated, where $\tau_0 > T$, the total pulse length.

$$h(t) = \begin{cases} s^*(\tau_0 + t_0 - t) & ;t > 0, \tau_0 \geq T \\ 0 & t < 0 \end{cases} \quad (2.45)$$

For the general case of the filter output at other delays the MF is expressed by:

$$s_0(t) = s(t) \otimes h(t) =_{K=1,t_0=0} \int_{-\infty}^{\infty} s(\tau)s^*(\tau - t)d\tau \quad (2.46)$$

For the case of $h(t) = s^*(t)$, being the so-called replica of $s(t)$, the right-hand side of the above equation becomes the auto-correlation function of $s(t)$.

In practice the replica of the transmitted wave is computed and stored for processing. For this project a number of replicas are generated and stored for CW and LFM in order to perform post-signal processing by using Matlab.

Expanding the discussion, as described by Turin in his report, *An Introduction to Matched Filters* [16], by taking the Doppler effect into account, the output of the MF $u_0(t)$ is expressed in terms of the input complex envelope $u(t)$, shifted by a certain Doppler frequency f_d. The Doppler-shifted complex envelope $u_D(t)$ is thus expressed by:

$$u_D(t) = u(t)exp(j2\pi f_d t) \quad (2.47)$$

Inserting Equation (2.60) into Equation (2.46), and by selecting $t_0 = 0,\ K = 1$ as before, leads to the result of the output of the MF $u_0(t, f_d)$ in terms of the delay τ and the Doppler frequency f_d.

$$u_0(t, f_d) = \int_{-\infty}^{\infty} u(\tau)exp(j2\pi f_d \tau)u^*(\tau - t)d\tau \quad (2.48)$$

By performing integral manipulations the above expression may be rearranged as follows:

$$\chi(\tau, f_d) = \int_{-\infty}^{\infty} u(t)u^*(t - \tau)e^{j2\pi f_d t}dt\,, \quad (2.49)$$

which forms one of the expressions of the ambiguity function. The ambiguity function is an important tool to evaluate signal designs for their performance in both range and Doppler determination. The function is discussed in more detail in Section 2.5.

When it comes to detecting targets having an unknown added Doppler component to their echo, most SONAR systems make use of a bank of MF. Using Equation (2.62) each MF may be

tuned to a specific Doppler frequency, thus optimizing the detection process for echoes which are Doppler shifted.

The MF is optimized for the detection of a signal in noise, thus having an optimal SNR at its output. The disadvantage of the MF is that the output has high side lobes, which is undesirable. Having high side lobes decreases the resolution of the filter when it comes to the resolution of multiple closely spaced echoes. To reduce side lobes a window function may be applied, which supresses side-lobes, but widens the main lobe. Consequently the final response will still not be perfect.

2.4.2 Inverse Filter (IF)

To improve upon the range resolution of the MF, the impulse response of the filter, with which the transmitted signal is being convoluted, needs to minimize the output peak of the convolution. The signal which has the narrowest output response is an impulse δ. To achieve a δ function as an output of the receiver, the filter $h(t)$ is chosen to be the inverse filter of the transmitted signal. A simple approach in explaining the IF is expressed by N. Sharma, *Trading detection for resolution in active sonar receivers* [17], as below:

$$s(t) \otimes h(t) = \delta(t) \tag{2.50}$$

therefore,

$$H(f) = \frac{1}{S(f)} \tag{2.51}$$

A received signal $r(t)$ comprised of two echoes is expressed below. One echo is not delayed in time, the other is delayed by τ. White Gaussian noise is added to the signal as $w(t)$.

$$r(t) = s(t) + as(t - \tau) + w(t) \tag{2.52}$$

Sending the received signal through the inverse filter as proposed shows that the IF is able to decompose a composite signal for any τ.

$$h(t) \otimes r(t) = \delta(t) + a\delta(t)(t - \tau) + w(t) \tag{2.53}$$

The above mathematical explanation of the IF is, however, insufficient because noise will flood the output of the filter. The IF is derived in more detail in the notes of A.J Wilkinson, *Notes on Radar/Sonar Signal Processing: Fundamentals* [14]. Wilkinson limits the bandwidth forwhich the scene's impulse response may be reconstructed to the bandwidth B of the transmitted signal. Outside the frequency band B the IF will amplify noise. In practice a windowing function limits the IF frequency band.

$$H(f) = \begin{cases} \frac{1}{S(f)} & ; -\frac{B}{2} \leq f \leq \frac{B}{2} \\ 0 & elsewhere \end{cases} \tag{2.54}$$

Similar to the MF, a replica is generated and stored in memory. Obtaining the replica by physically transmitting and receiving the pulse, the IF is capable of removing all non-linear system effects added to the signal, thus optimising the filter output. Ideally, a replica is obtained by transmitting and receiving a pulse, with the transmitter and the receiver transducers facing each other across certain distance. Adjusting the delay of the replica will result in the output of the IF being free of effects added by the system components. This replica acquisition process would, however, require a near infinite environment with a perfect medium, as reflections from inside the medium and the environment's boundaries would deteriorate the replica. For this project the replica is obtained by directly sampling the generated signal from the signal-generating unit.

In contrast to a MF, an IF is designed to deliver optimal resolution, compared to optimal detection of the MF. This leaves the IF with the problem of being non-optimal with regard to detection, thus experiencing problems in detecting signals which are submerged in noise. The journal article, *Trading detection for resolution in active sonar receivers* [17], by N. Sharma explains the trade-off between MF and IF precisely: "A matched filter cannot resolve some targets that it can detect, and an inverse filter cannot detect some targets that it can resolve."

2.4.3 De-Ramping

The de-ramping technique is mostly used in RADAR applications. Literature on the usage of the de-ramping technique in SONAR is limited. The reason for this being that this processing technique requires a continuous linear frequency-modulated pulse (FMCW) in order to function. Consequently, a continuous signal needs to be transmitted, which may become

problematic in an environment where reverberation is a limiting factor in the detection of targets.

The basic principle employed by the technique is multiplying the transmitted and received signals to obtain two signals, one having a frequency of the difference and the other that of the sum of w_T and w_R. Commonly only the difference signal is employed for calculations, as the frequency of the difference signal is lower. For the simple case shown below, where the transmitted w_T signal and received signal w_R is plainly sinusoidal, only Doppler information can be extracted from the signal being either the sum or the difference of w_T and w_R.

$$cos(w_R t) \cdot cos(w_T t) = \frac{1}{2} cos(w_R t + w_T t) + \frac{1}{2} cos(w_R t - w_T t) \qquad (2.55)$$

The Doppler frequency may be calculated by using Equation (2.8).

To obtain both Doppler and range information the transmitted pulse needs to be modulated. The modulation commonly used is LFM. In case of a received signal having a Doppler shift, there is an ambiguity between the changes in frequency due to Doppler Effect and due to range. The ambiguity between Doppler Effect and range is graphically explained in Figure 2.13. The increasing frequency of the transmitted signal is represented by the thin line, whereas the received signal is represented by the bold line.

The frequency of the received signal at a certain point in time is affected by the time delay τ it takes for the signal to travel to and from the target, as well as the Doppler frequency shift F_d.

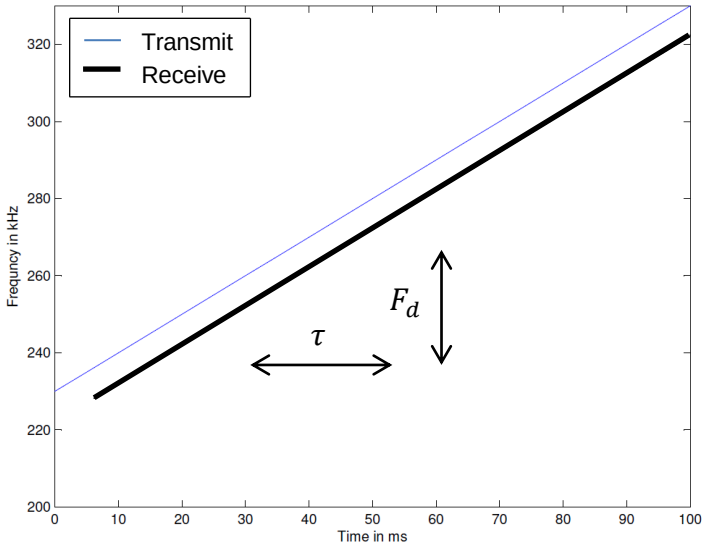

Figure 2.13 - LFM up chirp

To resolve the ambiguity, two sweeps of triangular LFM are commonly used. An example of a triangular signal sweep is shown in Figure 2.14. The difference frequency, commonly called the beat frequency, with added Doppler is shown as the dashed line. Chirping both up and down creates a beat frequency which has an added Doppler component and a subtracted Doppler component, depending on an up or down chirp. Averaging the beat frequency reveals the frequency pertaining to the range of the target. Taking either the positive or negative offset of the beat frequency to the average discloses the Doppler frequency of the target.

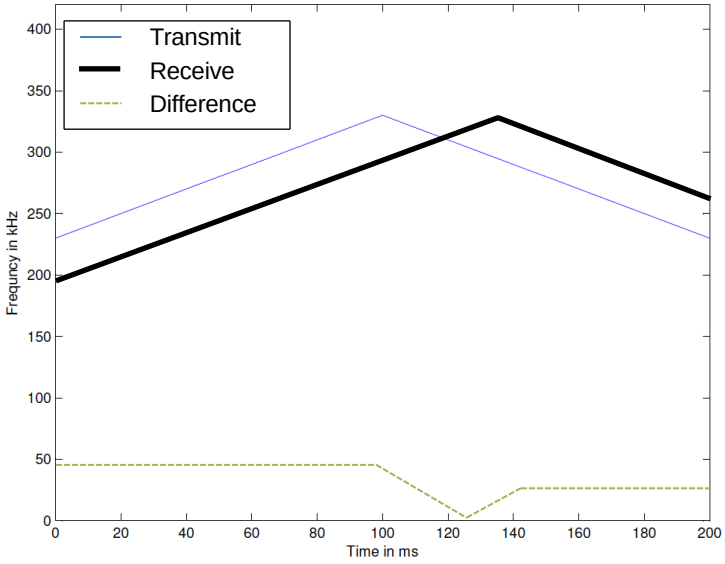

Figure 2.14 - Triangular FM

The following three equations describing frequency resolution Δf, range resolution ΔR and range R are obtained from the thesis of J. Hoole, *Implementation of a Low-cost FM-CW Radar* [18].

$$\Delta f = \frac{1}{T_{pulse}} \tag{2.56}$$

$$\Delta R = \frac{c}{2B} \tag{2.57}$$

$$R = \frac{fT_{pulse}c}{2B} \tag{2.58}$$

For the range and range resolution the bandwidth B is defined as being the bandwidth between the starting and stopping frequency of the linear sweep. The frequency f is the frequency corresponding to a target at range R.

2.5 The Ambiguity Function

The ambiguity function is a tool used to predict the performance of a pulse design in range and Doppler frequency determination, for both RADAR and SONAR applications. The function evaluates the performance of signals based upon the assumption that the signals are processed by a MF. The ambiguity function is defined by N. Levanon in his book, *Radar Signals* [15], as follows:

$$|\chi(\tau, v)|^2 = \left|\int_{-\infty}^{\infty} x(t)x^*(t-\tau)e^{j2\pi vt}dt\right|^2, \quad (2.59)$$

where

- $x(t)$ is the pulse to be investigated
- $x(t)^*$ is inverse of the pulse to be investigated
- τ is the time delay due to a target at a certain range
- v is the target velocity

It should be noted that the ambiguity function may be stated in terms of target velocity v or target Doppler frequency shift f_d.

$$|\chi(\tau, f_d)|^2 = \left|\int_{-\infty}^{\infty} x(t)x^*(t-\tau)e^{j2\pi f_d t}dt\right|^2, \quad (2.60)$$

where

- $x(t)$ is the pulse to be investigated
- $x(t)^*$ is inverse of the pulse to be investigated
- τ is the time delay due to a target at a certain range
- f_d is the Doppler frequency shift

The output of the ambiguity function is a three -plot, which has axes in range, Doppler and ambiguity.

The ideal ambiguity function is shown in Figure 2.15, where the ambiguity function is a spike of infinitely small width, peaking at the origin and being zero everywhere else. A pulse with the ambiguity function as shown below may be perfectly resolved in both range and Doppler frequency. Such a function is, however, not possible in terms of to the properties of the ambiguity function, as discussed by Levanon.

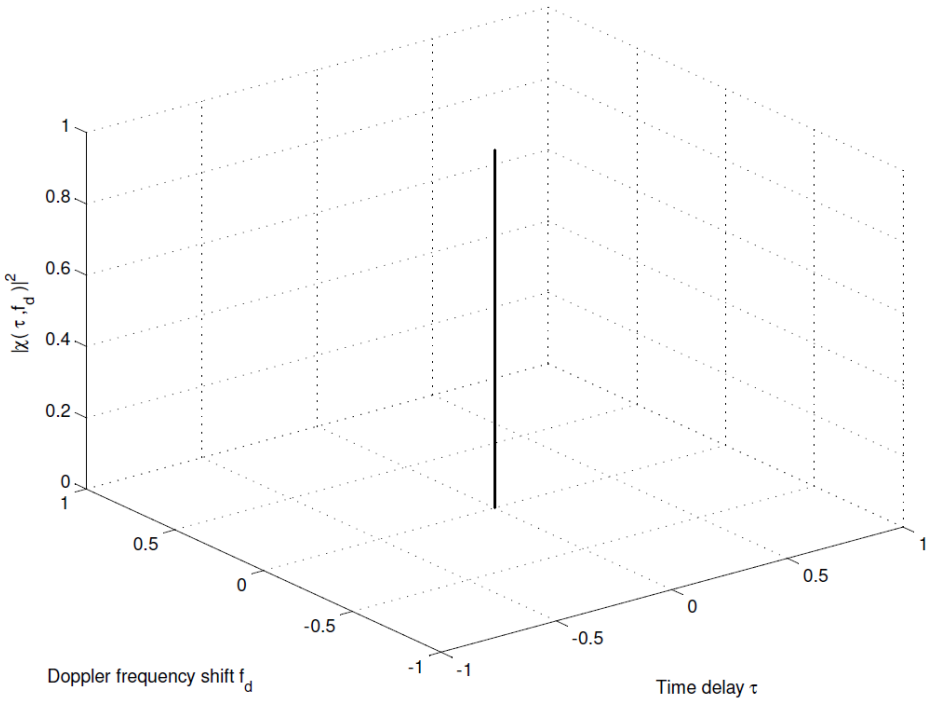

Figure 2.15 – Ideal Ambiguity Function

According to Levanon the ambiguity function has the following properties:

1) Maximum at (0,0)

$$|\chi(\tau, f_d)| \leq |\chi(0,0)| = 1 \qquad (2.61)$$

2) Constant volume

$$\int_{-\infty}^{\infty}\int_{-\infty}^{\infty}|\chi(\tau, f_d)|^2 d\tau\, df_d = 1 \qquad (2.62)$$

3) Symmetry with respect to the origin

$$|\chi(\tau, f_d)| = |\chi(-\tau, -f_d)| \qquad (2.63)$$

4) Linear FM effect

$$|\chi(\tau, f_d - k\tau)| \qquad (2.64)$$

Properties one and two dictate that when optimizing an ambiguity function to have a narrow peak at the origin, that peak cannot exceed a value of one, and that volume displaced has to reappear somewhere else. Property four explains that an ellipsoid will be sheared according to the frequency sweep rate k of a LFM pulse. Figure 2.16 illustrates the basic ambiguity function profiles for long and short CW pulse designs, as well as the sheared ellipsoid due to a LFM pulse design, in the presence of interference and a stationary target.

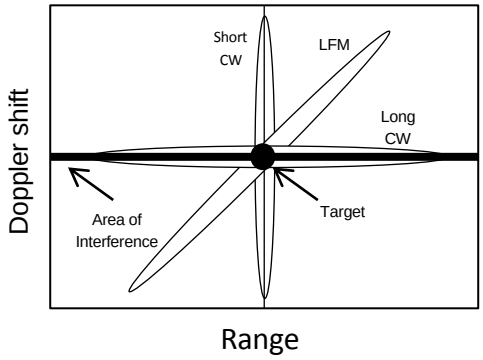

Figure 2.16 - Ambiguity function profiles for long CW, short CW, and LFM

The typical three-dimensional plot of an ambiguity function is shown in Figure 2.17, for the example of a simple CW pulse.

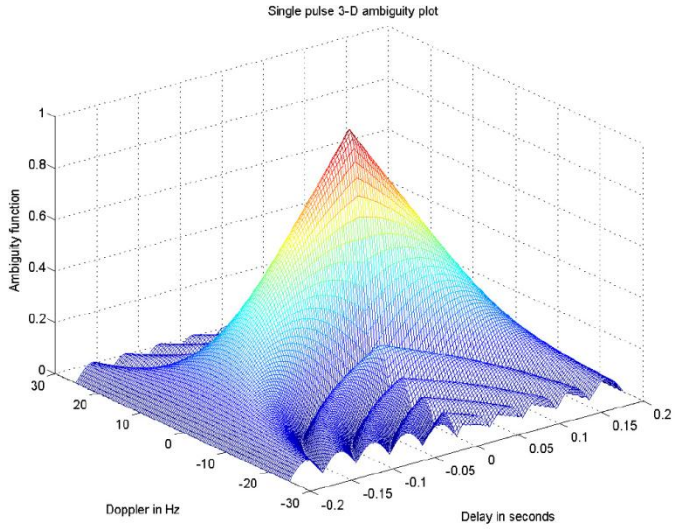

Figure 2.17 - CW ambiguity function

To gain more insight into the result of the ambiguity function, it is often favourable to plot the contour lines of the function. The contour plot of the above ambiguity function is depicted in Figure 2.18.

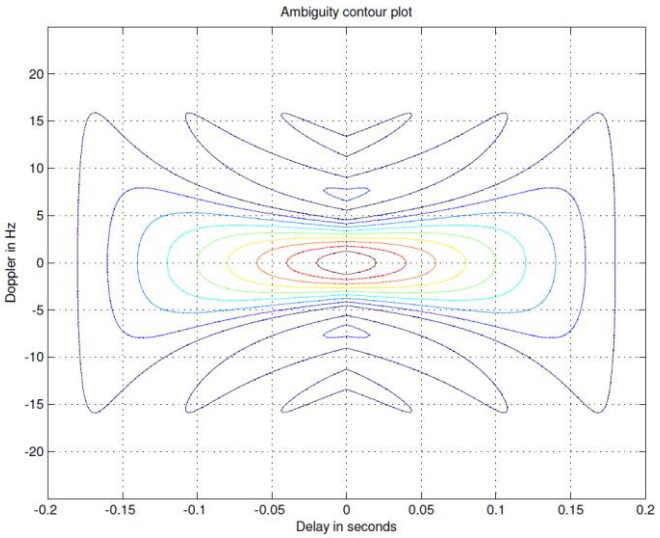

Figure 2.18 - CW ambiguity contour plot

To evaluate the ambiguity function of a pulse for range and Doppler resolution, the ambiguity function may be evaluated along zero delay $\tau = 0$ and zero Doppler $f_d = v = 0$ axes of the ambiguity plot, respectively.

The plots for zero Doppler and delay are shown in Figure 2.19, for the above CW ambiguity function example plot.

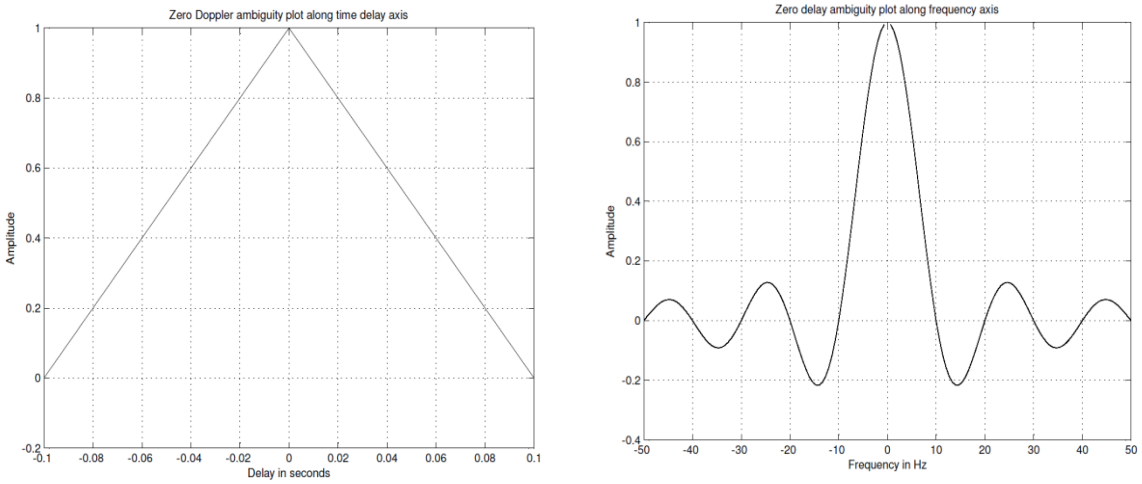

Figure 2.19 – CW zero Doppler and delay ambiguity function cuts

In his book, *Detection, Estimation and Modulation Theory* [19], H.L. Van Trees suggest that the ambiguity function as stated in Equations (2.59) and (2.60) is overestimating the Doppler frequency resolution performance. According to H.L. Van Trees the ambiguity function as stated, is for the evaluation of narrow-band signals only. H.L. Van Trees suggest that a signal exceeding the following condition is regarded as a wide-band signal:

$$\frac{2v}{c} \ll \frac{1}{BT} \tag{2.65}$$

Should the above condition not be satisfied the wideband ambiguity function shown below, defined by Kelly and Wishner [20], should be implemented.

$$|\chi(\tau,\eta)|^2 = \left|\eta^{1/2} \int_{-\infty}^{\infty} x^*(t)x(\eta(t-\tau))dt\right|^2, \tag{2.66}$$

where

$$\eta = \frac{(1+\frac{v}{c})}{(1-\frac{v}{c})} \tag{2.67}$$

For the purpose of this project LFM is however only used to determine range. Thus it is assumed that the narrow-band ambiguity function delivers satisfactory results.

2.6 Wave Forms

The selection of the signal wave form determines the ability of the SONAR system to resolve targets in range and velocity. The selection of the signal wave form thus depends upon the application of the SONAR. Besides maximum range, range and Doppler frequency resolution requirements, the environment the SONAR operates in must be considered when selecting a signal waveform. An environment with high reverberation requires a different signal selection from an environment with high noise.

The characteristic types of signal waveforms which are applicable for scanning the underwater environment may be classified into three main categories.

- Constant Wave Pulses (CW)
- Frequency Modulated Pulses (FM)
- Discrete Coded Waveforms

Each of the above, except the CW pulse, may be subdivided into numerous further subcategories. All three types of waveforms are investigated for their suitability to this project.

One type of pulse modulation which is omitted from this project's discussions is amplitude modulation. Amplitude modulation is generally becoming obsolete for nearly all signal processing applications. The dominant reason for this is that the theoretically optimal SNR, and therefore theoretical detection capabilities of a system, depends only on the noise power density and the total energy of the received signal. The bigger the SNR the better the probability of detecting targets. As the total signal energy depends on the pulse duration and its power efficiency, amplitude modulation is unfavourable, as it decreases the power efficiency.

2.6.1 Constant Wave

The oldest and simplest of waveform used in SONAR is a pulse of constant frequency f Hz and pulse length of T seconds. In some literature the CW pulse is also described as a constant frequency (CF) pulse. A CW pulse may be modelled by using the expression below:

$$v(t) = rect\left(\frac{t}{T}\right) cos(2\pi f_0), \tag{2.68}$$

where

- $\mathrm{rect}\left(\frac{\mathrm{t}}{\mathrm{T}}\right)$ defines the envelope of the pulse
- t is the total simulation time
- T is the pulse length
- f_0 is the centre frequency of the pulse

The effective bandwidth of a CW pulse is:

$$\frac{B}{Hz} = \frac{1}{T} \tag{2.69}$$

Due to the effective bandwidth of a CW pulse being the inverse pulse duration, the time-bandwidth product N of a CW pulse is unity.

$$N = BT \tag{2.70}$$

A time domain plot of a CW pulse is shown in Figure 2.20.

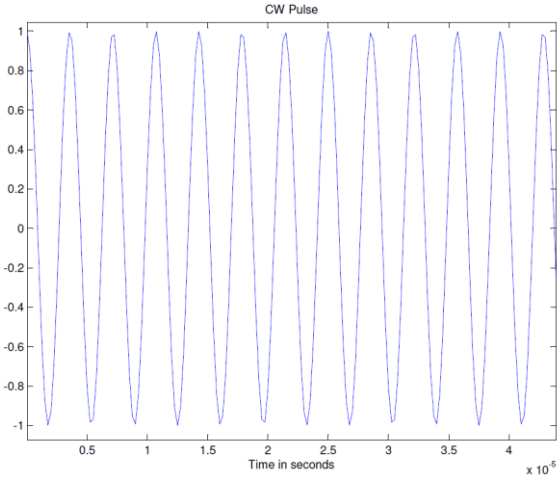

Figure 2.20- CW pulse in time domain

Range resolution of a CW pulse is given by Equation (2.7).

$$\frac{\Delta R}{m} = \frac{c}{2B} \tag{2.71}$$

For Doppler frequency resolution Bassam R. Mahafza, *Radar Signal Analysis and Processing using MATLAB,* states that the minimum resolvable Doppler frequency f_d is equal to the inverse of the total pulse duration T. Applying Equation (2.69) to Equation (2.8), the minimum resolvable Doppler frequency shift is expressed by:

$$\frac{\Delta v}{m/s} = \frac{Bc}{2f_0}, \tag{2.72}$$

where

B is the bandwidth of the pulse in Hz
f_0 is the centre frequency of the pulse

The dilemma CW is afflicted with is that a high range resolution is proportional to the bandwidth of the pulse. Thus the shorter a CW pulse the better it can resolve range. On the other hand, Doppler resolution is proportional to the pulse duration. The longer the pulse, the better a CW pulse can resolve Doppler frequency shifts.

The ability of a CW pulse to resolve range is, however, limited. As the pulse length is decreased, the transmitted power has to be increased in order to keep detection requirements. However, the maximum transmitted power cannot be increased indefinitely, as it is limited by cavitation. Ways around this problem would be the use of underwater explosives, which is impractical in most cases.

CW is therefore best used as a Doppler frequency resolving tool, where processing of CW may be thought of a noise limited process for all instances. A long CW pulse will produce a spectrum with a narrow peak and fast falling side lobes at zero Doppler frequency shift. Target Doppler frequency shifts will force target echoes to fall out of the reverberation spectrum, where reverberation power is low, making the target Doppler frequency shifts detection process a noise limited one. Figure 2.21 illustrates the above discussion in terms of the ambiguity function.

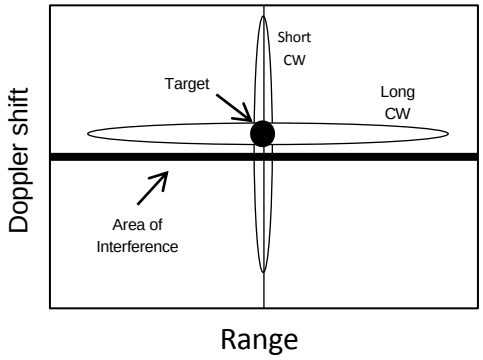

Figure 2.21 - Ambiguity function profiles for long CW and short CW and moving target

2.6.2 Frequency Modulation

The need for modulated pulses arose from the requirement of having high range resolution without compromising detection performance. It is thus desirable to increase the bandwidth B of a pulse without decreasing the corresponding duration of the pulse T, ultimately creating pulses that have a greater than unity time-bandwidth product.

The three most prominent modulation techniques found in literature are linear, sinusoidal and hyperbolic frequency modulation. Of these three techniques, linear frequency modulation is selected for investigated in this project. Besides being the most widely used modulation technique, the reason for choosing LFM is found in the readily available hardware. LFM may be

implemented by using low cost, off-the-shelf hardware, which may be used for a variety of pulse types discussed in this thesis.

Apart from increasing resolution, frequency modulation of the pulse also adds Doppler frequency tolerance to a signal when working with correlation filters. If Doppler frequency shifts are present on a received signal, and correlation filtering is utilized for range processing, CW required a bank of correlation filters, each tuned to a specific Doppler frequency, to solve for range. By contrast, frequency modulated pulses can generally do with only one filter, thus being referred to as Doppler tolerant. The obvious disadvantage to Doppler tolerance is that Doppler frequency shifts cannot be accurately determined, if at all.

Furthermore, modulated signals with substantial bandwidth have the ability to suppress interference, as energy is spread over a whole frequency band. Interference in this case is classified as general background noise combined with as reverberation.

For this project LFM is selected for investigation. The reason for choosing LFM above other modulation techniques is firstly, the availability of hardware for implementation, secondly, according to the conference proceedings of Victor Pjachev [21], LFM is found to provide the best reverberation suppression for low-Doppler frequency targets.

A LFM pulse may be modelled by the expression below:

$$x(t) = rect\left(\frac{t}{T}\right) cos(2\pi\left[f_0 t + \frac{1}{2}kt^2\right]), \qquad (2.73)$$

where

- $\mathrm{rect}\left(\frac{\mathrm{t}}{\mathrm{T}}\right)$ defines the envelope of the pulse
- t is the total simulation time
- T is the pulse length
- f_0 is the centre frequency of the pulse
- k is the linear frequency sweep rate

Figure 2.22 shows the frequency of a pulse being linearly swept up with time. The sweeprate k of the pulse with bandwidth B and duration T is defined by:

$$\frac{k}{Hz/second} = \frac{f_H - f_L}{T} = \frac{B}{T} \tag{2.74}$$

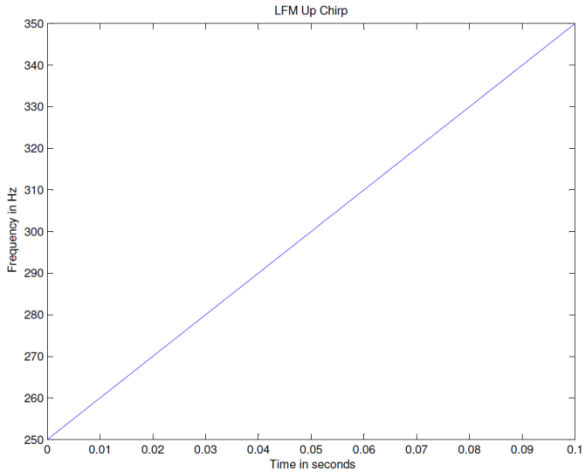

Figure 2.22 - LFM pulse frequency sweep

A time domain representation of a linear frequency modulated pulse is shown in Figure 2.23. For this instance, the frequency is swept from some lower frequency f_L to a higher frequency f_H over a certain period of time T, covering a frequency band B.

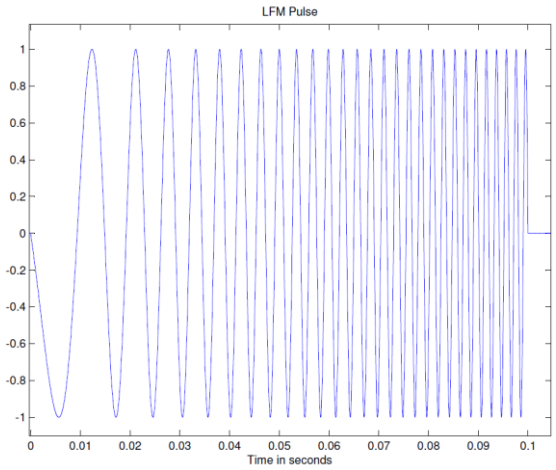

Figure 2.23 - LFM pulse in time domain

The frequency band covered during the linear frequency sweep is defined as the bandwidth B of the LFM pulse. Using correlation filters for range calculations, the bandwidth of a LFM pulse

is the frequency band the pulse is chirped in, contrary to the inverse of the pulse duration $\frac{1}{T}$, as is the case with CW. Applying Equation (2.7) for range resolution calculations, an improvement in range resolution may be observed, as compared to a CW pulse, without changing the pulse length T.

$$\frac{\Delta R}{m} = \frac{c}{2B} \tag{2.75}$$

Theoretically, the range resolution of a LFM pulse may therefore be increased indefinitely.

The phenomenon of improved range resolution is described as the compression ratio of a LFM pulse. Using a MF or IF to process a LFM pulse will compress the pulse from T seconds, to a length of $\delta T \approx \frac{1}{B}$. The time-bandwidth product, or compression ratio ξ is thus defined as:

$$\xi = BT \tag{2.76}$$

The compression ratio is an indication of how well range may be resolved, in comparison to an ordinary CW pulse. Using Equation (2.7), a CW pulse of length $T = 0.1$ seconds would result in a range resolution of 73 meters. Assuming a LFM signal of $T = 0.1$ seconds has a bandwidth $B = 100000$ Hz, the compression ratio of the signal using MF would be $\xi = 10000$. The system's range resolution would therefore be reduced by a factor of $1/10000$, as compared to the CW pulse.

Following the notes of A.J. Wilkinson, *Notes on Radar/Sonar Signal Processing: Fundamentals* [14], compressing a pulse by a factor ξ, also improves the SNR by the same factor ξ. Assuming a LFM signal of amplitude of A volts having added white noise of the form $S(f) = \frac{\eta}{2}$ V^2/Hz, band-limited to the bandwidth B, the SNR before the correlation filter is expressed as follows:

$$SNR_i = \frac{A^2}{(\eta/2)B} \tag{2.77}$$

After pulse compression the SNR is expressed by:

$$SNR_o = \frac{A^2 T}{(\eta/2)} \tag{2.78}$$

Finally, the SNR is shown to improve by:

$$\frac{SNR_0}{SNR_i} = BT = \xi \qquad (2.79)$$

The disadvantage of LFM is that it has a range-Doppler-coupling issue. A coupling between range and Doppler frequency occurs due to large Doppler frequency shifts in the signal received. The result is an error in range determination and a reduced target main lobe after filtering. Furthermore, smearing of the main lobe occurs after processing the received signal with a correlation filter, as the signals being correlated to not match perfectly anymore. Although the target main lobe is reduced, and the range is not perfectly accurate, a target can still be detected, thus making LFM a Doppler tolerant signal.

As with the de-ramping technique, the error in range may be compensated for by taking another measurement with a LFM pulse chirped in the opposite direction. Utilizing the average of the two range measurements will deliver an accurate range measurement. For the purpose of this project the range Doppler ambiguity problem is noted, but no provision is made for accurately solving the ambiguity.

Performing Doppler frequency resolution calculations on a LFM pulse is superfluous as the signal is, by definition, Doppler tolerant. The LFM pulse is therefore best suited to determine only the range of targets.

The ambiguity function and its contour plot for a LFM pulse with a sweep rate of $k = 0.5$, are plotted in Figure 2.24 and Figure 2.25, respectively. The property of the ambiguity shearing the ellipsoid for a LFM pulse is evident. The reader should also examine the ambiguity between Doppler and range resolution.
Increasing the sweep rate k of the pulse, thereby increasing the bandwidth B, and/or decreasing the total pulse length T, will shear the ambiguity function even further. Examining Figure 2.26 and Figure 2.27, the respective ambiguity function and contour plot of a LFM pulse with sweep rate $k = 3$, indicates an increase in range resolution. Doppler resolution is simultaneously decreasing. Further increasing k will ultimately result in the LFM ambiguity ridge running nearly along the delay axis of the ambiguity function, thus indicating a high range resolution and Doppler tolerance.

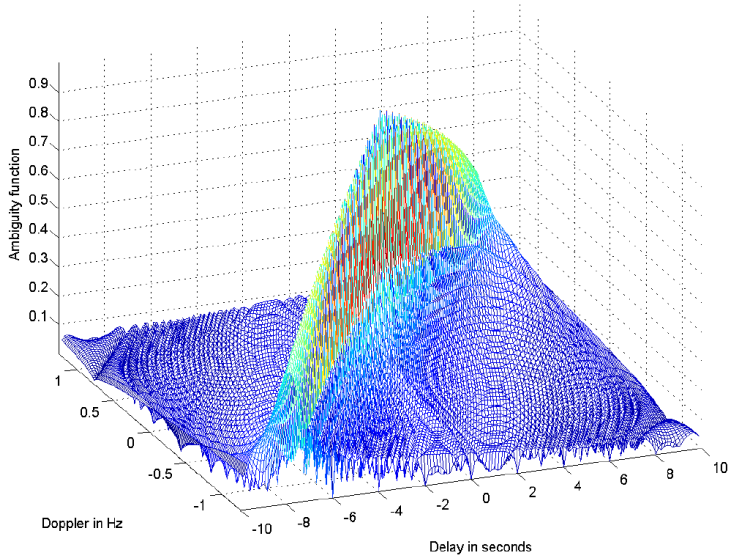

Figure 2.24 - LFM Ambiguity Function, k = 0.5

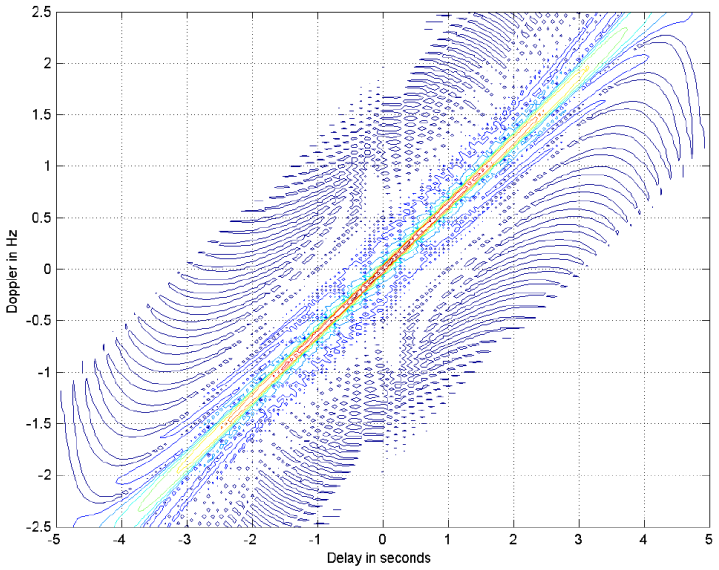

Figure 2.25 - LFM Ambiguity Contour Plot, k = 0.5

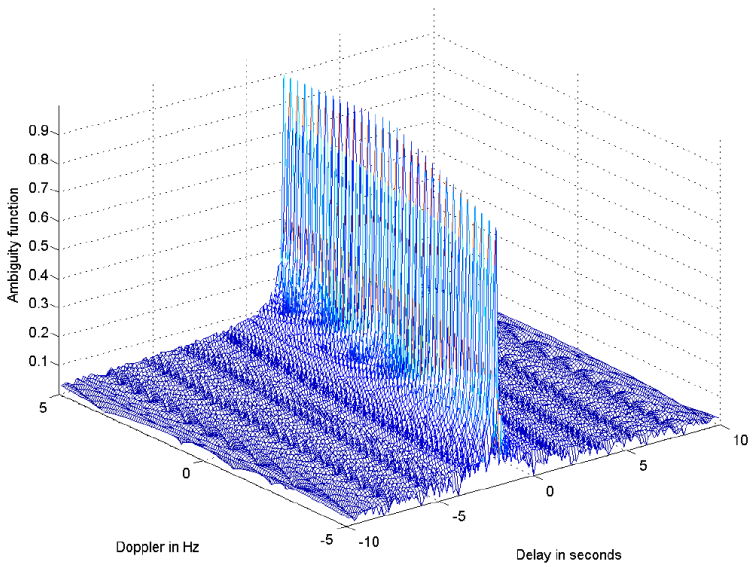

Figure 2.26 -LFM Ambiguity Function, k = 3

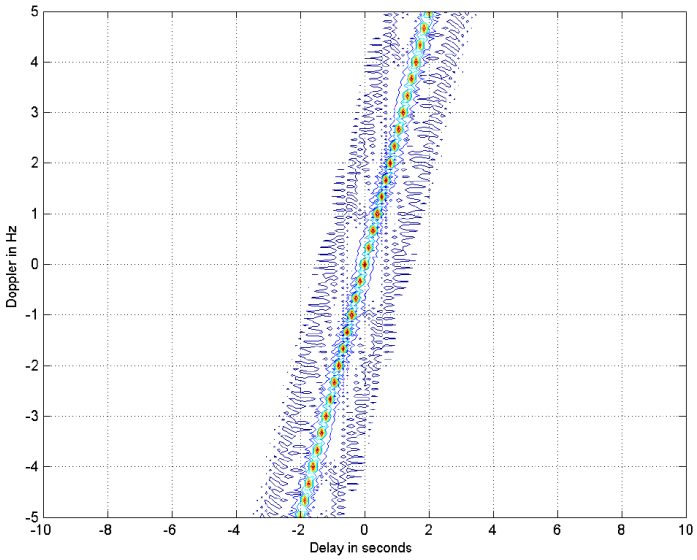

Figure 2.27 - LFM Ambiguity Contour Plot, k = 3

2.6.3 Discrete

The waveforms discussed in the previous two sections are generally referred to as being analogue signals. With advanced digital technology, discrete coded waveforms have evolved in both SONAR and RADAR applications. A discrete coded waveform commonly consists of a series of narrow-band pulses added together to form one pulse. Processing of discrete pulses is achieved as with analogue signals, by using a MF. As with LFM, discrete coded pulses exhibit pulse compression capabilities, when processed by a MF. What makes discrete coded waveforms potentially superior to analogue waveforms is their ability of resolving both range and Doppler. It should, however, be noted that discrete coded waveforms are more effective in improving on range, than Doppler characteristics according to B.R. Mahafza, *Radar Signal Analysis and Processing using Matlab* [6]. Discrete coded waveforms will thus be specifically evaluated for their ability to resolve targets with respect to range.

One of the major advantages of high end discrete coded waveforms, and the reason why they have become increasingly popular, is their feature of being difficult to detect. Furthermore, they have inherent anti-jamming capability, which makes them especially interesting for military applications. However, no anti-jamming capability is required for this project.

Discrete signals may be divided into three groups:

- Un-modulated pulse train codes
- Phase modulated codes
- Frequency modulated codes

The un-modulated pulse train divides a longer pulse into N sub-pulses. Each pulse will be rectangular and will have an amplitude of one or zero. Arranging the one and zero pulses in a certain way allows narrowing of the spike at the origin of the ambiguity function, and lower side lobes to a certain extent. Being the simplest form of discrete coding, un-modulated pulse codes are understood to deliver the worst results regarding range and Doppler resolution.

Phase modulated codes may again be subdivided into binary-coded and poly-phase coded pulse trains. Binary coding allows for the phase of a sub-pulse to be chosen either as zero or π. As before, the aim is to divide a long pulse of length T into N smaller sub-pulses. Each sub-

pulse will then have a width of $t_b = \frac{T}{N}$. By arranging the sub-pulses in a certain manner, the side lobes of the ambiguity function will be reduced, and the main peak will resemble that of the un-modulated pulse train codes. One way of arranging the sub-pulses is dictated by Barker codes. Barker codes present a unique way of arranging the sub-pulses, in order to reduce the side lobes of the ambiguity function, and sharpen the main lobe.

The number of Barker codes is limited to seven, with the longest code B_{13} having thirteen code elements. The B_{13} Barker code also exhibits the largest side lobe reduction of -22.3 dB. The width of the autocorrelation function of a Barker code is $2t_b$ and has a peak of size N, being the number of elements in the code, while the side-lobes are of unity size. The B_{13} code and its auto correlation function are shown below. Note that the main lobe has a size of thirteen, while the side lobes are unity.

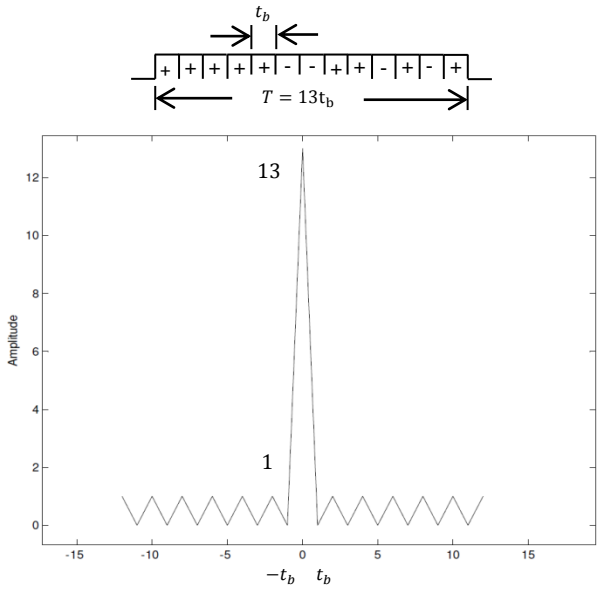

Figure 2.28 - Barker code of length 13 with auto-correlation function

For most cases a side-lobe reduction of -22.3 dB of the auto-correlation is insufficient. The peak of the main lobe is also not narrow enough for accurate range measurements after MF. To increase resolution capabilities, the Barker codes must be increased in length. To lengthen a Barker code, codes may be combined, for example, the B_5 code may be inserted into the B_4 code, to form a B_{54} code. In his book, *Radar Signal Analysis and Processing using Matlab* [6], B.R. Mahahafza indicates that the compression ratio ξ of such a code equals:

$$\xi = MN, \qquad (2.80)$$

where M represents the length of the code inserted into the code of length N. The maximum achievable compression ratio is only $\xi = 143$, which is obtained by utilizing the B_{13} and B_{11} codes. A problem arising from the extended codes is that the side-lobes are no longer uniform. The ambiguity function of a B_{54} barker code is shown below, with side lobes reaching 40% of the main lobe. Furthermore, although Barker codes can resolve Doppler frequency, the modulation is sensitive to Doppler frequencies larger that $1/T$.

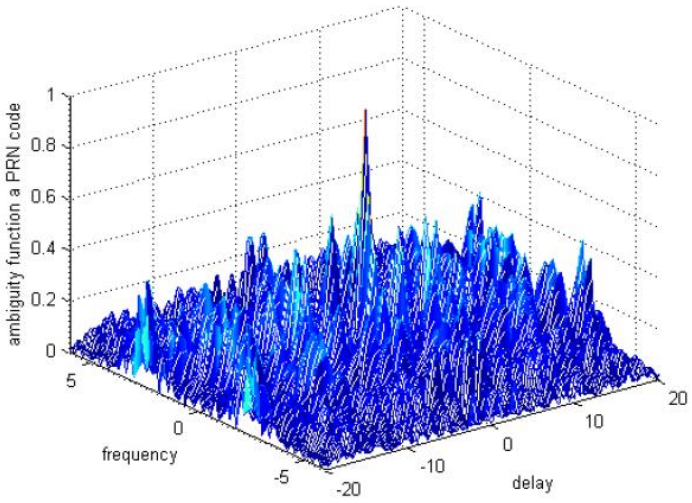

Figure 2.29 - Ambiguity Function for B_{54} Barker Code [6, p. 240]

Much longer binary codes may be generated by using pseudo-random number (PRN) codes, which exhibit superb side-lobe suppression characteristics, depending on the code length implemented. An ambiguity function for a 31-bit PRN coded waveform is shown in Figure 2.30. The compression ratio ξ of such pulses is dependent upon the number of elements in the pulse. The problem with PRN codes thus arises with their processing. Very long pulses are required to achieve a large compression ratio. Although algorithms exist, as described in the article, *Efficient Computer Decoding of Pseudorandom Radar Signal Codes* [22] *,* by E. Mayo, which considerably reduces the processing requirements to decode PRN codes, the processing requirements are still substantial for very long pulses.

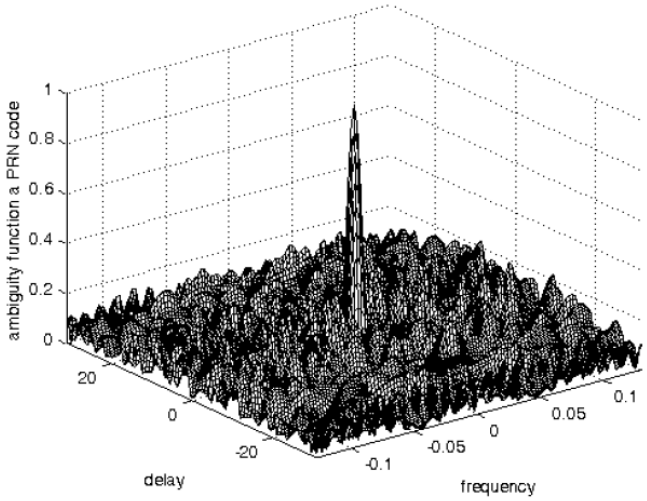

Figure 2.30 - Ambiguity function of a 31-bit PRN code [6, p. 246]

Poly-phase codes allow the phase of a pulse to be complex, rather than restricting the phase to zero and π. Besides Barker codes, Frank codes make use of poly-phase coding. Frank codes sweep the phase in a linear manner. The compression ratio of Frank codes is described by B.R. Mahahafza as being:

$$\xi = N^2, \qquad (2.81)$$

where N is the number of sub-pulses. The ambiguity function of a 16-bit Frank coded waveform is plotted in Figure 2.31. It should therefore be noted that the ambiguity function of a Frank code resembles the ambiguity function of a LFM pulse. Judging from the ambiguity function, resolving both Doppler frequency and range will be as problematic, as it is with LFM.

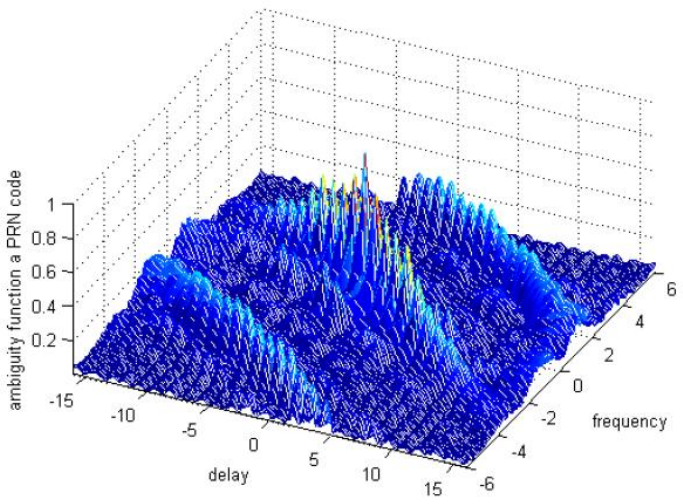

Figure 2.31 - Ambiguity function of 16-bit Frank code [6, p. 250]

The final type of discrete modulation discussed is frequency code modulation, which is of great interest in on-going research. As before, a relatively long pulse is sub-divided into N smaller pulses of length $t_b = \frac{T}{N}$, where the sub-pulses are referred to as bursts. Each burst is spaced Δf apart from the other. A specific technique of selecting the frequency of the bursts in a random manner was introduced by Costas[2]. Costas codes, like Barker codes, are readily available. The generation of Costas codes represents a theory of its own, and is not discussed in this text. An example of a 8 level Costas code is shown in Figure 2.32.

[2] J.P. Costas, *A Study of Class of Detection Waveforms Having Nearly Ideal Range-Doppler Ambiguity Properties* [35]

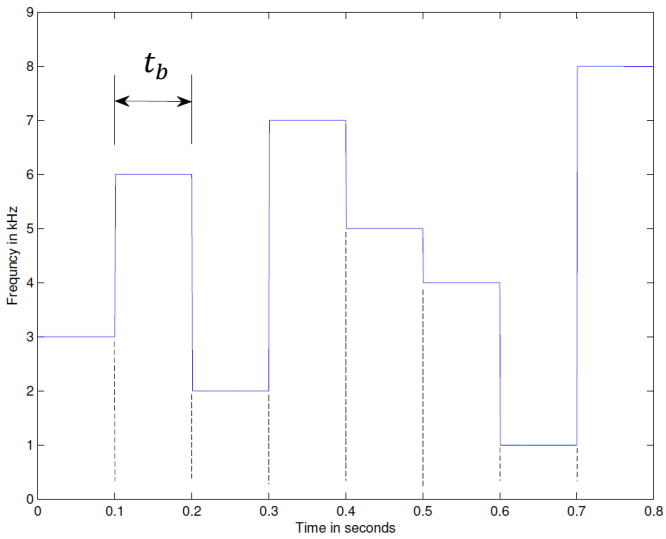

Figure 2.32 - Costas Frequency Coding

According to the article, *Improving Ambiguity Function of Costas Signal* [23], by K. Hassan Aboulnour, the pulse compression ratio of a Costas-coded signal is defined as:

$$\xi = N^2, \tag{2.82}$$

Furthermore, a Costas signal requires the frequency spacing to be related to the length of each bit by:

$$\Delta f = \frac{1}{t_b} \tag{2.83}$$

Costas-coded signals are becoming increasingly popular. Besides resolving both Doppler frequency and range, Costas-coded signals have reverberation suppression characteristics similar to LFM, according to the article, *Improved Active Sonar Performance using Costas Waveform* [24], by S.P. Pecknold. The article reveals promising practical data on using Costas waveform in both deep- and shallow-water applications.

Furthermore, Costas-coding allows for a water mass to be scanned at a higher rate than common LFM SONARs, because the MF is able to identify individual Costas waveforms from among received waveforms. The ambiguity function of a 22-bit coded Costas waveform is shown in Figure 2.33. A narrow peak may be observed, which can resolve both range and Doppler. Additionally, the function features very low side-lobes.

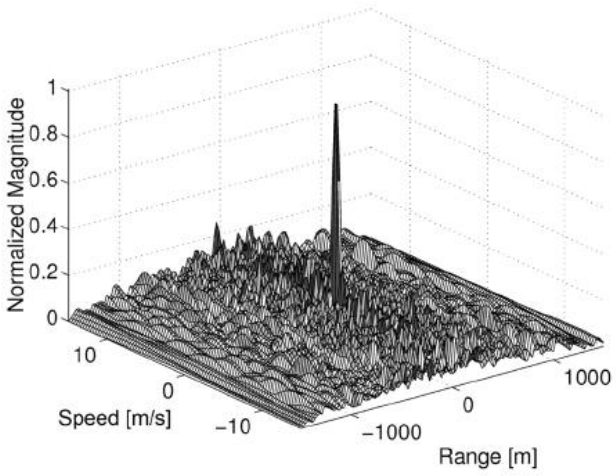

Figure 2.33 - Costas 22-code ambiguity function [24]

Methods to improve on Costas signals are discussed in various articles. K. Hassan Aboulnour, *Improving Ambiguity Function of Costas Signal* [23], proposes increasing the product of $t_b \Delta f$ dictated by Equation (2.83), beyond unity. Side lobes may be significantly reduced by selecting a specific relationship between the burst length t_b and the frequency step Δf. N. Levanon, *Modified Costas Signal* [25], proposes adding time lag between bursts, in order to reduce side lobes as well. Furthermore, Levanon proposes the addition of separate LFM to each burst, thus narrowing the main lobe of the ambiguity function and reducing side lobes. By alternating between ramping a burst up and down, further improvements in side-lobe reduction may be observed.

In general it may be concluded that discrete coded waveforms are superior to analogue waveforms, in the sense that discrete coded waveforms can resolve both range and Doppler frequency. The problem for this project, however, is the required range resolution of $\Delta R = 1 \text{ cm}$ or better. Discrete coded waveforms require extremely long codes to achieve the compression ratio exhibited by LFM. The disadvantage of generating and receiving discrete long codes is a drastic increase in hardware, due to the large processing requirements. For a LFM pulse to obtain a range resolution of 1 cm, a compression ratio of $\xi = 10000$ is required, which is discussed in more detail in Chapter 3. For Costas-coded waveforms, where the compression ratio increases exponentially with the code length, a code of bits 100 would be required to obtain a compression ratio similar to LFM. Referring to Section 4.6.1 the DDS used

to generate the signals for this project can only achieve a 16 bit frequency modulation, which equals a compression ratio of $\xi = 256$, compared to a LFM pulse exhibiting a compression ratio of $\xi = 10000$. Keeping the pulse length at $T = 0.1$ s, an 16 bit Costas coded waveform could thus only achieve a range resolution of $\Delta R = 28.5$ cm, according to the pulse compression theory.

Discrete coded waveforms are best suited for the detection of targets at longer ranges, where range resolution is less of an issue. Discrete coded waveforms are therefore not investigated further for this project.

Chapter 3

PULSE DESIGN AND PERFORMANCE PREDICTIONS

This chapter's discussion entails the selection and design of signal waveforms according to the requirements of Section 1.2. Furthermore, the signal waveforms are tested and simulated for their ability to detect targets, as well as resolving targets in range and Doppler frequency.

3.1 Pulse Design Requirements

Following the discussion on signal waveforms in Section 2.6, the pulses selected to resolve Doppler frequency shift and range are CW and LFM, respectively. The requirements for range and Doppler frequency resolution are recapped below:

- Maximum range of 50 m
- High accuracy in range resolution ΔR, ideally to the nearest 1 cm
- Maximum detectable target velocity of $3\ \mathrm{m/s}$
- Accuracy in velocity resolution Δv no worse than $0.1\ \mathrm{m/s}$
- Reverberation resistant

3.1.1 CW Pulse Design Considerations

The challenge for the CW pulse design is to achieve the velocity resolution Δv as required, which is inherently coupled to the length of the pulse. The relatively low maximum detectable speed is not a concern for design. To determine the minimum pulse length Equation (2.8) is rearranged as follows:

$$\frac{1}{\Delta f_d} = T = \frac{c}{2\Delta v f_0}, \tag{3.1}$$

where

- Δf_d is the Doppler frequency shift due to the velocity of the target
- $\Delta v = 0.1\ \mathrm{m/s}$ is the velocity resolution
- $f_0 = 280\ \mathrm{kHz}$ is the center frequency of the CW pulse
- $c = 1476\ \mathrm{m/s}$ is the speed of sound in water

The centre frequency f_0 of the pulse is selected to be in the centre of the pass band of the band pass filter discussed in Chapter 4.
Applying Equation (3.1) leads to the minimum CW pulse length of:

$$T = 26 \text{ ms}$$

To ensure that the velocity resolution requirement is met with noise added to the signal, and using non-ideal hardware, the CW pulse length for practical implementation is selected as being:

$$T_{CW} = 100\ ms \tag{3.2}$$

Therefore, the resulting theoretical radial target velocity resolution according to Equation (3.1) is:

$$\Delta v_{CW} = 0.026\ ms \tag{3.3}$$

The velocity resolution is thus overdesigned by a factor of 3.8, which is obtained by dividing the required velocity resolution specification by the designed velocity resolution.

The ambiguity function of a CW pulse with the specifications as described in this section is shown in Figure 2.17. The plots along the zero Doppler frequency and zero range axes are shown in Figure 2.19. Examining the plot cut along the zero delay axes shows that a Doppler frequency shift of 10 Hz is resolvable, which equals a target velocity of 0.026 ms.

3.1.2 LFM Pulse Design Considerations

Selected a LFM pulse fulfils the design requirements for a reverberation-resistant pulse. The design of the LFM pulse of this section focuses on range resolution requirements, rather than the maximum detectable range. Implementing a MF, the maximum detectable range theoretically depends only on the energy of the pulse, not on the type of pulse, as shown in Section 2.4.1. The energy of a LFM pulse depends on the pulse length, as well as the instantaneous power output level of the final amplification stage. Fixing the pulse length of the LFM pulse to the CW pulse length with $T_{LFM} = 100$ ms, results in the design for maximum detectable range being only limited by the of transmitted signal power. The discussion takes place in the next section, and extends to Chapter 4, where signal amplification requirements are investigated.

The range resolution ΔR of a LFM pulse is described by Equation (2.7), where the bandwidth B is the frequency band across which the pulse is chirped. Rearranging Equation (2.7) to determine the required bandwidth, by using the speed of sound as for the CW calculations:

$$B = \frac{c}{2\Delta R}, \tag{3.4}$$

results in

$$B = 73.8\ kHz$$

To compensate for added signal noise, non-ideal hardware and processing in practice, the bandwidth is overdesigned as being:

$$B = 100\ kHz \tag{3.5}$$

The resulting theoretical range resolution according to Equation (3.4) is now:

$$\Delta R = 0.73\ cm \tag{3.6}$$

Compared to the velocity resolution, which is overdesigned by a factor of 3.8, the range resolution is overdesigned by a factor of 1.4. This factor is obtained as it was done with the velocity resolution, by dividing the designed resolution by the specified resolution.

The ambiguity function plot of the LFM pulse design is shown in Figure 3.1. Due to the high compression ratio, the main ridge is skewed to such an extent that it runs nearly parallel to the zero delay axis. The Doppler resolution of the function is, however, overstated as the designed pulse does not satisfy the requirements for the narrow-band signal, as specified by Equation (2.65). This is of no concern though, as the LFM pulse is intended to be applied for range measurement only.

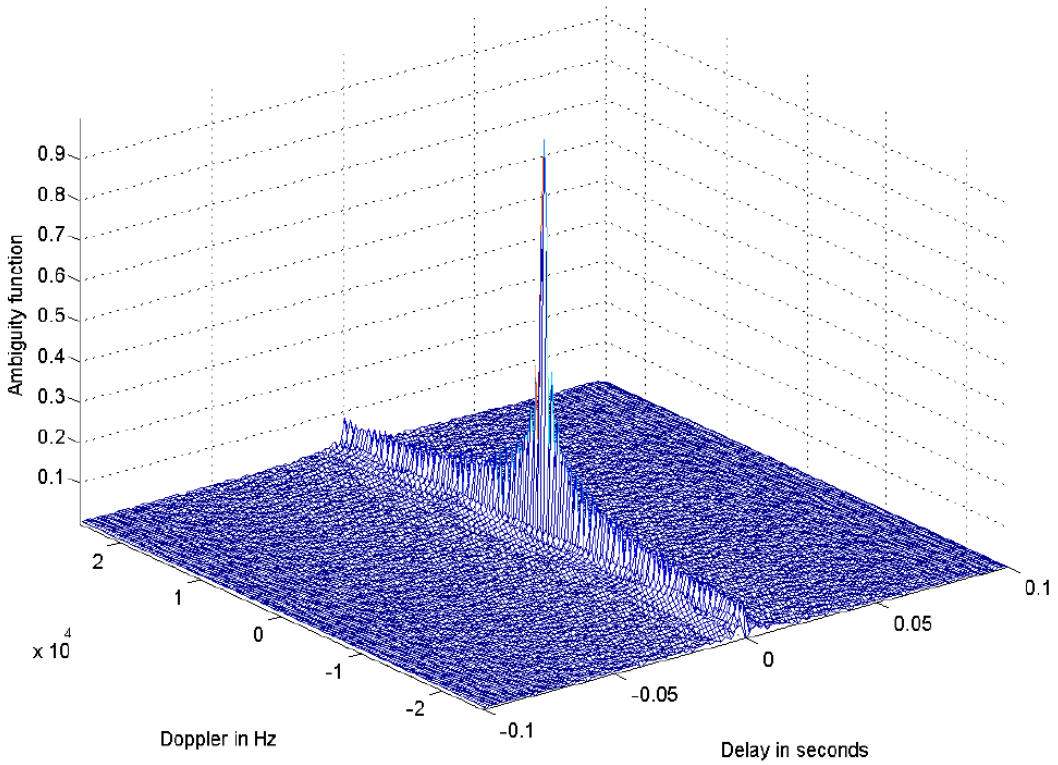

Figure 3.1 – LFM Ambiguity Function Plot

Figure 3.2 shows the ambiguity function by using a cut along the zero Doppler frequency axis, which provides an indication of the range resolution capabilities of the designed LFM pulse. The plot confirms the range resolution calculated in Equation (3.6). The reader should note the different time scaling of Figure 3.1 compared to Figure 3.2, as well as the dB amplitude scaling of Figure 3.2 compared to Figure 3.1.

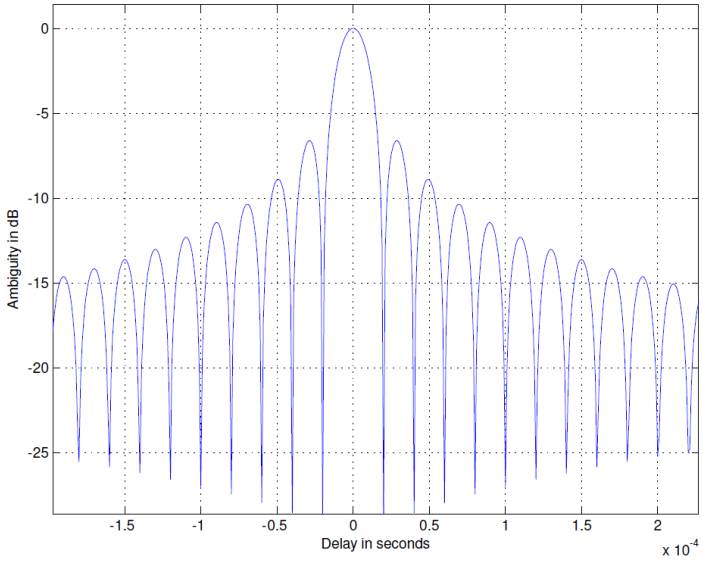

Figure 3.2 – LFM Zero Doppler Frequency Ambiguity Plot

3.2 Power Calculations

Ultimately, the SONAR equation indicates whether a system design can detect a target, thus verifying whether a pulse design meets the given range, noise and reverberation requirements. In this case the SONAR equation is used to determine the required transmit power, in order to detect a specified target at the maximum required range. According to the calculated required transmit power the signal amplification is designed in Chapter 4.

3.2.1 CW

To determine the minimum power requirements for a CW pulse resolving a target at 50 m, the Sonar equation can be rewritten into the form shown below, where the equation is solved for the transmitted power.

$$10logP = DT - 170.7dB - DI_t + 2PL - TS + (NL - DI_r) \qquad (3.7)$$

$$10\text{logP} = 20.97 - 170.7 - 29.4dB + 2(68) - 46 + (34 - 29.4)$$

Using CW to resolve Doppler frequency shifts, the SONAR equation becomes noise limited only as described in Section 2.6.1. Solving the above equation for the case of a CW pulse by applying the relevant equations from Section 2 with:

- Target sphere diameter $r_s = 1$ cm
- Range $= 50$ m
- $d = 25$,

where d forms part of the detection threshold DT of Equation (2.36).

Delivers a result of:

$$P_{acoustic} = 7.1 \text{ W}$$

The minimum acoustical power required to resolve a target in Doppler at 50 m using a CW is $7.1\,W$. To take into account the efficiency loss of the transducers, the minimum applied electrical power is estimated to be 55% higher than the actual acoustical power.

$$P_{electrical} = 11 \text{ W}$$

3.2.2 LFM

In case of a LFM pulse the SONAR equation is expressed as shown in Equation (3.8). It should be noted that the only difference to the case of CW is that the LFM detection is a reverberation limited process, and the DT is adjusted by a factor of $10logB$.

$$10logP = DT - 170.7dB - DI_t + 2TL - TS + (RL - DI_r) \qquad (3.8)$$

As the LFM pulse has the same length as the CW pulse, detection is guaranteed.

3.3 Simulations

Both CW and LFM pulse designs are simulated by applying Matlab to verify the capacity of the designed pulses to resolve range and Doppler frequency. Furthermore, MF and IF as well as de-ramping processing techniques are simulated. The user may choose between CW, LFM and 10-bit Costas coded waveforms for simulation purposes. However, Costas coded waveforms have been found to be not suitable for the purpose of this project, as described in Section 3.6.3, and will thus not be discussed further. The Matlab simulation accepts the following input parameters:

- Centre frequency of pulse f_0
- Bandwidth of the pulse B (not applicable for CW)
- Pulse length T
- Any number of targets at any range
- The radius of the target sphere(s) ($1\ \mathrm{cm}$)
- The velocity of each target
- Standard deviation of white Gaussian receiver input noise (20% of received signal by default)
- Standard deviation of white Gaussian transmitter signal noise (0.5% of received signal by default)
- Amplifier output voltage ($24\ \mathrm{V}$)
- Combined transducer gains (5)
- Water temperature ($20\ ℃$)
- Salinity ($0.005\ \mathrm{ppm}$)
- Operating depth ($2\ \mathrm{m}$)
- Sampling rate of ADC ($1\ \mathrm{MHz}$)
- Windowing function (Hanning)

The specifications in brackets indicate settings used for simulation results stated in the following sub-sections.

3.3.1 CW

The Matlab simulations concerning the designed CW pulse are shown in Figure 3.3 and Figure 3.4. The various gains of the SONAR equation, as set out in the previous section, are taken into account for the simulation. The first figure shows the simulation result for two spherical targets at a range of $50\ \mathrm{m}$ with velocities of $0.1\ \mathrm{m/s}$ and $3\ \mathrm{m/s}$, respectively. The simulation shows that the designed CW pulse is able to resolve Doppler frequency shifts at the maximum range, as required. The second figure shows two targets at ranges of $5\ \mathrm{m}$ and $8\ \mathrm{m}$, respectively, with velocities of $0.1\ \mathrm{m/s}$ and $0.2\ \mathrm{m/s}$, respectively. Both target velocities are easily resolvable.

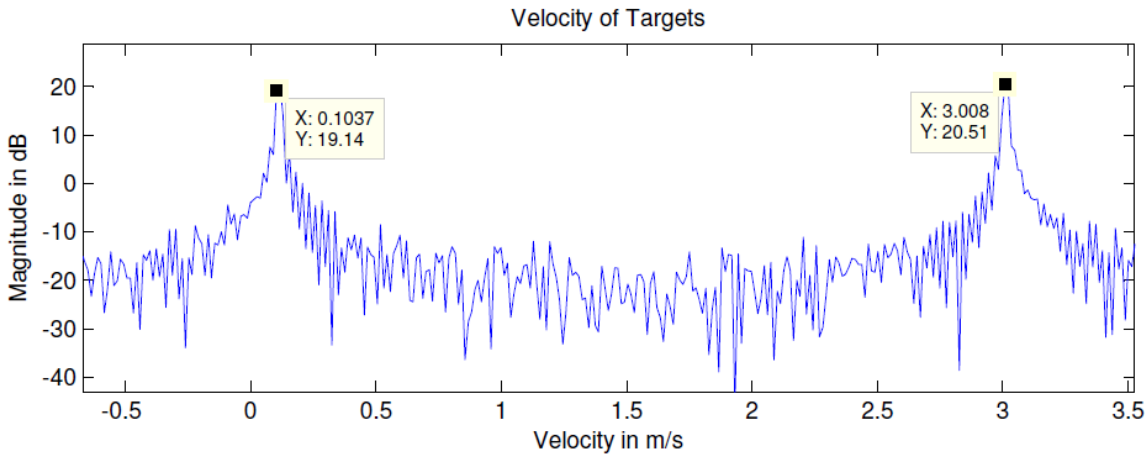

Figure 3.3 – Target velocity of two targets at 50 m range

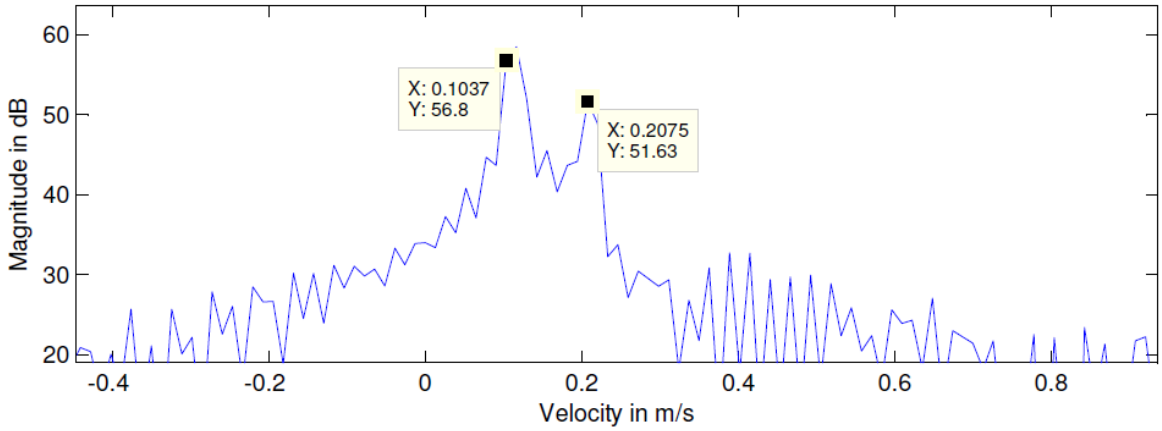

Figure 3.4 – Two targets at different range and velocity

3.3.2 LFM

The simulations for evaluating the LFM pulse design are accomplished by applying the settings as for the CW evaluation. Figure 3.5 and Figure 3.6 indicate the simulation results for three targets at ranges of $9\,\mathrm{m}, 26\,\mathrm{m}$ and $50\,\mathrm{m}$, using IF and MF processing, respectively. The amplitude for all the targets is indicated in $\mathrm{dB\ re\ 1\mu Pa}$, as well as giving an indication for the average noise figure. The simulation proves the theoretical ability of the LFM pulse to detect multiple targets up to a range of $50\,\mathrm{m}$. There is no difference in performance to be deduced from the figures, between the MF and IF .

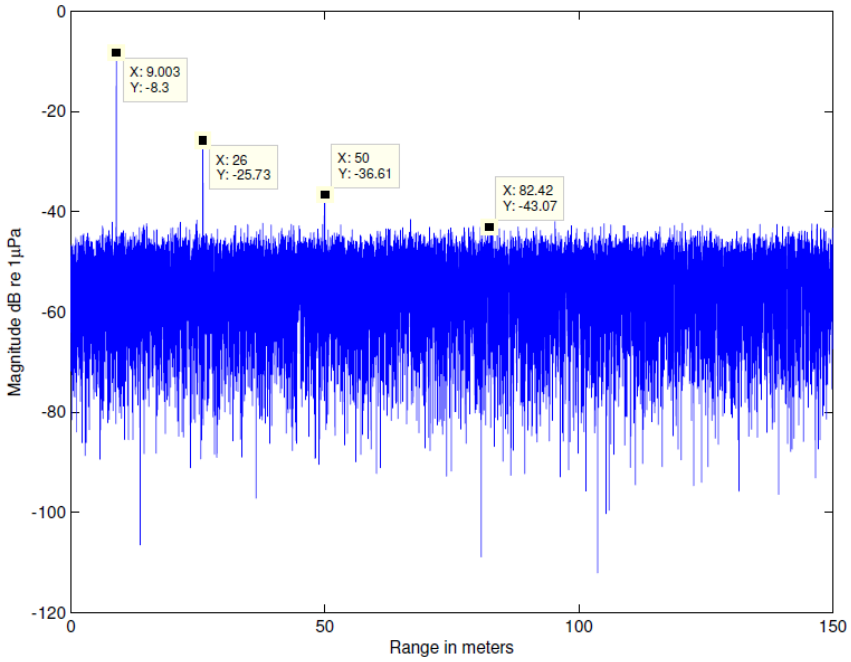

Figure 3.5 – IF range response to three targets

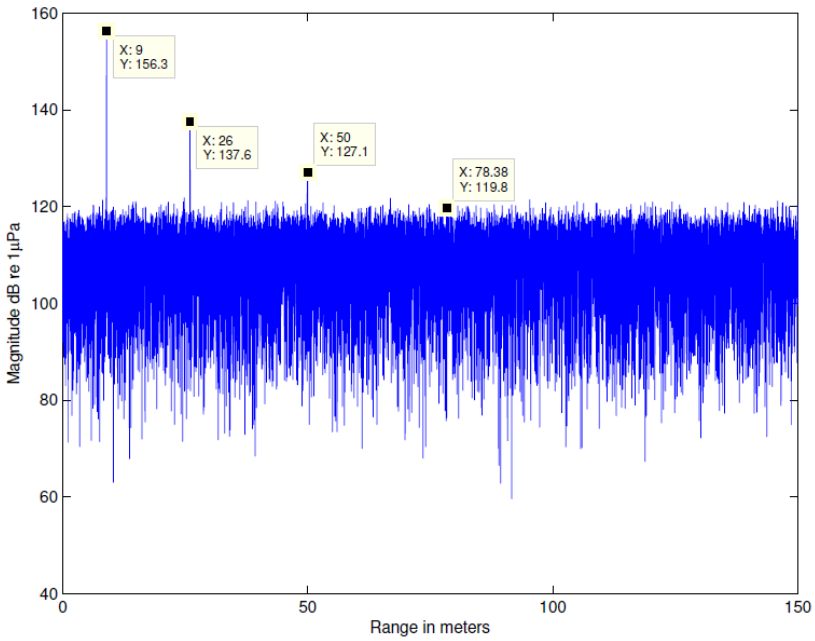

Figure 3.6 - MF range response to three targets

Figure 3.7 indicates the simulation result when applying the de-ramping technique for processing the range of two targets. Although, according to Equation *(2.57)*, the technique should yield the same range resolution as by using MF or IF, however the simulation proves differently. The width of the main lobe of the targets in *Figure 3.7* indicates that a range resolution of 1 cm is not possible, as they are too broad, which will become more clear when comparing the main lobe of targets using MF or IF.

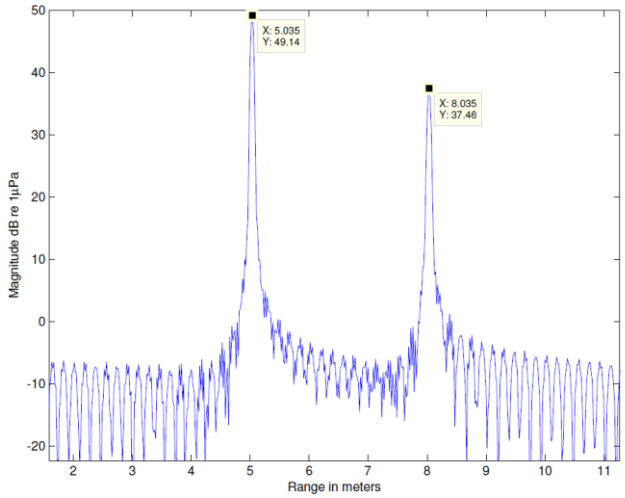

Figure 3.7 – Simulation output using de-ramping technique of targets at 5m and 8m range

In comparison to Figure 3.7, the simulation outputs for two targets at the same ranges as for the de-ramping technique, and using a MF (left hand side) and an IF (right hand side), are shown in Figure 3.8. The target's main lobes in respect of both filters are much narrower than is the case for the de-ramping technique.

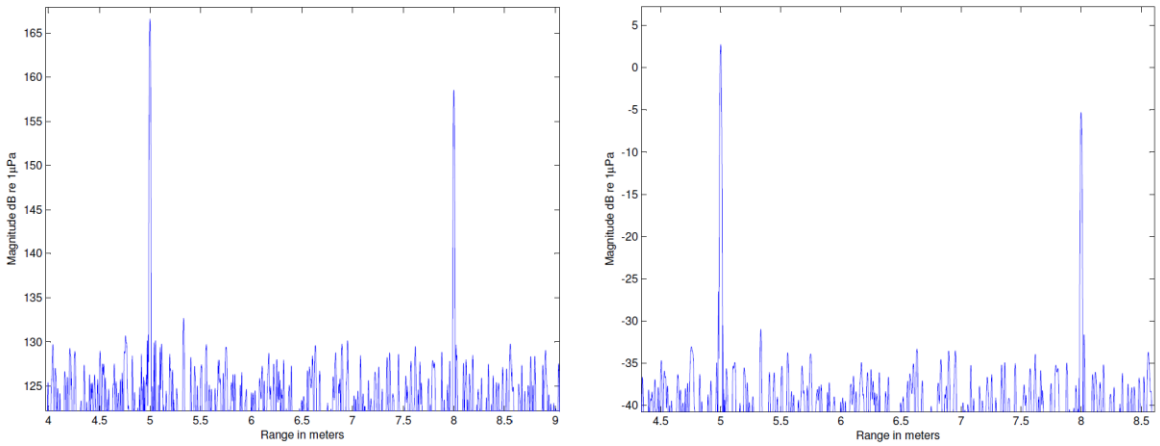

Figure 3.8 – MF and IF simulation outputs of two targets at 5m and 8m range

"Zooming in" on the main lobe of the target at $5\ \mathrm{m}$ for both MF and IF outputs, in Figure 3.9, indicates that the width of both main lobes is $10\ \mathrm{mm}$ at $3\ \mathrm{dB}$ below the peak. Spacing the two lobes at a distance of $1\mathrm{cm}$ apart will lead to the lobes combining and appearing as one. A range resolution of $1\ \mathrm{cm}$ will thus not be achievable. However, when changing the window function of the IF filter to a Kaiser window, the width of the lobe improves to $7\ \mathrm{mm}$, as shown in Figure 3.10. A definite advantage of the IF in resolving targets, as described in literature, cannot be confirmed in simulation. Further simulations and experiments are conducted, using only a Kaiser window for the IF, unless stated otherwise. The window function for the MF as a Hanning window remains unchanged, as no improvement could be observed when applying a different window.

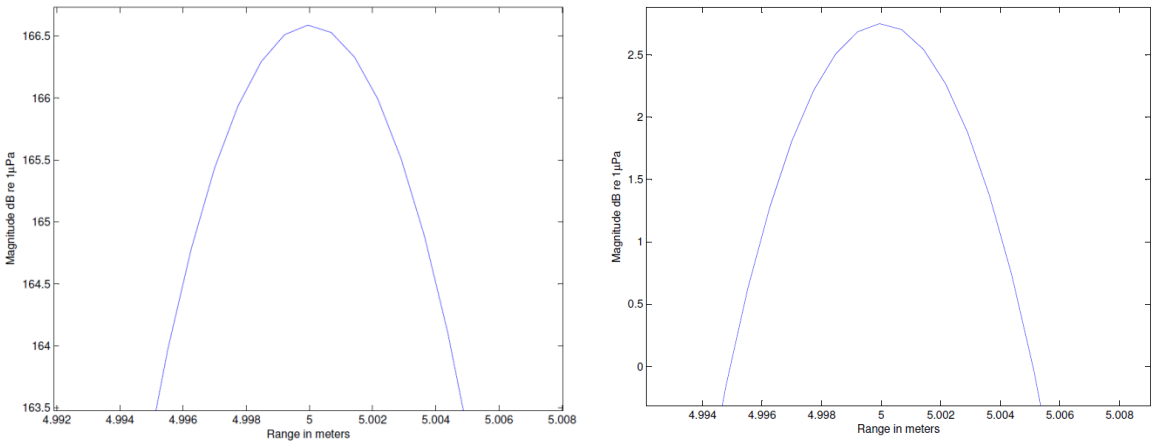

Figure 3.9 – Width of main lobe for MF and IF at 3dB below peak

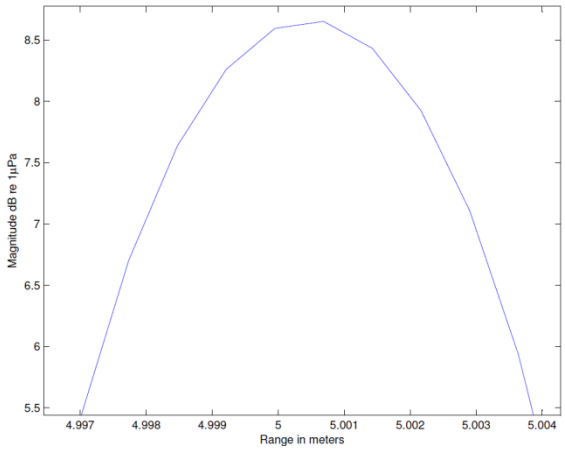

Figure 3.10 – Width of main lobe IF at -3dB from peak when using Kaiser window

The following six plots show the outputs of the MF and IF, respectively, for targets spaced at $1\ cm, 1.5\ cm$ and $2\ cm$ from each other. Examining the relevant plots, reveals that the designed LFM pulse is not capable of resolving $1\ cm$. However, it can resolve targets spaced at $1.5\ cm$ from each other. No superiority regarding the range resolution of the IF can be deduced from the simulations. Inspecting *Figure 3.12* and *Figure 3.13* demonstrates that the MF performs just as good as the IF.

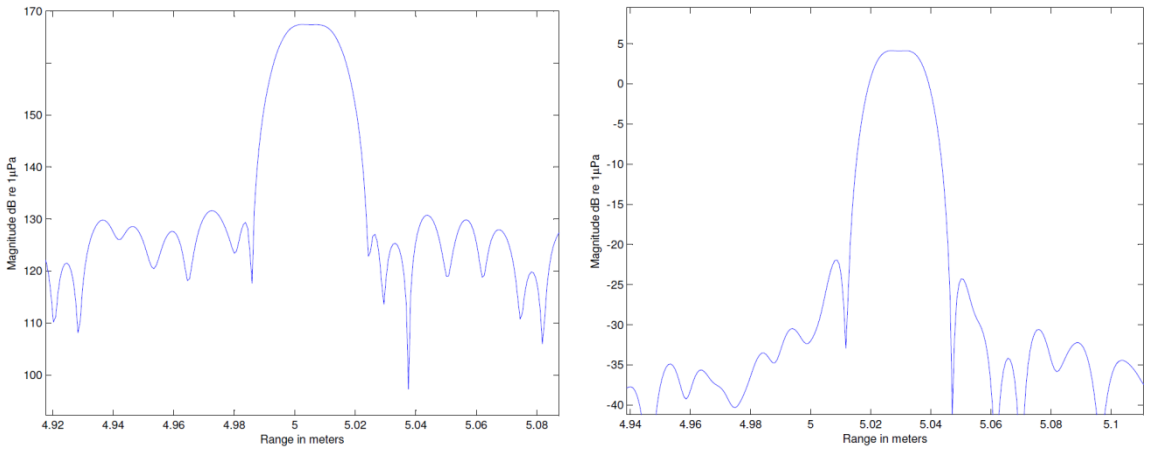

Figure 3.11 - MF and IF outputs for two targets spaced 1 cm apart

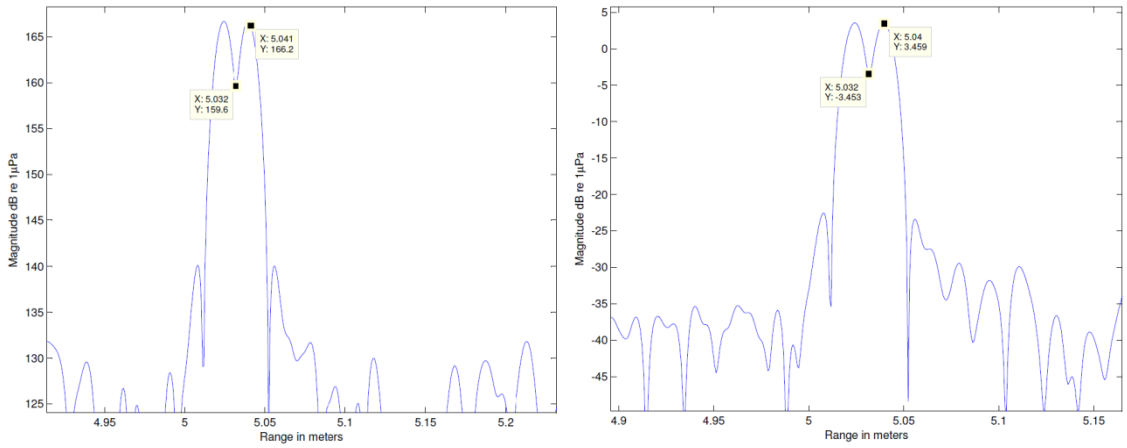

Figure 3.12 - MF and IF outputs for two targets spaced 1.5 cm apart

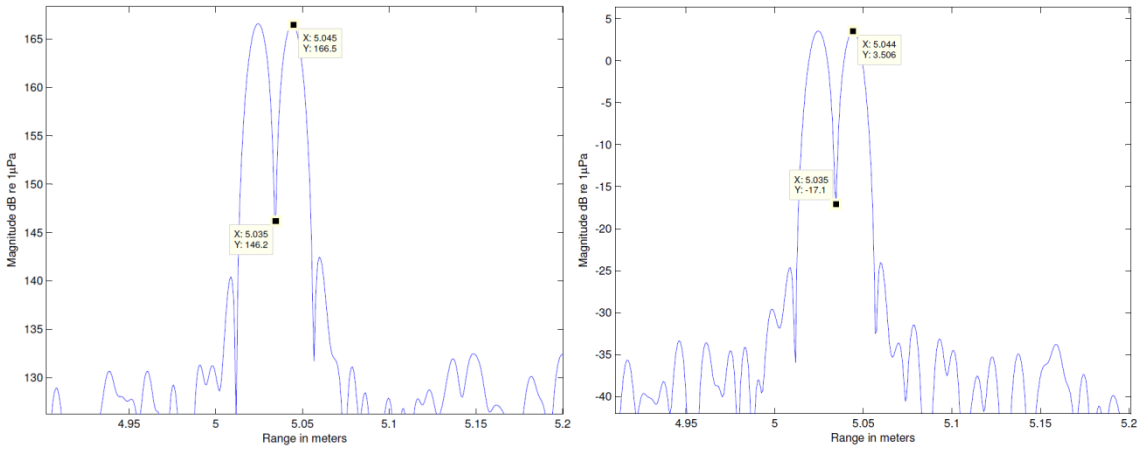

Figure 3.13 - MF and IF outputs for two targets spaced 2 cm apart

The range-Doppler coupling issue of LFM is shown in Figure 3.14, both for MF and IF. Two targets are simulated. One target is stationary at a 5 m range. The second target has a range of 8 m to the SONAR platform and approaches the SONAR platform at a radial incoming velocity of 3 m/s. As discussed in Section 2.6.2, there is an error occurs in range calculation because of the added Doppler frequency shift of the signal returning from the moving target. According to the simulation, the error in range for a target moving at 3 m/s is 0.8 m. As anticipated, too, a smearing of the main lobe may be observed, as well as a reduction in amplitude of the main lobe, as compared to Figure 3.8.

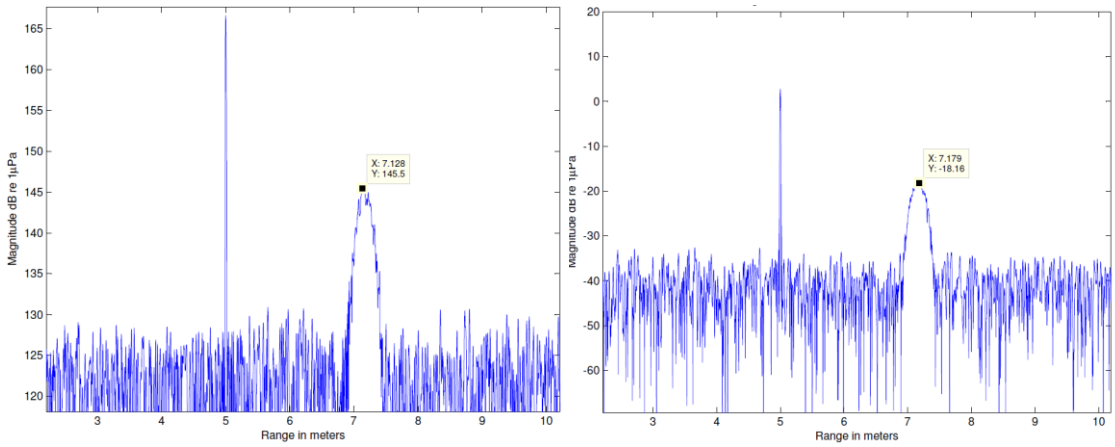

Figure 3.14 – LFM range-Doppler coupling

3.4 Pulse Design Conclusions

The designed CW pulse, with $T = 0.1$ s, is capable of resolving and detecting the target velocities at the required range, as specified.

The de-ramping technique is shown to be inefficient in yielding accurate range resolution, as the target's main lobe is not narrow enough. For the LFM pulse the requisite ideal range resolution of 1 cm is not met when using a MF or IF. However, a range resolution of 1.5 cm is indeed possible. The reason for this is that the calculation of Equation (3.4) assumes ideal conditions. This means that the equation does not take noise, losses or non-perfect sampling and processing into account.

The range resolution may be met by increasing the bandwidth of the LFM pulse. For purposes of this project, and due to hardware constraints, the LFM pulse will be implemented as designed in Section 3.1.2. The intention of this project is to select sensor theory applicable for AUV applications in a closed environment, and to show the accuracy of the selected theory in a practical implementation. Furthermore the simulation model developed of the process should be proved for accuracy as well.

The range-Doppler coupling issue of the LFM pulse is inspected. An error of $0.8\,\mathrm{m}$ in range determination was found to be coupled to a target velocity of $3\,\mathrm{m/s}$. The error may be nullified by taking the average range between an up- and down-chirp. For a moving platform the frequency of replica may be adjusted according to the speed of the platform, thus the Doppler frequency shift created the platform's own movement is nullified.

Chapter 4

HARDWARE DESIGN

4.1 Basic Hardware Layout

In order to keep the platform as flexible as possible for a quick and easy evaluation of different signals, processing of signals is performed posterior. The basic functioning of the platform is illustrated in Figure 4.1. The Section heading in which each component is discussed individually is indicated in each component block.

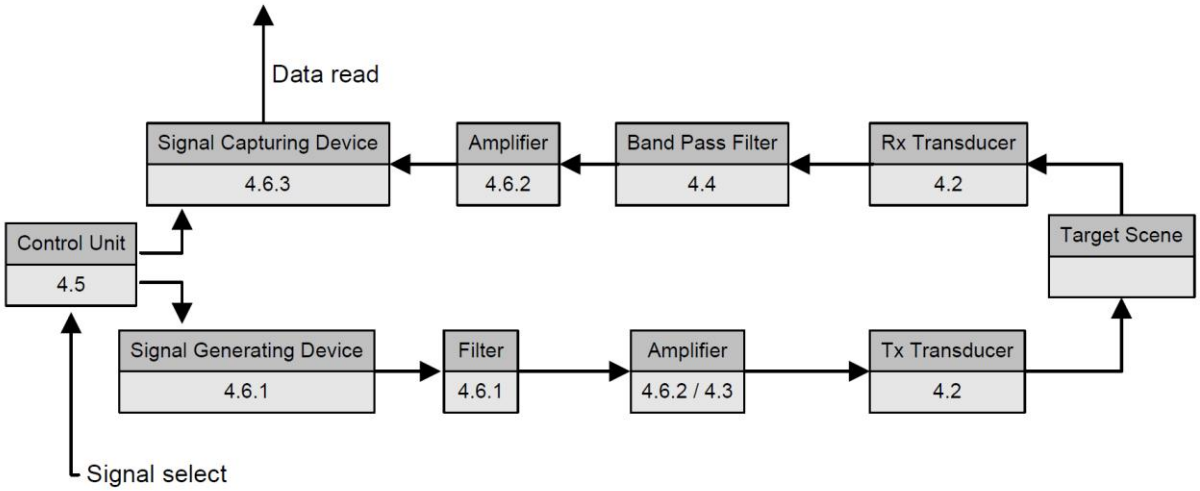

Figure 4.1 - Basic Hardware Layout

After a desired signal is selected by the user, it is generated by the DDS. After being filtered and amplified the signal is transmitted via a transducer into a water volume. Signals being reflected from targets inside the water volume are picked up by a second transducer. The acoustic signal received is transformed into a voltage signal by the receiver transducer. The voltage signal generated is filtered, and amplified by a low noise amplifier before being passed on to a data capturing device. The captured data is read by a personal computer and analysed by using appropriate software.

To keep the design simple, no quadrature modulation is implemented, as explained in Section 2.3.

4.2 Transducers

Transducers, also referred to projectors, are generally prohibitively expensive, especially wide band transducers, which are required for this project. Thus the hardware components that are defining nearly all the other parameters of this project are the transducers, which were borrowed from CSIR. The projectors obtained from CSIR were designed as wide-band-proof concept entities, and are therefore non-ideal regarding their impedance and beam pattern. The image below shows the Rx and Tx transducers. An additional disadvantage of the transducers is that they are identical. Both are designed to function as transmitting projectors. It would be preferable for the receiving transducer not to be resonant in the same region, to avoid phase distortions.

Figure 4.2 - Rx & Tx Transducers

The two transducers work on the piezoelectric principle. When a voltage-generated signal is applied to the terminals of the transducer on the transmitting side, the signal is converted into an acoustic pressure wave by the transducer. On the receiving side, the other piezoelectric transducer converts the received acoustic pressure wave reflections back to voltage signals.

The diameter D and maximum allowable applied voltage signal V_{max} of the transducers are as follows:

$$D = 4.4 \text{ cm}$$
$$V_{max} = 100 \text{ V}$$
$$V_{peak\ to\ peak} = 200 \text{ V}$$

The active operating region of the transducers lies in a band between $200\ \text{kHz}$ to $400\ \text{kHz}$. This band was suggested during a meeting with Mr. Johannes van Jaarsveld [26] at CSIR, upon examining the results obtained in Section 4.2.2. Although measurements revealed active bands at higher frequencies, these potential operating bands undeemed not suitable, as the available bandwidth at these frequencies is too narrow for the purposes of this project. The available band is therefore defined between:

$$f_{low\ min} = 200\ \text{kHz}$$
$$f_{high\ max} = 400\ \text{kHz}$$

4.2.1 Beam Spread

Due to the round face of the transducers the beam pattern of the projector is of a conical nature. The angle at which the signal spreads is fixed by the diameter D of the projectors' surface and depends on the wave length λ of the transmitted signal. Following the technical notes on piezoelectric transducers from Olympus [5], the spreading angle α is defined as follows:

$$sin\left(\frac{\alpha}{2}\right) = \frac{0.514\lambda}{D}, \qquad (4.1)$$

where

- $\frac{\alpha}{2}$ = Half Angle Spread between -6 dB points in metric degrees

Applying the above equation to the case of the lowest and highest possible frequency it is established that the spread angle decreases from $230\ \text{kHz}$ to $330\ \text{kHz}$ as shown below:

$$\alpha_{230kHz} = 7.9°$$
$$\alpha_{330kHz} = 6°$$

4.2.2 Transducer Compensation

For maximum power transfer, efficiency and uniform power distribution across a wide frequency band, the impedance of the transducers with their cabling must be matched with a suitable network to the impedance of the supplying and receiving components. All components of the SONAR platform are designed to have an input and output impedance

of $50\ \Omega$. To match impedances, the impedance of each of the projectors was measured by using a Hewlett Packard 4285A bridge. The results for both transducers are plotted below.

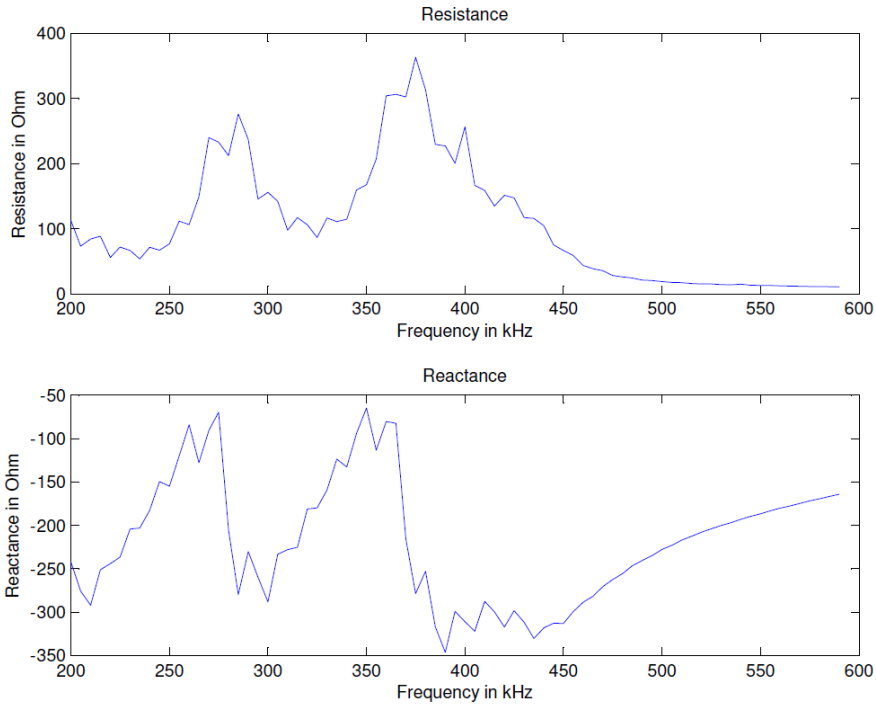

Figure 4.3 - Natural Impedance of Tx Transducer

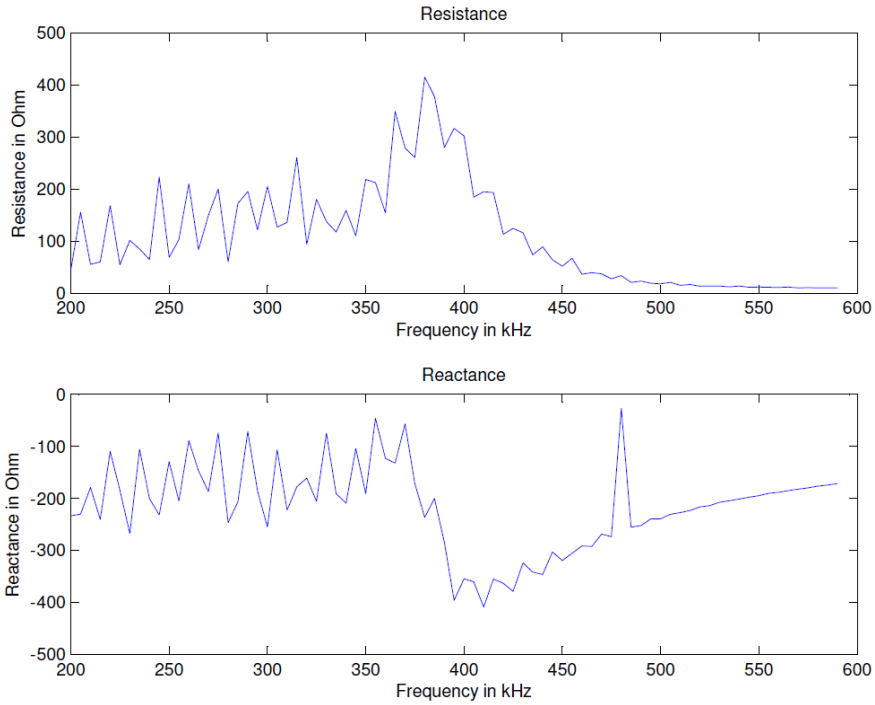

Figure 4.4 - Natural Impedance of Rx Transducer

A lumped network compensation is designed to match the transducers to a standard impedance of $50\ \Omega$. In his book *Microwave and RF Design of wireless Systems* [11], Davis M. Pozar examines various methods of creating a lumped compensation network. To simplify the design process, a software package named SMITH, developed by Prof. Fritz Dellsperger from the Berne Institute of Engineering Architecture, is applied to design a suitable compensation circuit.

The lumped network compensation process allows for an impedance to be matched at one specific frequency only. To create an operational band that is as linear as possible, each transducer is matched to $50\ \Omega$ at $380\ \mathrm{kHz}$. The impedance at lower frequencies will consequently not be matched to $50\ \Omega$ but will linearly approach the ideal $50\ \Omega$ impedance. The lumped compensation network selected is shown in Figure 4.5, where Z_L represents the impedance of the T_x transducer. The properties for the network's components are determined by following the Smith Chart compensation technique of adding shunt and series components as required. The compensation process is shown in Figure 4.6. Starting at point 1) components are added consecutively to reach the centre of the chart at 4), which is set up at $50\ \Omega$.

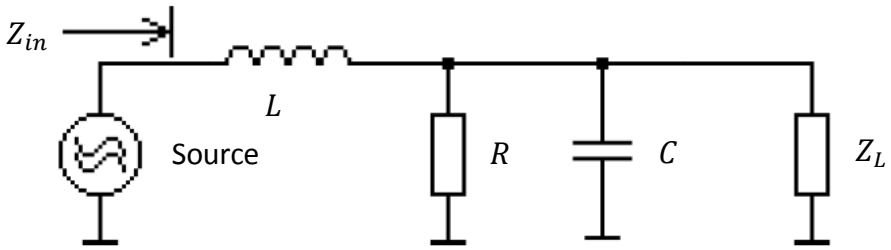

Figure 4.5 - Lumped Network for Tx Transducer

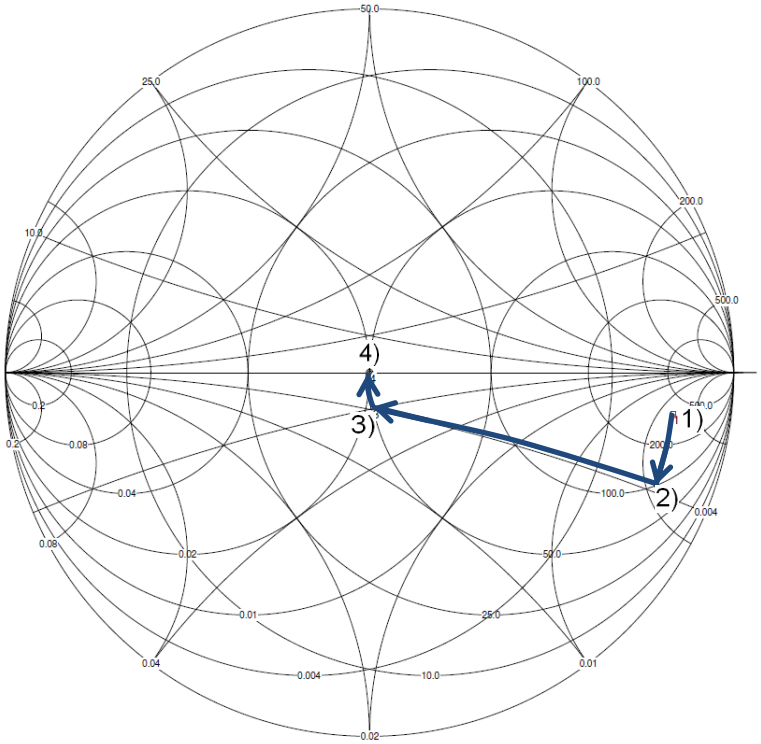

Figure 4.6 - Smith Chart Compensation

Matching the transducer's impedance of $(363 - j278)\ \Omega$ at $380\ \text{kHz}$ to $50\ \Omega$, results in the following component properties:

$$1 - 2\ )\ L = 4.3\ \mu\text{H}$$
$$2 - 3)\ R = 57\ \Omega$$
$$3 - 4)\ C = 1\ \text{nF}$$

For implementation of the T_x compensation circuit, special attention is paid to selecting suitably rated components capable of withstanding the high power output of the final stage amplifier.

The same steps are followed for the design of the R_x compensation circuit as for the T_x circuit. In contrast to the T_x design, source and load of Figure 4.5 are switched, as for the R_x case the receiver transducer represents the source instead of the load Z_L. For the R_x case, the source needs to be compensated for. No special care is necessary when implementing the circuit with regard to component power ratings, as the received signal will be of low power. The properties of the components for the R_x compensation circuit are as follows:

$$L = 4.4\ \mu\text{H}$$
$$R = 57.8\ \Omega$$
$$C = 1.2\ \text{nF}$$

Components with ratings as near as possible to the calculated values are chosen for implementation.

The impedance of both transducers is measured and illustrated in Figure 4.7 and Figure 4.8 after the lumped compensation network has been added.

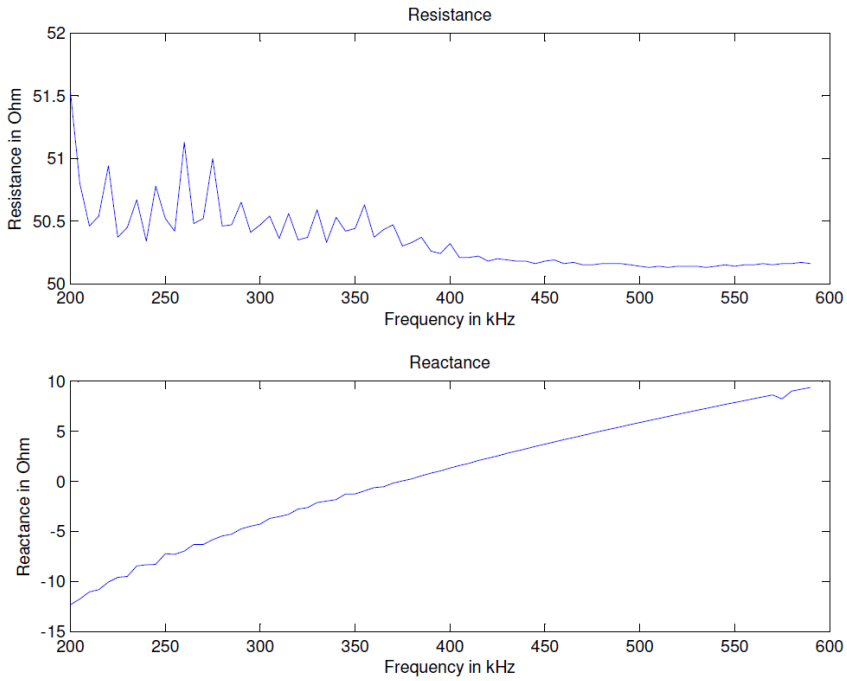

Figure 4.7- Impedance of Tx Transducer with Lumped Network

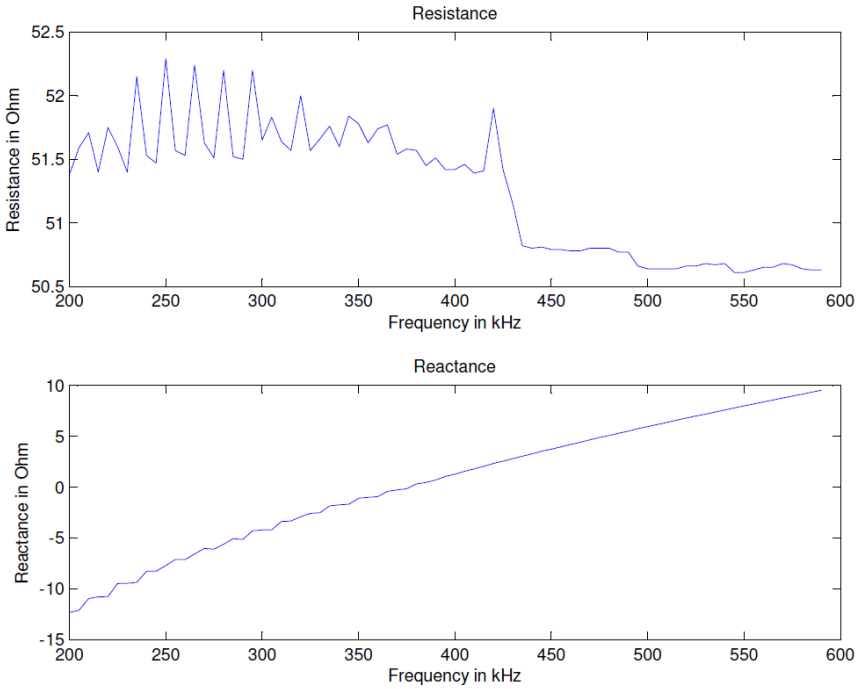

Figure 4.8 – Impedance of Rx Transducer with Lumped Network

4.2.3 Directivity

The directivity gain of the transducers is established empirically. For purposes of the experiment, the transmitter and receiver projectors are placed, facing each other at a distance satisfying the minimum range required, described by Equation (2.6). Pulses at frequencies covering the intended operating band are generated, transmitted and received again. The voltage V of each pulse at the sending and receiving terminals of the respective transducer is noted. The power P of the signals at the respective frequencies is calculated by using Equation (4.2), where the compensated transducer impedance is assumed to be $50\ \Omega$.

$$\frac{P}{W} = \frac{V_{rms}^2}{R} \tag{4.2}$$

The gain of the transducers may be calculated by using the Friis equation below, which is commonly used in the RADAR environment to determine antenna gain.

$$\frac{P_r}{P_t} = G_t G_r \left(\frac{\lambda}{4\pi R}\right)^2 (1 - |\Gamma_t|^2)(1 - |\Gamma_r|^2)|a_t \cdot a_r^*|^2 e^{-\alpha R} \tag{4.3}$$

where

- P_r and P_t represent received and transmitted power respectively
- G_r and G_t represent receive and transmit gain respectively
- R is the distance between the transducer faces
- Γ_t and Γ_r are the reflection coefficients of the transmitter and receiver transducers respectively
- a_t and a_r are the polarization coefficients of the transmitter and receiver transducers respectively
- α is the absorption coefficient of the medium

The transducers being identical, it is assumed that they have the same gain. G_t and G_r are consequently replaced with G. The polarization vectors a_r and a_t are not applicable in this case and may be omitted, because the projectors only transmit and receive compressional waves.

The average directivity gain per transducer is found to be:

$$DI = 24.4\ dB \tag{4.4}$$

The experimentally determined measured gain is found to be less than the expected theoretical value predicted in Section 2.1.10. This is due to omitting the efficiency of the transducers from calculations.

Figure 4.9 shows the calculated versus the measured directivity gain of the transducers. A large spike in gain is observed centred around $350\ \mathrm{kHz}$. The spike is due to the transducers being resonant at the same specific frequency. Signals at $350\ \mathrm{kHz}$ will be considerably distorted by the transducers themselves and the rest of the signal processing system, which cannot handle such large gain spikes.

Consequently, to keep the system's operating range as linear as possible, and the signals as undistorted as possible, the operating bandwidth of the SONAR is chosen to be lower than $350\ \mathrm{kHz}$. The band between $230\ \mathrm{kHz}$ and $330\ \mathrm{kHz}$ is identified as a favourable band to work in. In the $100\ \mathrm{kHz}$ bandwidth, the transducers have a positive, almost linear gain increase of approximately $10\ \mathrm{dB}$ when added together.

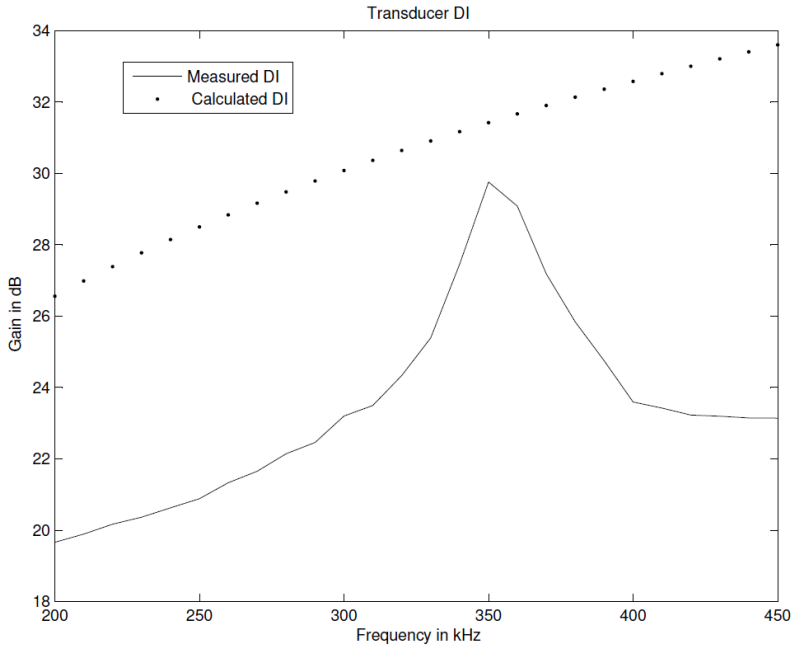

Figure 4.9 - Measured versus Calculated DI Gain of transducer

4.3 Amplifier

The transmitting amplifier stage consists of two amplifiers. The pre-amplifier is a low-power, ultra-low noise amplifier with variable gain. The second stage, is a high-power fixed gain amplifier drives the transmitting transducer. The pre-amplifier is described in more detail in Section 4.6.2. It is used to amplify the signal of the DDS to $2\ \mathrm{V}$, which is the maximum input voltage of the main amplifier. The variable gain of the pre-amplifier allows the user to adjust the output power of the platform, adding extra flexibility to the platform's design during the evaluation process.

The remainder of this section is dedicated to the selection and design of the main amplifier.

4.3.1 Specifications

The main amplifier's characteristics are defined largely by the transducers. Besides the requirement of a linear signal response across the desired operating bandwidth described earlier, the desired properties for the amplifier relating to the transducer's characteristics are as follows:

- $V_{max} = 100\ \mathrm{V}$
- $I_{max} = \frac{V_{max}}{R} = 2\ \mathrm{A}$
- $f_{max} = 400\ \mathrm{kHz}$
- $B = 100\ \mathrm{kHz}$
- $Slew\ Rate$[3] $= 2\pi f_{max} V_{max}(1 \cdot 10^{-6}) = 251\ \mathrm{V/\mu s}$

The APEX PA107DP operational power amplifier from CIRRUS LOGIC matches the above requirements. The amplifier is specifically designed as a driver for piezoelectric projectors. The features of the amplifier are the following:

[3] Slew rate is calculated according to PA107DP [27] datasheet.

- Power Bandwidth $170\ \mathrm{V_{peak\ to\ peak}}$, $2\ \mathrm{MHz}$
- Output Voltage up to $180\ \mathrm{V_{peak\ to\ peak}}$
- Voltage input of maximum $2\ \mathrm{V_{peak\ to\ peak}}$
- Slew Rate $2500\ \mathrm{V/\ \mu s}$
- Rated RMS output current $\pm 1.5\ \mathrm{A}$
- Peak output current $\pm 5\ \mathrm{A}$

The small signal response of the amplifier is shown in Figure 4.10. The amplifier exhibits a linear phase response and a linear decrease in gain of about $-10\ \mathrm{dB\ per\ decade}$ across the desired frequency band. Together with the increasing gain from the transducers, this results in almost a constant gain across the frequency band used.

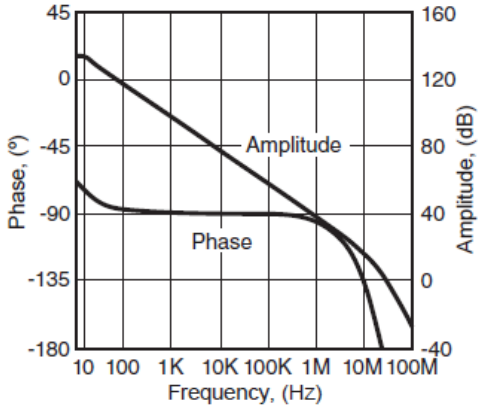

Figure 4.10 – Amplifier Small Signal Response [27]

It should be noted that the amplifier as specified above, is an ideal fit for the available transducer, but over-designed for this project's requirements. For the case of a CW pulse, the minimum required electrical power applied to the transmitting transducer, in order to resolve a target in Doppler, as specified at $50\ \mathrm{m}$, is calculated to be $11\ \mathrm{W}$. This is shown in Section 3.2.1 Assuming that the projectors are purely resistive with $R = 50\ \Omega$, the required voltage swing is equal to:

$$V = 2\sqrt{P \cdot R} = 46\ \mathrm{V_{peak\ to\ peak}}$$

However, as the platform is intended as a basis for further research, the proposed amplifier is thought to be a good compromise.

4.3.2 Circuit Design

The PA107DP amplifier chip may be implemented in an ordinary feedback circuit as displayed in Figure 4.11, where the ratio of R_F / R_{IN} determines the gain of the circuit.

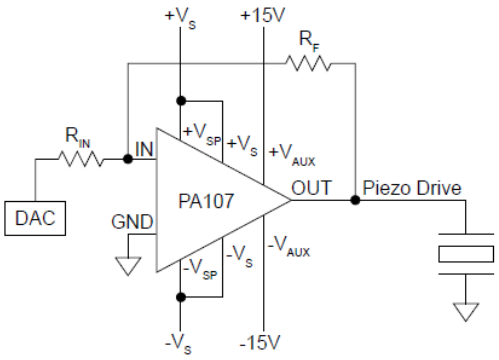

Figure 4.11 - Main Amplifier Basic Circuit [27]

Given the maximum allowable input voltage of $V_{IN} = 2\ \mathrm{V_{peak\ to\ peak}}$ the ratio of R_F / R_{IN} is chosen to be 47. This ratio allows for an input signal of $V_{IN} = 2\ \mathrm{V_{peak\ to\ peak}}$ to be theoretically amplified to an output of $94\ \mathrm{V_{peak\ to\ peak}}$. The maximum gain of the amplifier is designed to be higher than required to allow for non-ideal system characteristics and unforeseen gain losses in the system.

- $R_F = 47\ \mathrm{k\Omega}$
- $R_{IN} = 1\ \mathrm{k\Omega}$

To allow for lower gains, four $47\ \mathrm{k\Omega}$ resistors have been added in parallel to R_F in an open circuit configuration, which may be added into the circuit one by one, by placing a jumper on the appropriate header. The headers are shown on the right hand side of Figure 4.12.

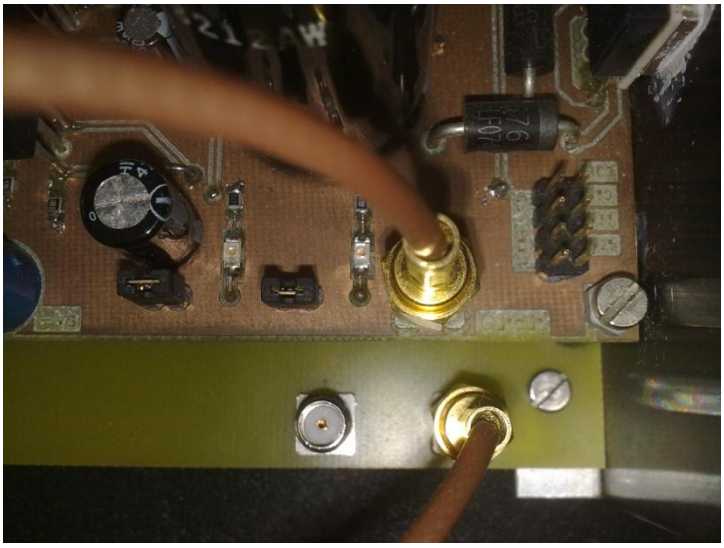

Figure 4.12 – Amplifier gain-select headers

The amplifier circuit design in conjunction with the transducer compensation circuit is successfully simulated for linear output behaviour by using LTspice.

4.3.3 PCB Design Considerations

The PA107DP operational amplifier chip requires a primary and an auxiliary supply voltage, as well as various stabilising and feedback components. The maximum supply voltages designed for, are:

- $V_{primary} = \pm 80\ \mathrm{V_{DC}}$
- $V_{\mathrm{auxiliary}} = \pm 15\ \mathrm{V_{DC}}$

Special care is taken in the selection of suitable components and PCB design, to prevent the contingency of catastrophic reverse voltage application. Ordinary laboratory bench power supplies are used to power the amplifier circuit. The PCB is designed to enable quick connecting and disconnecting of power supply cables.

To protect the various components of the amplifier circuit from a large inrush current during start up, a soft-start circuit is designed and implemented by using power MOSFETs.

Figure 4.13 shows the amplifier PCB.

Figure 4.13 - Main Amplifier

4.3.4 Power Dissipation

Calculations for determining the minimum rating of heat sink required are performed according to the data sheet specifications of the chip amplifier.

$$R_{SA} = \frac{T_C - T_A}{PD + PD_Q} - 0.1 = 2\ ℃/W \qquad (4.5)$$

where

- T_C *is* the maximum allowable case temperature $= 85\ ℃$
- T_A is the ambient temperature $= 23\ ℃$
- $PD = \frac{V^2_{peak\ to\ peak}}{2\pi^2 R} = 25.9\ \text{W}$
- $PD_Q = 0.035 \cdot V_{primary} + 0.021 \cdot V_{\text{auxiliary}} = 3.115\ \text{W}$

A heat sink with $R_{SA} = 0.6\ ℃/\text{W}$ is selected to allow for higher ambient temperatures and non-ideal case-to-sink heat transfer properties.

4.4 Band Pass Filter

The input of the platform's receiver side consists of a band pass filter which is implemented to limit noise received. To keep the platform as versatile as possible regarding the receiver's bandwidth, the band pass filter is chosen to have cut-off frequencies which cover the frequency band of interest, plus an additional $50\ \mathrm{kHz}$ bandwidth to both sides, to allow for possible alterations during the test phase:

- $f_{low} = 180\ \mathrm{kHz}$
- $f_{high} = 380\ \mathrm{kHz}$

4.4.1 Filter Design

To achieve a flat pass band with linear phase response and low additional noise, a passive Butterworth filter design is implemented. As the pass band is quite substantial, the band pass design is achieved by adding suitable high- and lowpass filters in series. Both filters are designed to be 6^{th} order units to achieve sharp cut-offs.

The design process is accomplished by following the lecture notes of the *Electronics 315* course of the University of Stellenbosch, Electrical and Electronic Engineering Department [28]. A basic n^{th} order low-pass filter is used, as shown in Figure 4.14. The cut-off frequency of the filter may be adjusted to any desired value by means of k_f. The low pass filter can then be converted into a high pass filter by using prescribed transformations. Furthermore, the standard input and output resistances R_S and R_L may be adjusted by using the impedance scaling factor k_z.

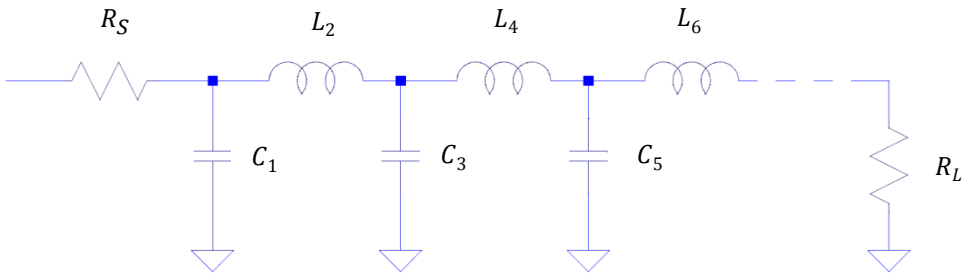

Figure 4.14 - Passive Low Pass Filter

The component values for a 6^{th}order passive Butterworth low pass filter, with R_S and R_L equal to $1\ \Omega$, and a cut-off frequency of $\Omega_0 = 1\ \mathrm{rad/s}$ are given by the class notes below.

- $C_1 = 0.5176\ \mathrm{F}$
- $L_2 = 1.4142\ \mathrm{H}$
- $C_3 = 1.9319\ \mathrm{F}$
- $L_4 = 1.9319\ \mathrm{H}$
- $C_5 = 1.4142\ \mathrm{F}$
- $L_6 = 1.4142\ \mathrm{H}$

For the low-pass filter to have a cut-off frequency of $f_{low\ pass} = 380\ \mathrm{kHz}$ and impedances of R_S and R_L equal to $50\ \Omega$, the above components are scaled as follows:

$$L_{scaled} = \frac{L_{unscaled} \cdot k_z}{k_f}, \tag{4.6}$$

$$C_{scaled} = \frac{C_{unscaled}}{k_f \cdot k_z} \tag{4.7}$$

where

- $k_z = 50/1$
- $k_f = f_{cut-off} \cdot 2 \cdot \pi$

The high-pass filter with a cut-off frequency of $f_{high\ pass} = 180\ \mathrm{kHz}$ is designed by following the same principles as for a low-pass filter. The component values of a basic high-pass filter, which has the same properties as the basic low-pass filter previously discussed, is given by:

- $L_1 = 1.932$ H
- $C_2 = 0.707$ F
- $L_3 = 0.5176$ H
- $C_4 = 0.5176$ F
- $L_5 = 0.707$ H
- $C_6 = 1.932$ F

For practical implementation of the filter, standard component values resembling the theoretical ones as closely as possible ones are selected.

4.4.2 Filter Simulation and Measurements

The designed band pass filter is first tested by using LTspice before implementation. Figure 4.15 shows the result of the filter output, using LTspice simulation software. For purposes of simulation, the exact component values are used as for the practical filter implementation. Practical measurements confirm the simulation.

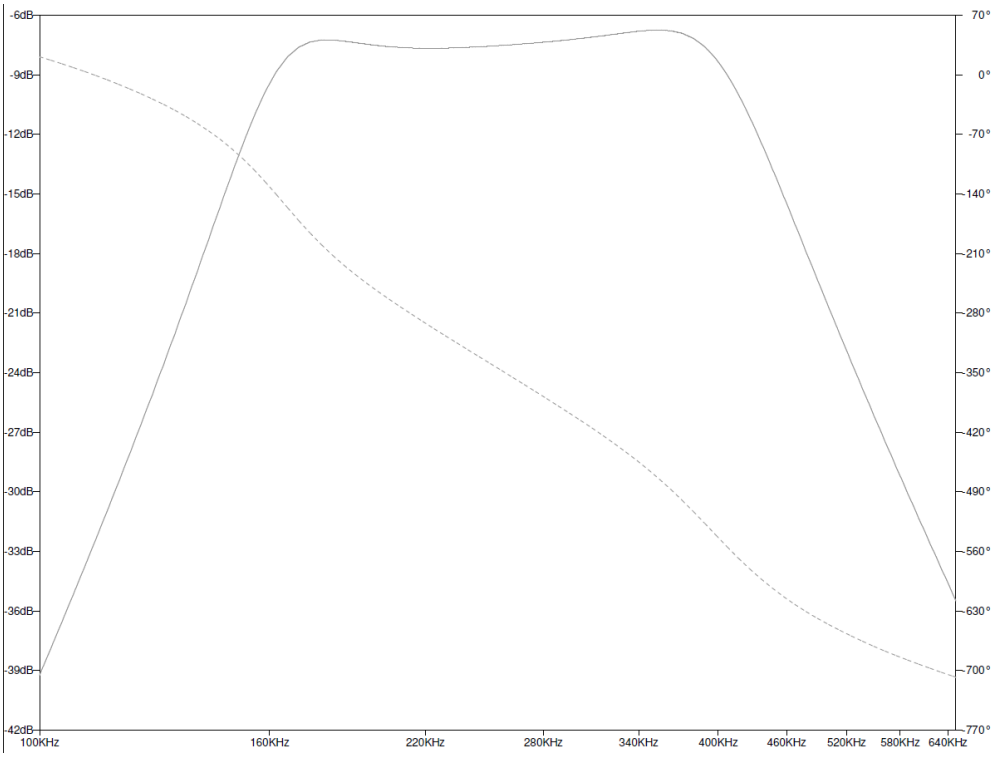

Figure 4.15 - LTspice BP Filter Simulation

4.5 Power Supply

The development boards described in the following section require numerous different voltages for powering purposes. To simplify the process of powering the entire SONAR platform, a power supply PCB is designed. The input and output voltages are the following:

- $V_{in} < 12\ \mathrm{V_{DC}}$
- $V_{out\,1} = 1.8\ \mathrm{V_{DC}}$
- $V_{out\,2} = 3\ \mathrm{V_{DC}}$
- $V_{out\,3} = 5\ \mathrm{V_{DC}}$
- $V_{out\,4} = 0 - 5\ \mathrm{V_{DC}}$
- $V_{out\,5} = 0 - 5\ \mathrm{V_{DC}}$

Standard voltage regulators are used for the PCB design. Heat dissipation and power ratings of voltage regulators are considered during the design process.

For implementation, care is taken to prevent a reverse supply voltage to the circuit.

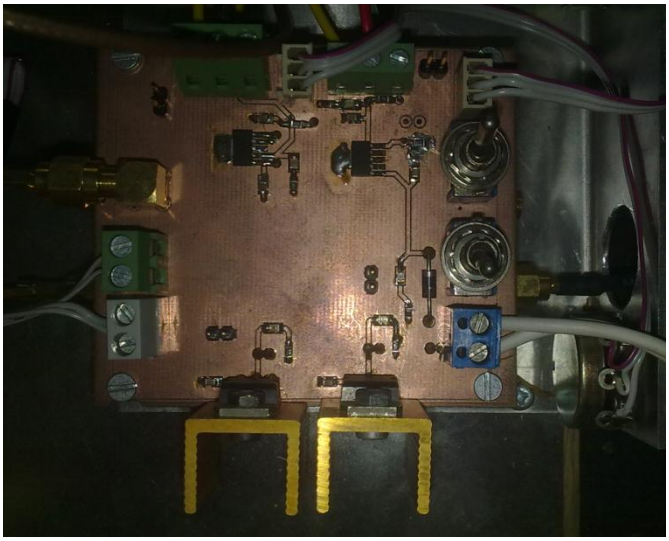

Figure 4.16 - Power Supply PCB

4.6 Development Boards

As the platform is a proof-of-concept type of implementation, and to accelerate the hardware development process, various development boards are used to realise the hardware design of Figure 4.1. Following the signal processing path, the development boards used, are:

- Signal Generation – Direct Digital Synthesiser
- Pre-Amplifier – Low-noise variable gain amplifier
- Signal Capturing – ADC in conjunction with a First In First Out (FIFO) data capturing chip
- Control Unit – ESL avionics board

For the SONAR platform to function, a pulse is required to be generated and captured in total. This process occurs within a few milliseconds, depending on the pulse design. The development boards therefore need to be accurately controlled in order for a signal to be generated by one board, and correctly captured again by another.

The problem arising from using development boards for generating and capturing signals is, that the boards are designed by the manufacturer to be used individually. Each board is specifically designed for the evaluation of the main component featured by the board. Hence there is no direct provision for the boards to communicate with each other in order to function as sub-components in an integrated processing circuit.

To synchronise the signal sending-and-receiving process a former avionics board from the ESL laboratory housing a dsPIC is used to interact with both the DDS and FIFO boards.

4.6.1 DDS

Direct Digital Synthesisers have become readily available in a variety of configurations and with substantial processing capabilities lately. The advantage of using a DDS as compared to an analogue synthesizer is low cost, micro-Hertz tuning resolution and high configurability, which are some of the most important features of this project's platform. A DDS allows for the implementation of frequency, phase and amplitude modulation, as well as the possibility of mixing some of the modulations to a certain extent.

A simple DDS consists of four basic components, viz. a phase accumulator, a lookup table, a DAC and a low-pass filter. The phase accumulator is incremented with each system clock cycle and accesses a sine function, stored in the lookup table. By accessing the lookup table according to the output of the phase accumulator in a defined sequence, any required sine wave may be digitally synthesized. The digital wave is then converted into an analogue signal by a DAC. To obtain a smooth near-perfect sine wave, the output of the DAC is filtered by a low-pass filter.

The output frequency of the DDS depends on the rate at which the addresses to the look up table are changed. For modulation purposes, the addresses are generated by adding a constant, specified by the phase increment register (PIR), to the phase accumulator. For most common DDS's the rate at which additions occur is a constant, resulting in linear modulation only. The number added by the PIR, changing the output frequency, may be defined by the user. The frequency resolution of the DDS in turn depends on the number of bits in the PIR. A block diagram of a simple DDS is shown in Figure 4.17.

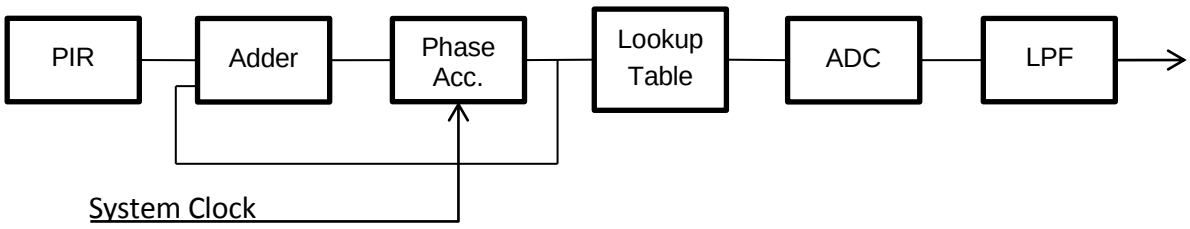

Figure 4.17 - Simple DDS block diagram

The DDS used for this project is mounted on the AD9959/PCB development board made by Analog Devices. The evaluation board is shown in Figure 4.18. The AD9959 chip itself has four synchronised DDS cores which may generate independent output signals, which may be individually modified in frequency, phase and amplitude. Further features of the AD9959 chip, according to the AD9959 datasheet [29], are:

- Maximum output rate of 500 MSPS
- Maximum output frequency of 200 MHZ
- 4 integrated 10 bit DACs
- 16-level modulation of frequency, phase or amplitude

- Linear modulation of frequency, phase or amplitude
- 32-bit frequency tuning
- 14-bit phase offset resolution
- 10-bit output amplitude scaling resolution
- Serial I/O port interface
- Selectable 4x to 20x reference clock multiplier (PLL)
- Selectable reference clock crystal oscillator between $20\ \mathrm{MHz}$ and $30\ \mathrm{MHz}$

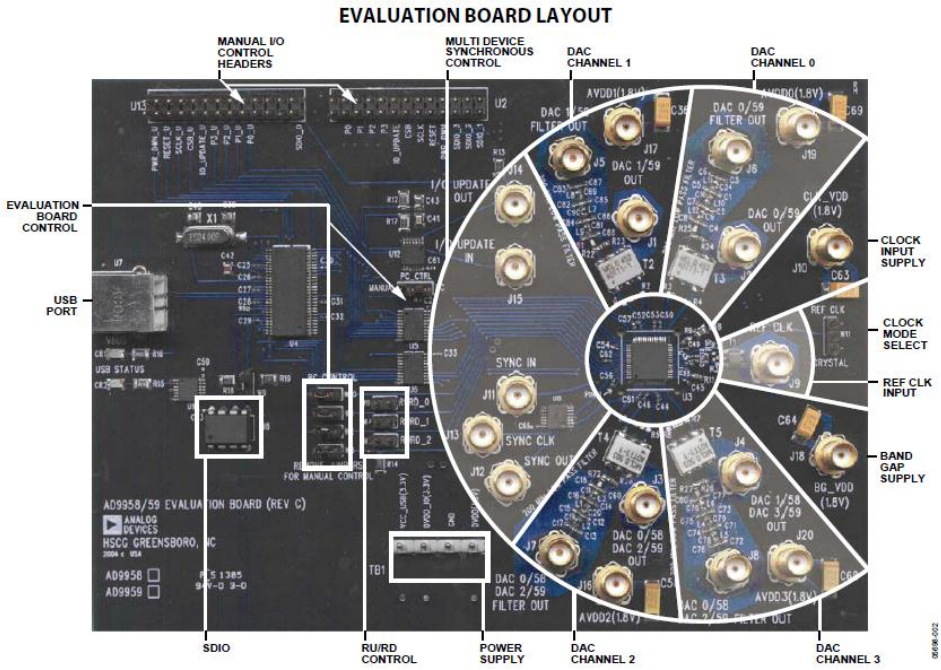

Figure 4.18 - DDS Evaluation Board [29]

The evaluation board requires $1.8\ \mathrm{V}$ to power the DDS cores, as well as $3.3\ \mathrm{V}$ to power the USB and SPI I/O ports. Furthermore, the board requires a clock signal. The signal may be supplied by an external signal generator or preferably for this project, by a crystal oscillator. The clock of the crystal may be multiplied by means of an internal PLL, before being passed on as system clock. The selection regarding the system clock is made on the frequency tuning resolution. For the LFM pulse, $100\ \mathrm{kHz}$ bandwidth centred at $280\ \mathrm{kHz}$ is required. To obtain a good linearity during a frequency sweep while still obtaining a high output rate, the following setup is selected:

- $Crystal = 28\ \mathrm{MHz}$

- $PLL = 5$

The resulting system clock and frequency tuning resolution are:

- $f_{system} = 140$ MHz
- $f_{tuning} = 0.0326$ Hz

Various types of operations are supported by the DDS and may be explored in more detail in its datasheet. The operations applicable to this project are the ones supporting a CW and LFM pulse. The CW pulse is easily implemented by a constant signal output. For the LFM pulse, the DDS is programmed to do a linear sweep between a predefined starting and stoping frequency. The amplitude ramp-up and ramp-down function is added for both operations. Ramping up the signal when starting the pulse, and de-ramping the signal just before the end of the pulse, reduces spectral noise considerably.

The evaluation board is programmed and controlled via the USB port by default, with the relevant software being installed on a personal computer. However, the board also features external control and I/O headers by which the DDS chip may be programmed and controlled. Utilizing the external headers requires the user to change a few jumper settings. Changing the board to 'manual' control renders the USB port inoperable. Therefore the DDS control registers need to be set up via the SPI port supported by the I/O headers.

Setting up the control registers and controlling the ramping of the signal via the external control headers is accomplished by a dsPic, which is housed by the Control Unit. The functionality of the Control Unit is discussed in more detail in Section 4.6.4.

Power design is not an issue for this project at this point and is only considered for power supply design purposes. However, for future reference and AUV applications where power constraints are a concern, it should be noted that the power requirements of the board depend on how many cores are being used, and on the type of application performed by the core. The power requirement ranges between 315 mW and 420 mW per core in active mode. All unused cores are thus switched into power-down mode, where each core only consumes 13 mW.

4.6.2 Pre-Amplifier

The pre-amplifier evaluation board employed for this project is the AD8332-EVALZ supplied by Analog Devices. The board features the variable gain (VGA) ultralow noise preamplifier (LNA) AD8332. Another feature of the board is the programmable input impedance, which is naturally chosen to be $50\,\Omega$ to match the rest of the system's impedance. Further specifications of the board are as follows [30]:

- $V_{supply} = 5\ \mathrm{V_{DC}}$
- $V_{variable\ supply} = 0 - 5\ \mathrm{V_{DC}}$
- $P = 250\ \mathrm{mW}$
- $V_{out} = 2\ \mathrm{V_{peak\ to\ peak}}$
- $Linear\ gain\ up\ to\ 90\ \mathrm{MHz}$

The pre-amplifier is used for the receiving and transmitting signal processing side of the platform. It is specifically selected as its maximum output voltage swing is ideal for the main amplifier and the ADC. Both, main amplifier and ADC have maximum input voltages of $V_{in} = 2\ \mathrm{V_{peak\ to\ peak}}$.

On the transmitting side, the amplifier functions as a buffer between the DDS and the main amplifier. Besides boosting the signal, the pre-amplifier protects the DDS in case of an amplifier failure.

For both sides the pre-amplifier acts as a gain control unit. By varying the $V_{variable\ supply}$ input voltage the output voltage is controlled. A pod is implemented for both boards enable the user to manually vary the gain for each one.

The reason for choosing a dual pre-amplifier board is to give the platform the option of IQ channel signal processing, should it be required at a later stage.

4.6.3 ADC and FIFO

For capturing the received signal, the dual AD9248 ADC evaluation board is used in conjunction with the HSC-ADC-EVALB (FIFO) evaluation board. Both development boards feature dual signal processing capability and are supplied by Analog Devices. The power requirements for both boards are the following:

- $V_{in} = 6\ \mathrm{V_{DC}}$
- $I_{max} = 2\ \mathrm{A}$

The FIFO evaluation board is a general data capturing board which supports a number of ADC evaluation boards. With the FIFO board, as with the DDS evaluation board, direct control of the board is very limited. Although the FIFO board features a SPI port, this can only be used to programming certain output parameters of the ADC board, if SPI communication is supported by the ADC. The AD9248 ADC does not support a SPI interface. The only way of program the FIFO ADC board and read data from it is by using the supplied evaluation software from Analog Devices. The software, installed on a personal computer, communicates with the board via USB interface. Data can be captured and read, after the FIFO is initialised. Data from the interleaved ADC board is written into the FIFO memory chips at a clocking speed supplied by the ADC board when requested by the user by software command. Once the FIFO registers are full, the data capturing process is terminated and the data is sent to the evaluation software via USB interface. Captured data may be exported from the evaluation software to Excel, from where it may be re-imported by using Matlab.

The AD9248 ADC evaluation board has an output capable of delivering 14 bits of resolution at 65 MSPS, which allows amply for both dynamic range and Nyquist criterion requirements. Its maximum input specification $V_{in} = 2\ \mathrm{V}$ complies with the maximum output of the pre-amplifier. The board itself is very simple in that only a clock signal is required for it to output 14 bits of data per channel, at the frequency of the clock signal. The data is continuously passed on to the FIFO evaluation board together with the clock. The clock frequency thus defines the sampling frequency of the ADC and the FIFO. Calculations regarding dynamic range and Nyquist criterion are shown below:

- $V_{recieve\ max} = 2\ \mathrm{V}$

- $V_{reive\ min} = \frac{Amplifier\ output\ voltage}{(2*maximum\ range)^2} = \frac{23V}{100^2} = 2.3\ \text{mV}$
- $V_{ADC\ \text{min.}resolvable} = \frac{2V}{2^{14\ bit}} = 0.122\ \text{mV}$

The above calculations confirm that the dynamic range of the ADC is adequate for the purposes of this project.

The minimum sampling frequency required to satisfy Nyquist sampling theorem for a band pass signal may be deduced from Figure 4.19, which was obtained from an IEEE article, *The Theory of Bandpass Sampling,* by R. Vaugan [31]. The figure links the minimum sampling frequency fs to the lowest frequency of the band pass signal f_u by the bandwidth of the signal B. Having a minimum frequency of $230\ \text{kHz}$ and a bandwidth of $100\ \text{kHz}$ for the case of the LFM pulse, f_u thus equals approximately $2B$. Figure 4.19 dictates a minimum sampling frequency of $4B$, or $f_{s\ min} = 400\ \text{kHz}$. Unfortunately, the approach requires f_u to be an exact multiple of B. The pulse needs to be adjusted accordingly for the evaluation of low sampling rate requirements.

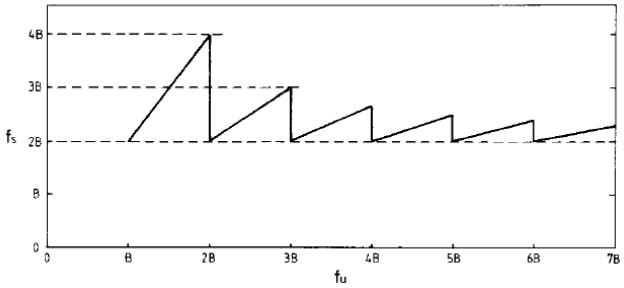

Figure 4.19 - Minimum Sampling Frequency for Band Pass Signal with Bandwidth B [31]

Nevertheless, for this project no constraint is given with regard to the sampling rate. The sampling rate must therefore be chosen to be at least twice the highest frequency of the band pass signal in order to satisfy Nyquist's theorem. The highest frequency of the band pass signal is $f_{max} = 330\ \text{kHz}$. The sampling frequency is selected as:

$$f_s = 1\ MHz \qquad (4.8)$$

To be able to cope with the ADC board, the FIFO evaluation board naturally has a much higher sampling ability of 133 MSPS. The standard FIFO memory chip size supplied with the FIFO evaluation board is $16\ \text{bit}$ wide and $32\ \text{kilobit}$ deep. Sampling 14 bit of data at $f_s =$

1 MHz would fill the memory chip in 32 milliseconds. However, the CW and LFM signals are designed to have a pulse length of 100 milliseconds. Keeping to a non-IQ channel sampling design and a LFM pulse design, where f_u is not a multiple of B, larger FIFO memory chips are required. Both FIFO memory chips are consequently replaced with 256 kilobit sized memory chips. Hence, the maximum sampling interval of the platform is increased to $T_{sample} = 256$ milliseconds. Allowing for the time of 67.75 milliseconds a pulse needs to travel to and from a target at 50 m, the maximum permissible pulse length is:

$$t_{pulse\ max} = 188.25\ milliseconds \tag{4.9}$$

Selecting a dual processing channel for both boards allows IQ channel processing capability to be added the platform at a later stage. Adding IQ channel processing as well as choosing f_u to be a multiple of B would considerable reduce sampling frequency requirements.

The ADC interleaved with the FIFO is shown in Figure 4.20.

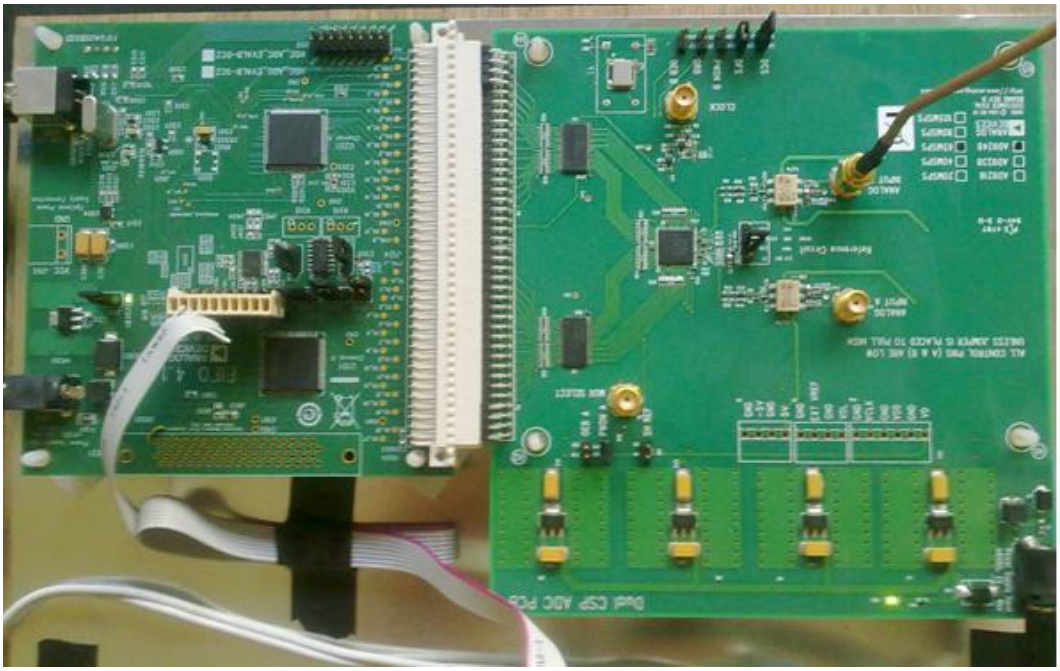

Figure 4.20 - ADC and FIFO

4.6.4 Control Unit

The control unit (CU) consists of an obsolete servo board as shown in Figure 4.21, which is supplied by the Electronic Systems Laboratory of the Electrical and Electronic Engineering Department of the University of Stellenbosch. The on-board components relevant to this discussion are a 30F5011 dsPIC, a $9.6\ \mathrm{MHz}$ crystal supplying a clock signal, a $3.3\ \mathrm{V}$ voltage regulator and $MAX3232$ line driver/receiver for serial communication. The voltage regulator is changed from the original $5\ \mathrm{V}$ regulator to a $3.3\ \mathrm{V}$ regulator for the dsPIC, to facilitate communication with the DDS via SPI, as the SPI port of the DDS has a $3.3\ \mathrm{V}$ communication standard. Consequently, the MAX3232 line driver/receiver has to be changed to comply to the new operating voltage.

Figure 4.21 - Servo Board

The control unit has three main tasks:

- Program the DDS to output desired pulse
- Monitor FIFO write enable
- Control the DDS

Apart from programming and controlling the DDS, the CU forms the synchronisation link between the DDS and FIFO board. In contrast to the DDS evaluation board, which may be controlled externally by the CU, the FIFO evaluation board is only controllable by using the evaluation software on a personal computer. A synchronisation link is created by letting the CU monitor the write-enable port of the FIFO evaluation board memory chips. As soon as the user requests data by using the evaluation software, the command is sent to the FIFO evaluation board. The on board FPGA of the FIFO board pulls the write-enable control pin of the FIFO chips low, which starts the data acquisition process. The CU senses the write-enable

signal of the FIFO memory chip and starts the signal transmission process of the DDS. Figure 4.22 shows the synchronisation process between the FIFO and DDS evaluation boards.

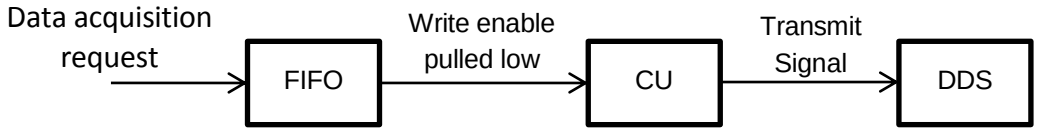

Figure 4.22 - FIFO & DDS Synchronisation

For an accurate synchronisation between the FIFO and DDS evaluation boards, the required instruction rate of the CU must be sufficiently high. The instruction rate is calculated according to the dsPIC30F datasheet [32]:

$$t_{instrution\ rate} = \frac{4 \cdot postscaler}{PLL_{CU} \cdot f_{crystal}} = \frac{4}{8 \cdot 9.6MHz} = 52\ ns \qquad (4.10)$$

Compared to a total pulse length of 100 ms the instruction rate as calculated above is more than sufficient to allow for accurate synchronisation and DDS control.

Programming the DDS is accomplished by the CU utilizing the SPI communication protocol. By sending the correct instruction commands as specified in the datasheet, the DDS may be set up to do any modulation mentioned previously in Section 4.6.3. To start/stop the modulation and ramp the signal amplitude up and down, the CU has control over five external control headers of the DDS. Furthermore, the CU is capable of powering the DDS down, as well as sending a reset command to the DDS.

For operation mode the user preselects the signal to be generated by the DDS, by sending a specific character to the CU from a personal computer via serial port communication. By requesting data from the FIFO evaluation board, using the supplied evaluation software, a SONAR signal is then sent and captured. The captured data is automatically sent to the personal computer and may be accessed by MATLAB for post-signal processing to evaluate the sent signal for its range and Doppler detection and resolution capabilities. Figure 4.23 explains the interaction of the various hardware components graphically. Following the numbering from one to eight describes the operation of the SONAR platform.

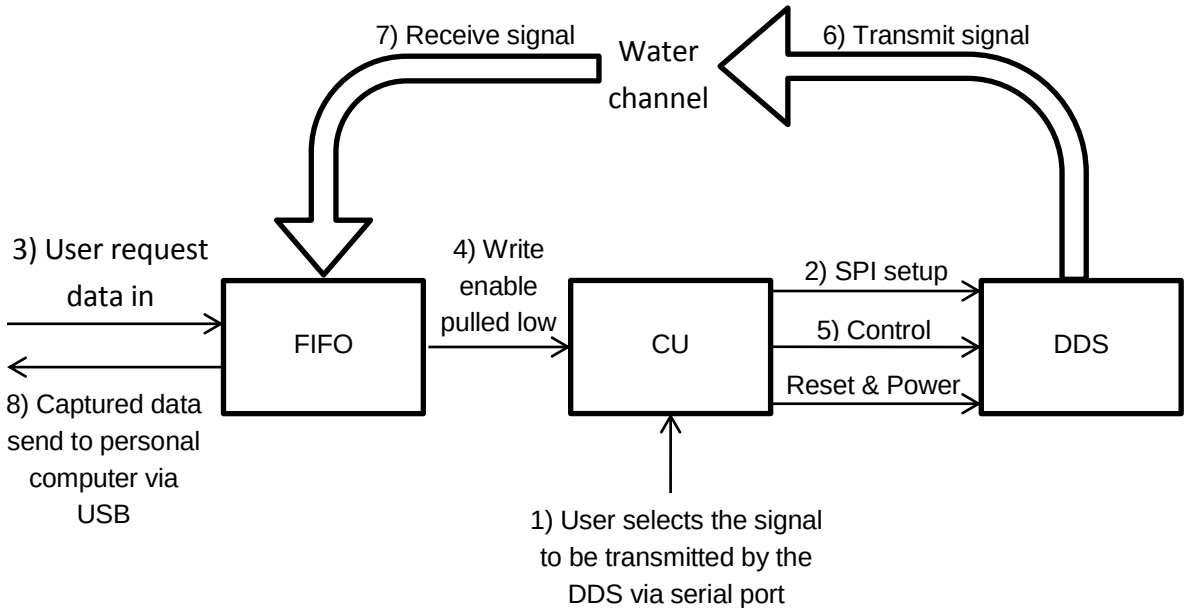

Figure 4.23 – SONAR platform operation

4.7 General Remarks

It is common practice in SONAR and RADAR applications to implement some type of automatic gain control on the received signal. The gain control automatically amplifies the received signal in such a way as to cancel the effect of spreading and absorption losses which the transmitted signal undergoes before being received again. Depending on the type of signal and signal processing, several different implementations are available. Depending upon the application, the implementations range, from simple filters or time-based amplification, to complicated implementations which actively track the signals received and sent, and amplify them accordingly.

The aim is to create a received signal which is linear in gain with time. Using an automatic gain control enables a system to detect echoes originating from distant targets equally well as echoes originating from close targets. Not using any type of gain control could result in the echoes from close targets swamping the echoes form distant targets.

Because of the very short maximum required range for this project, no gain control is implemented in hardware. Software based gain control would be possible, but proved to be less effective and is thus omitted, too.

Chapter 5

MEASUREMENTS AND RESULTS

The SONAR platform is tested in a towing tank at the CSIR facilities in Stellenbosch, as well as the towing tank facilities of the Department of Mechanical & Mechatronic Engineering (M&M) of the University of Stellenbosch. The dimensions of the CSIR towing tank, followed by the M&M facilities are as follows:

- 3 m wide x 100 m long x 2-2.5 m deep
- 4 m wide x 88 m long x 3.5-4 m deep

A towing tank is an ideal testing facility for purposes of this project, in that the tank has similar closed environment characteristics as those found in a harbor.

5.1 Test Setup

The towing tank facilities at both CSIR and M&M feature an electrically powered trolley, which runs on rails which are mounted on top of each tank's side walls. The trolleys can be controlled to run forward and backward at user selected speeds. The speed is determined by adjusting the setting of an analogue pod. The speed of the CSIR trolley may be calculated by converting the output EMF voltage of a small electric motor, which is connected to the drive train of the trolley. The relationship between the EMF voltage and the speed of the trolley, was determined empirically, and is shown in Appendix A.1. The M&M trolley has an onboard speedometer, which indicates the speed of the trolley in $\mathrm{m/s}$.

The SONAR platform is set up on each trolley in a similar way. The two transducers are mounted inside a plastic bracket as indicated in Figure 4.2. The bracket in turn is fixed to the tip of a carbon pole, which is attached to the trolleys. The experiment setup is shown in Figure 5.1 and Figure 5.2.

Spherical lead sinkers, acting as targets are suspended in the tank by fishing lines. For experiments regarding velocity readings the trolley is driven back and forth, while taking measurements. For accurate range resolution measurements the trolley is kept stationary and the targets are arranged as required.

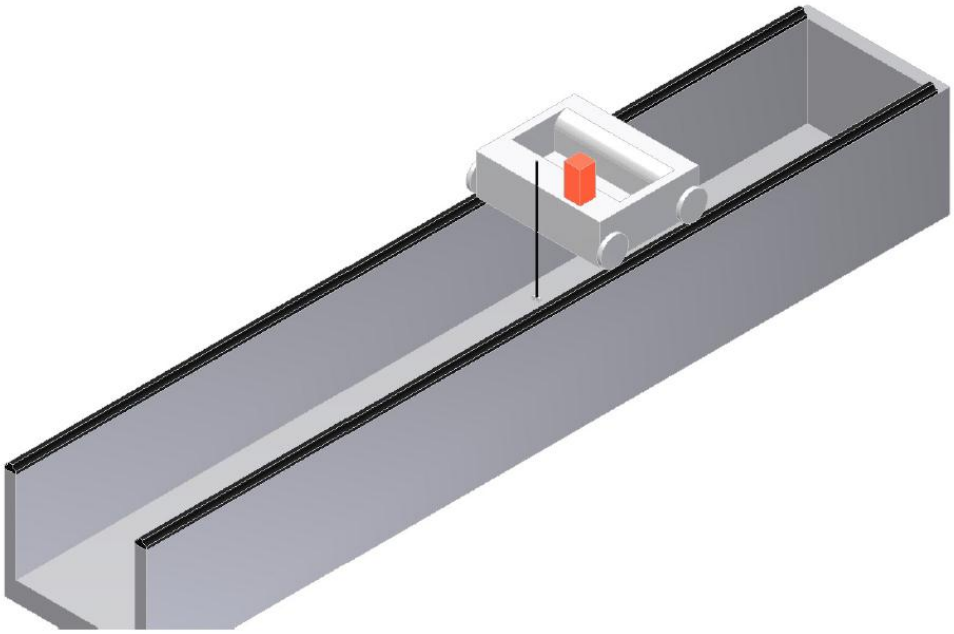

Figure 5.1 – CSIR towing tank experiment setup

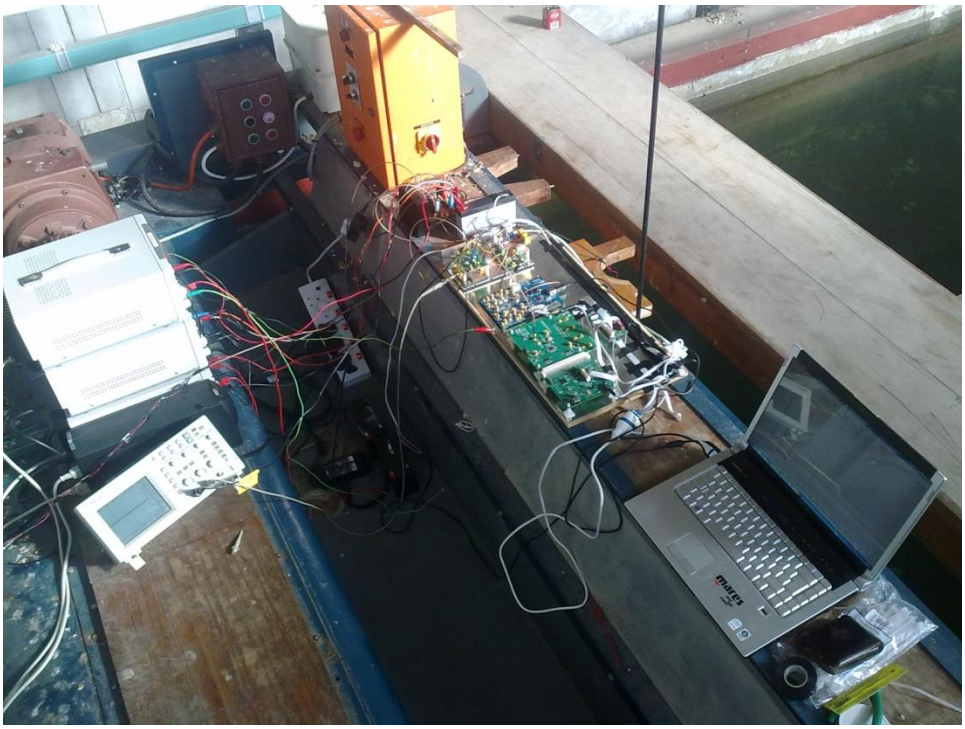

Figure 5.2 – Experiment setup aboard trolley in towing tank

5.2 CW Measurement Results

A second pole is attached to the relevant trolley at sufficient distance in front of the transducers for measurements. Taking CW velocity measurements when driving the trolley, two target velocities will appear after processing. One target velocity will be $0\ \mathrm{m/s}$, which is the velocity of the second pole that seems to be stationary in relation to the SONAR. The second velocity will be that of the trolley in relation to the tank's confining wall.

By inspecting Figure 5.3Figure 5.5, which represent the measurement results, it is shown that the velocity resolution is within the requirement of $0.1\ \mathrm{m/s}$ is met by the design. Experiments exceeding a trolley speed of $0.33\ \mathrm{m/s}$ are impossible with the proposed experimental set-up, as the resulting drag on the transducers will bend the fixing pole to breaking point.

Experiments for velocity readings lower than $0.2\ \mathrm{m/s}$ are performed at the M&M facilities, because the trolley at the CSIR facilities cannot be accurately controlled at such low speeds, as indicated by the speed conversion table shown in Appendix A.1.

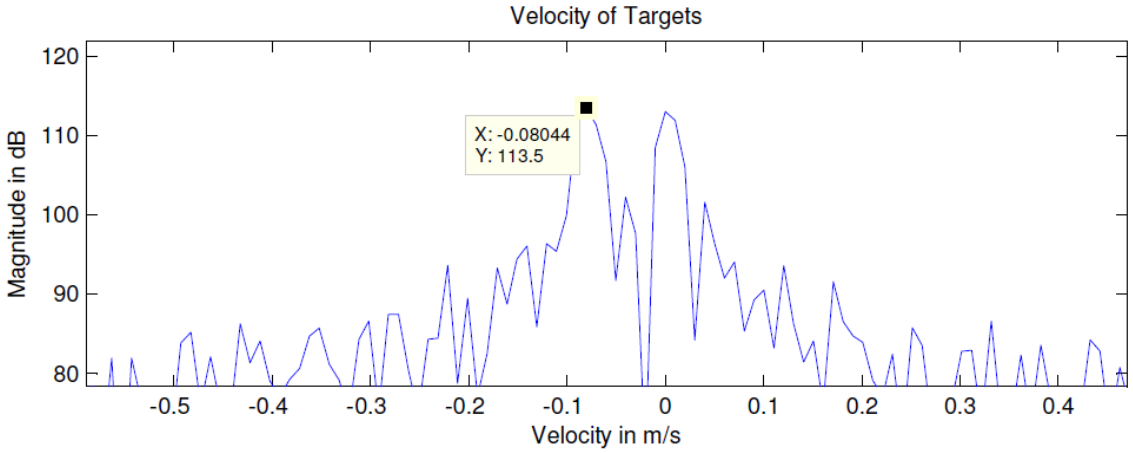

Figure 5.3 – CW velocity reading at trolley speed of 0.08 m/s

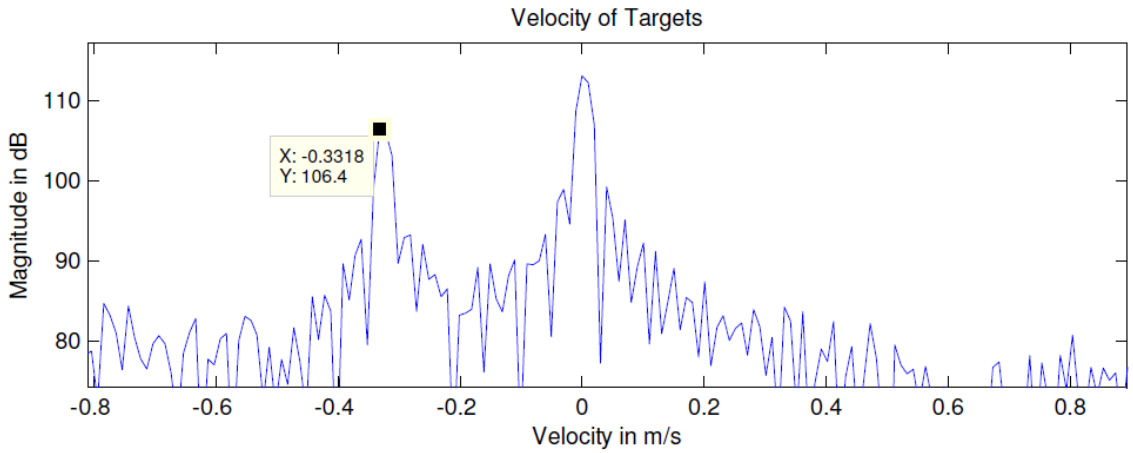

Figure 5.4 – CW velocity reading at trolley speed of 0.33 m/s

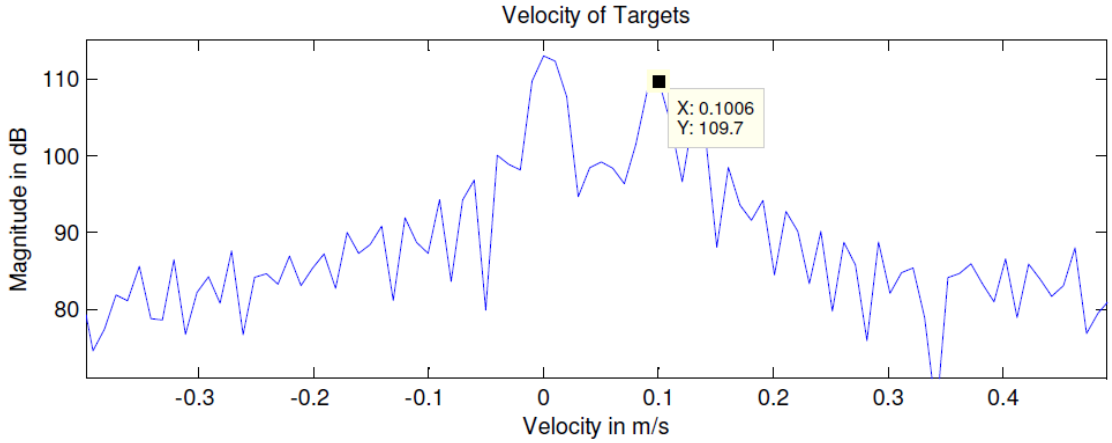

Figure 5.5 – CW velocity reading at trolley speed of -0.1 m/s

5.3 LFM Measurement Results

The measurement set-up for LFM pulse evaluation is similar to the one described for the CW pulse evaluation. However, for accurate range resolution determination the suspended targets are being moved, instead of the trolley. The distance between the targets id measured using a ruler.

Figure 5.6 Figure 5.7 show the results of a target sphere at a range of $51\ \mathrm{m}$, using an inverse filter (IF) and a matched filter (MF), respectively. The back wall of the CSIR towing tank may be recognised at a range of $96\ \mathrm{m}$, with the wave generator in front of the wall. For this specific

echo a lot of noise may be observed at ranges closer than $20\ \mathrm{m}$. This is, however, not the general case as may be noted by examining Figure 5.8, which shows two targets at close range. The T-shaped back wall of the M&M towing tank can be observed as well. The target at $116\ \mathrm{m}$ is the echo from the back wall of the towing tank, which is again reflected by the front wall of the towing tank, and excites the receiving transducer from behind. The noise at close range in Figure 5.6 and Figure 5.7 will not mask a nearby target, because the amplitude of the target's echo will exceed the amplitude of the noise, as indicated in Figure 5.8. Comparing the MF results of Figure 5.7 and Figure 5.8 indicates that the echo of a nearby target will exceed the noise amplitude by more than $10\ \mathrm{dB}$.

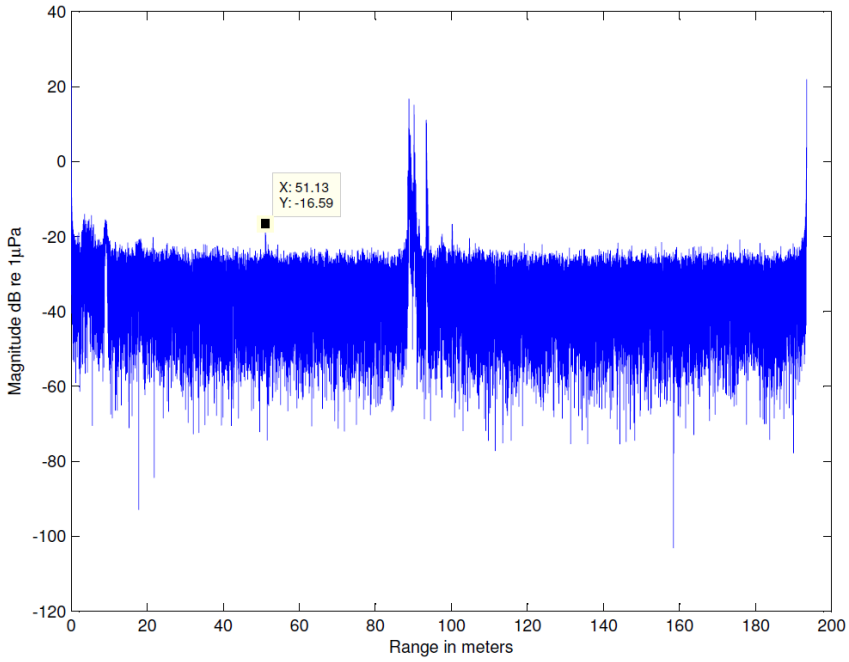

Figure 5.6 – Target at 51 m range, using IF

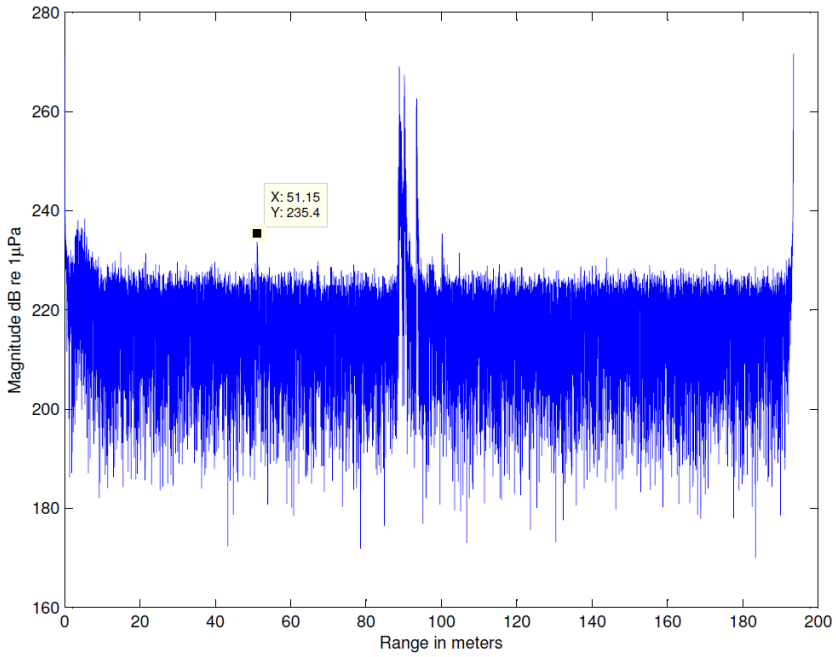

Figure 5.7 – Target at 51 m range, using MF

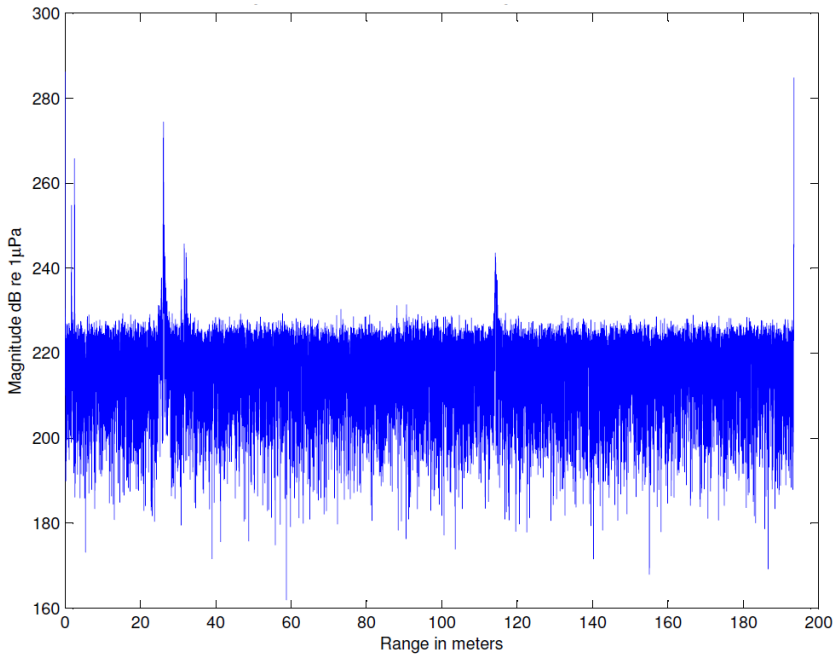

Figure 5.8 –Nearby target, using MF

"Zooming" in on the peaks of the main lobes for both MF and IF to determine the width of the lobes at $3\ \mathrm{dB}$ below the peak, reveals similar results to those obtained during simulations. The width of the target's main lobe at 3 dB below peak is found to be $13\ \mathrm{mm}$ applying a MF, and $8\ \mathrm{mm}$ applying an IF. The range resolution for both filters in practice is therefore expected to be poorer than simulated, which is be expected, since non-ideal system characteristics influence the signal processing path. The overall system performance is expected to be poorer, due to the received noise not being Gaussian as assumed during the simulation. Furthermore, the received signal will contain reverberation components, which are not incorporated in the simulation.

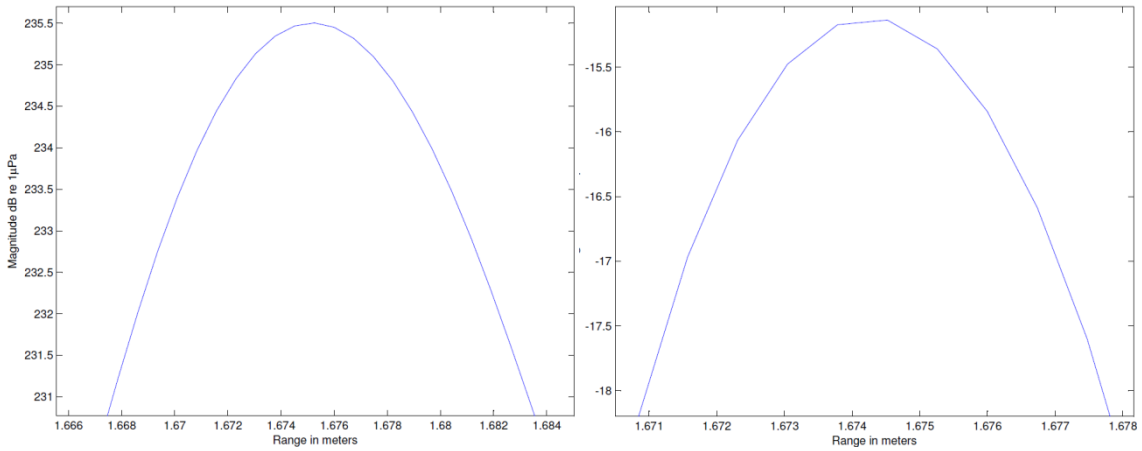

Figure 5.9 – Width of main lobe for MF and IF at 3dB below the peak

The $8mm$ main lobe width for the IF is obtained by using a Kaiser window, as stated in Section 3.3.2. Although a higher resolution should be possible when using a Kaiser window for the IF, as compared to using as Hanning window, the disadvantage in practical experiments is the appearance of ghost targets of significant amplitude, as shown in Figure 5.10. This is due to the Kaiser window allowing too much noise to pass through the IF. The IF will thus amplify the noise, thereby producing ghost targets. Figure 5.11 shows the IF output using a Hanning window, processing the same data as for Figure 5.10.

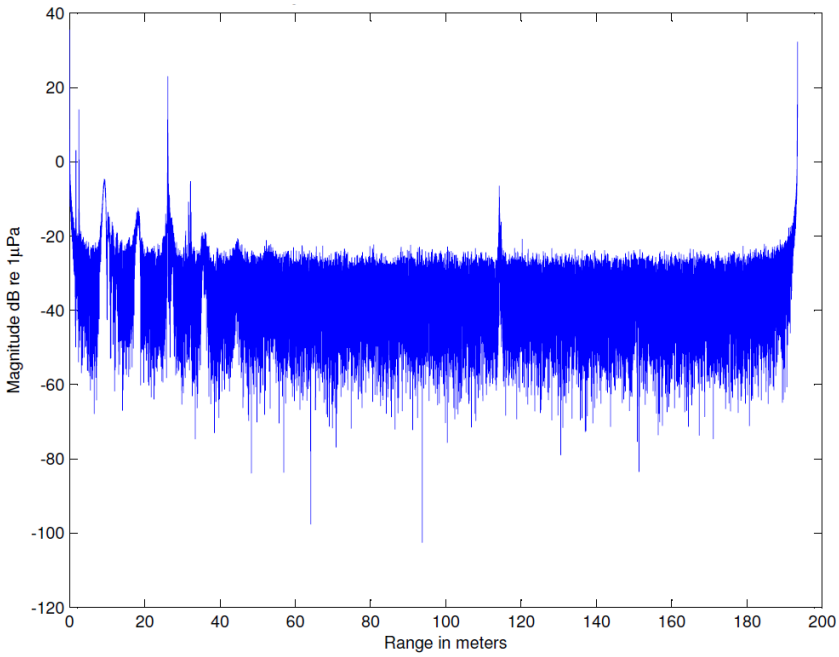

Figure 5.10 – IF using Kaiser window

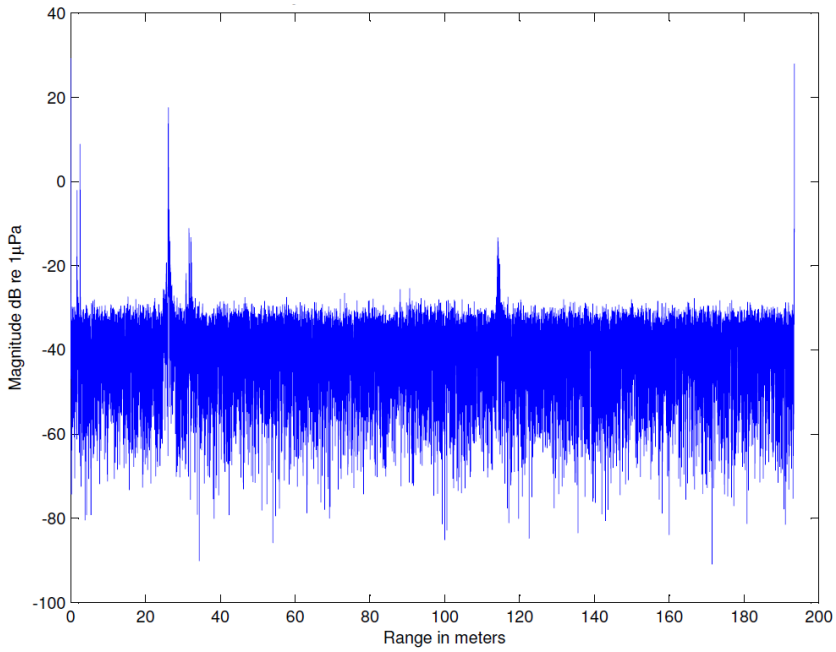

Figure 5.11 – IF using Hanning window

The plots in respect of range resolution performance for the MF and IF, respectively, for two spheres of diameter $1\ \mathrm{cm}$, separated by $17\ \mathrm{mm}$, are indicated by Figure 5.12 and Figure 5.13. Examining the two figures it is noted that the MF is unable to resolve the two targets. The IF

can easily resolve the two targets, by utilizing a Kaiser window, thus being the superior filter for range resolution. However, using a Hanning window for the IF, as indicated in Figure 5.14, yields a similar result as the MF, which utilizes a Hanning window as described in Section 3.2.2. The advantage of using a Hanning window for the IF, is the reduction in side lobes as compared to the Kaiser window. This is due to the shape of the respective filters. This observation supports the argument of the Kaiser window allowing too much noise to pass through the IF.

The advantage of the MF, as discussed in Section 2.4, is its superiority regarding SNR. The results shown in Figure 5.12 and Figure 5.13 indicate that the MF has a SNR of more than 40 dB compared to approximately 15 dB of the IF.

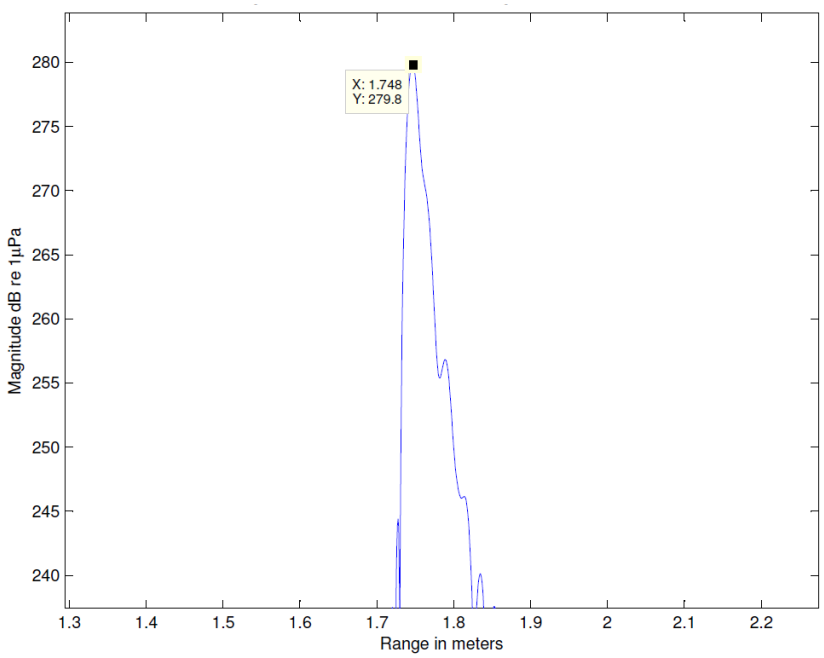

Figure 5.12 – MF (Hanning) result of two spheres 17 mm apart

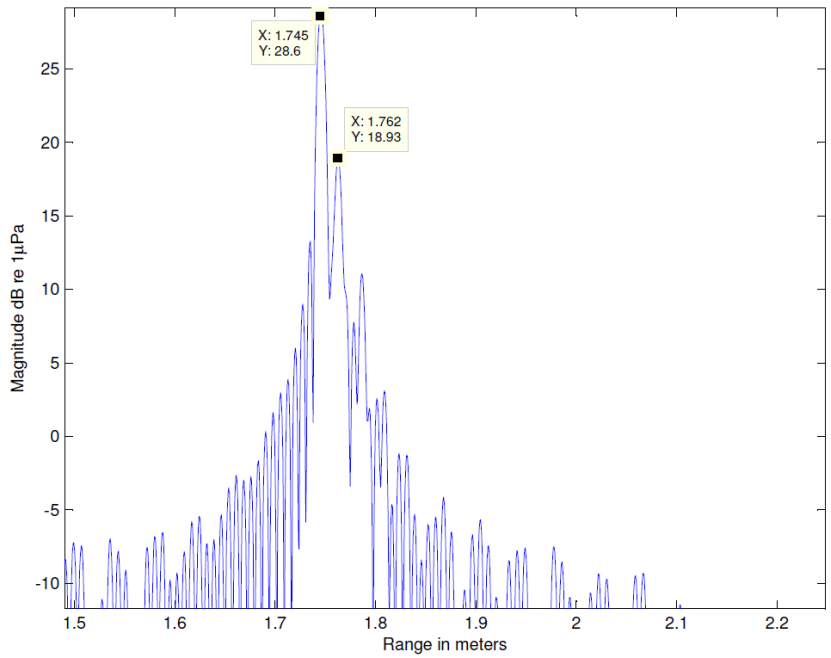

Figure 5.13 – IF (Kaiser) result of two spheres 17 mm apart

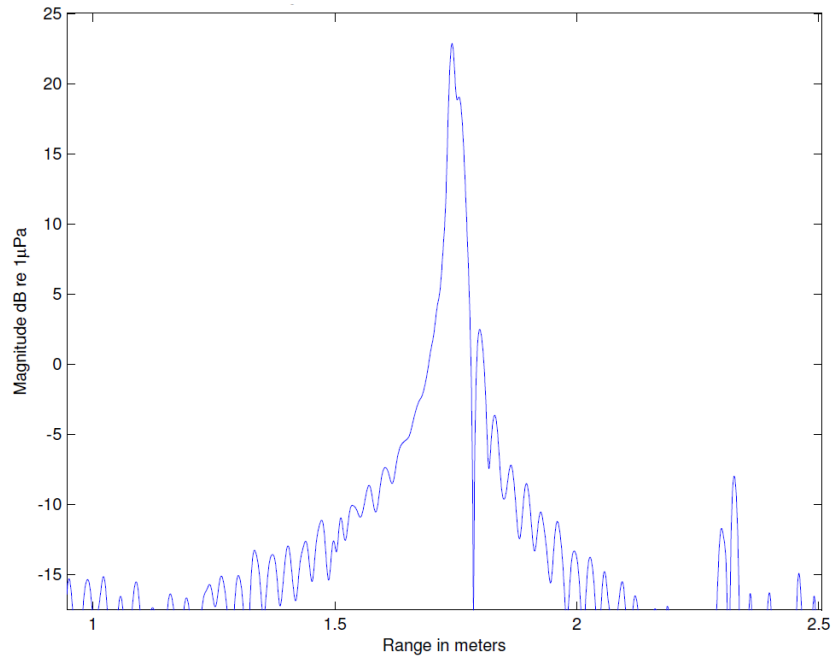

Figure 5.14 – IF (Hanning) result of two spheres 17 mm apart

The results of the target spheres separated by $24\ \mathrm{mm}$ and $33\ \mathrm{mm}$, respectively, are shows in Figure 5.15 and Figure 5.16. Both filters can resolve the targets very well.

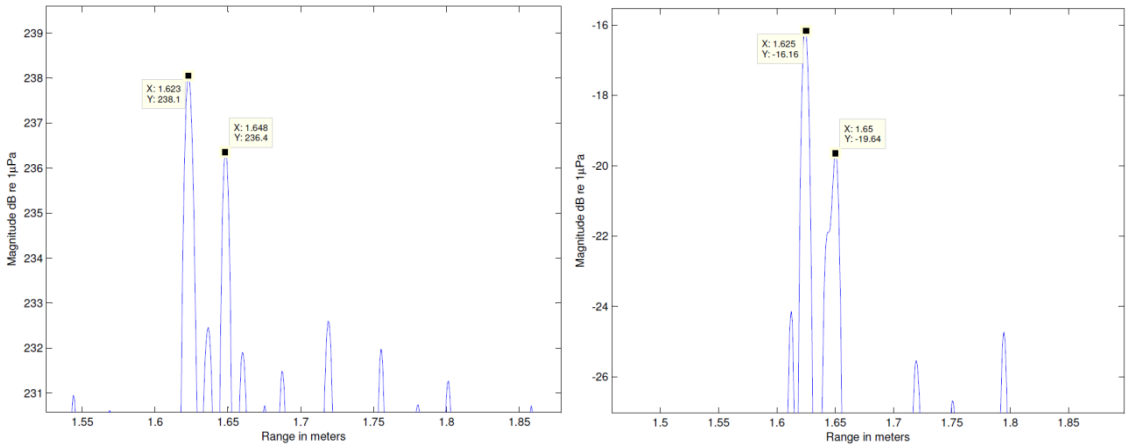

Figure 5.15 – MF (Hanning) & IF (Kaiser) results of two spheres 24 mm apart

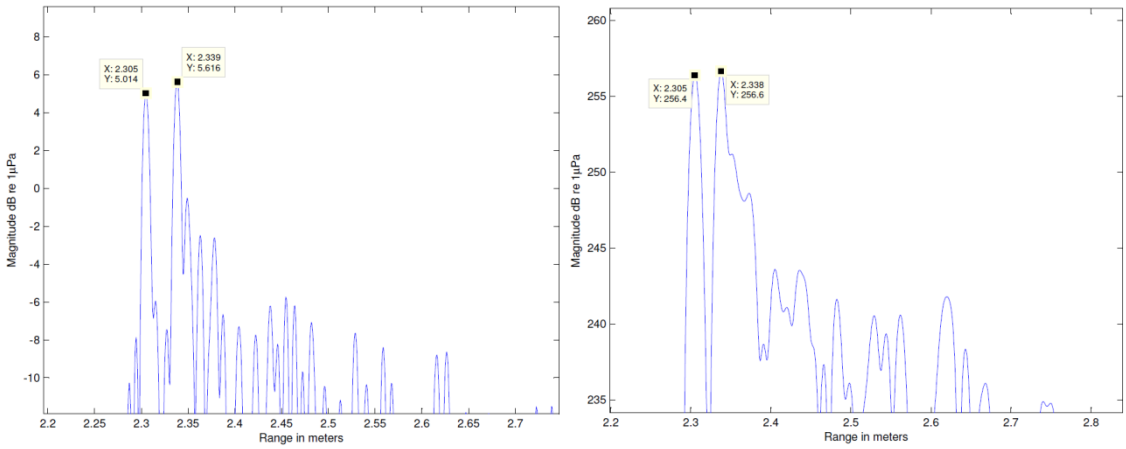

Figure 5.16 – MF (Hanning) & IF (Kaiser) results of two spheres 33 mm apart

The effect of the Doppler frequency shift on the LFM pulse is indicated in Figure 5.17, where an IF was utilized in conjunction with a Hanning window. The result is found to be the same as simulation result shown in Figure 3.14.

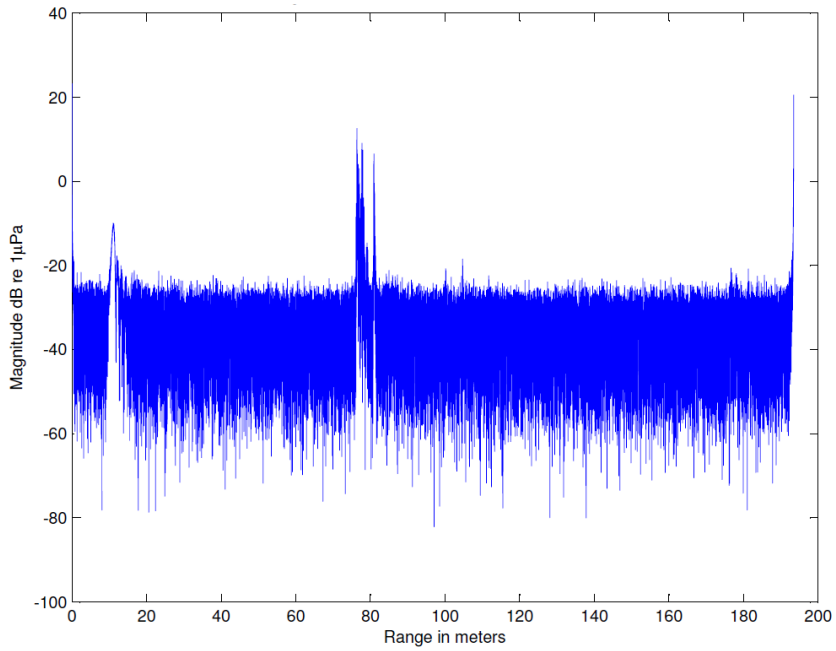

Figure 5.17 – Smearing of target main lobe due to added Doppler frequency shift

Chapter 6

CONCLUSION

6.1 Conclusion

The theory, design, simulation and testing of a SONAR platform for AUV applications in a closed environment have been discussed. The platform was built by using inexpensive, off-the-shelf components to reduce development costs to a minimum.

After thorough investigation it was decided to utilise a CW pulse for determining Doppler frequency, and a LFM pulse for range measurements, respectively, where the LFM pulse was selected for its ability to suppress reverberation. Both pulse types have been known since the early days of SONAR and are classified as analogue pulses. Modern digital coded waveforms were investigated as well, but were found to be ineffective for purposes of this project. Although digital coded waveforms can resolve both Doppler frequency shift and range, and are thus superior to their analogue counterparts, they do not achieve the high range resolution requirements of this project, without utilizing sophisticated hardware and excessive processing power. Costas coded waveforms are thus of great interest to projects with looser range resolution constraints and more powerful hardware.

Simulation and testing revealed that, although the pulse design for resolving Doppler frequency met the required specifications, as well as the maximum detection range requirements, the range resolution achieved did not meet the anticipated range resolution. However, it should be noted that the pulse applied for resolving Doppler frequency resolution, was overdesigned by a factor of 3.4, while the pulse used to resolve range was overdesigned by a factor of 1.4, as described in Chapter 3. Nevertheless, a range resolution accurate to $14\ \mathrm{mm}$ was achieved for the designed LFM pulse, when using an IF. To decrease the range resolution, the bandwidth B of the LFM pulse may be further increased. The bandwidth is, however, limited by the hardware specifications, and cannot be increased indefinitely.

Although the LFM pulse features Doppler resistant characteristics, a coupling between Doppler frequency shift and range measurement may be observed. The coupling issue may be resolved as explained in the text, or overcome by utilizing a hyperbolic frequency modulated pulse. Hyperbolic frequency modulated pulses are Doppler resistant, as compared to LFM pulses,

which are Doppler tolerant. However, to implement hyperbolic frequency modulated pulses, more expensive hardware is required for generating the pulse.

During practical tests the MF and IF performed according to the theory discussed, with the IF yielding a better range resolution and the MF featuring the better SNR. The filters performed equally well during simulations, which may be explained by the simulated noise being only Gaussian white noise.

The simulation model developed for the process proved to be significantly accurate. Simulation results and practical measurements were found to be in close correlation, with minimal variations due to reasons discussed above.

The hardware components of the platform were selected in such a way that the platform may be extended for further research and development. Although the hardware performed very well, some problems were experienced.

Development boards were used for hardware implementation to speed up the design process. The problem arising when using development boards is the limited control over the board itself. Another problem experienced, was due to cable failures and poor connections between the respective boards and PCBs. The cables which carry the signal between the various sub-system components tend to break at the SMA connector. Bad connections were the result of SMA connectors not making proper contact after connecting and disconnecting them several times. Furthermore, it was found that the platform is sensitive to EMC. Ever so often the DDS would reset due to EMC generated by switching on the main amplifier, or by operating the towing tank trolley.

For a final design it is thus advisable to create a PCB, which houses all the sub-components used for this project's design. This would not only solve EMC and connection problems, but also allow full access to all system's sub-components. Moreover, the total cost for the platform would be reduced, as development boards are usually expensive.

6.2 Further Development

The SONAR platform discussed in this text lays the foundation of knowledge for further research and development. New pulse designs may easily be evaluated on the platform, because it is highly configurable. Furthermore, the platform features the option for extension to test quadrature channel sampling, thereby reducing sampling requirements.

The next step in the development is to devise an imaging SONAR which may be mounted on to an AUV. The imaging SONAR may be applied for functioning as a collision avoidance SONAR and, as the name suggests, as an imaging SONAR for inspecting foreign objects in the water, on ship hulls and on the ocean floor. For the current platform to function as an imaging SONAR, the current transducers need to be replaced with an array of transducers featuring a narrow fan-shaped beam pattern. A narrow beam from the transducers will allow for an improved azimuth resolution. Having an array of transducers will allow for implementation of electronic beam steering control. The required transducer beam pattern is shown in Figure 6.1, where the beam may be steered in the vertical plane.

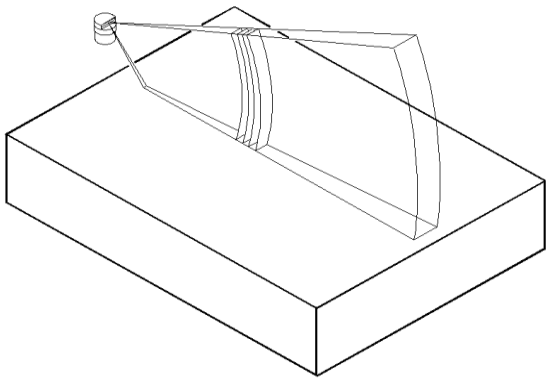

Figure 6.1 – Imaging SONAR transducer beam [33]

Adding a mechanical rotation SONAR head will enable the imaging SONAR to “look” sideways, as shown in Figure 6.2.

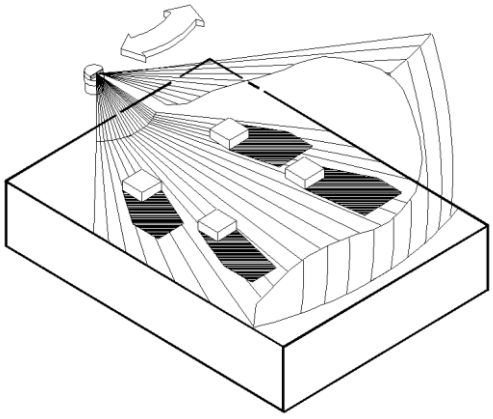

Figure 6.2 – Rotary scanning imaging SONAR [33]

Replacing the transducers of the platform, it may be applied for implementing and testing synthetic aperture scanning as well. Synthetic aperture SONAR is commonly found in a side-scan SONAR. A side-scan SONAR produces high resolution images by scanning the area of interest to its sides with a high range resolution SONAR, while travelling at a fixed speed and water depth. Processing the acquired SONAR data in a prescribed way produces high resolution images of the scanned area. Implementation of a side-scan SONAR is envisaged in Figure 6.3

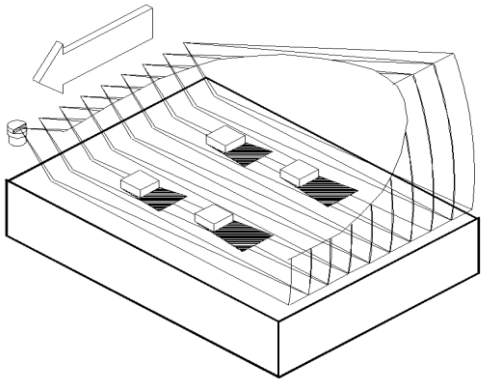

Figure 6.3 – Side scan SONAR [33]

Having developed an imaging SONAR, the ultimate goal is to apply the SONAR for developing an intelligent sensor. The sensor will communicate with a standard vehicle control unit, which is being developed for airborne, land based and marine autonomous vehicles, by the Electronic Systems Laboratory of the University of Stellenbosch. The control unit will be capable of steering the vehicle and mapping the surroundings by using various sensors, which may be added to the control unit in a plug-and-play fashion. Each sensor will therefore need to pre-process gathered data, and only communicate relevant information to the control unit. Furthermore, the data exchange will be a fixed one. A possible protocol for exchange of information could be, that the sensor informs the control unit about a target and the target's range. Moreover, the sensor will convey information concerning the certainty of the target being present. Information regarding the target may also be extracted and communicated. For example, a SONAR may determine whether the target is organic or inorganic, by evaluating the phase of the returned signal.

BIBLIOGRAPHY

[1] H. G. Urban, Handbook Of Underwater Acoustic Engineering, Bremen: STN ATLAS Elektronik GmbH, 2002.

[2] F. Jay, IEEE standard dictonary of electrical and electronic terms, New York: Institute of Electrical and Electronic Engineers, 1984.

[3] E. Bovio, D. Cecchi and F. Baralli, "Autonomous underwater vehicles for scientific and naval operations," *Annual Reviews in Control,* vol. 30, no. November, pp. 117-130, 2006.

[4] M. I. Skolnik, An Introduction to Radar Systems, New York: Mc Graw Hill, 1988.

[5] O. NDT, "Olympus Ultrasonic Transucers Technical Notes," 2006. [Online]. Available: http://www.olympus-ims.com/data/File/panametrics/UT-technotes.en.pdf. [Accessed 12 04 2011].

[6] B. R. Mahafza and A. Z. Elsherbeni, MATLAB simulations for radar systems design, Florida: Chapman & Hall, 2004.

[7] A. D. Waite, Sonar for Practicing Engineers, West Sussex: John Wiley & Sons Ltd, 2002.

[8] L. Kinsler, A. R. Fray, A. B. Coppens and J. V. Sanders, Fundamentals of Acoustics, 4th edn, New York: Wiley, 2000.

[9] R. J. Urick, Principles of Underwater Sound for Engineers, New York: McGraw-Hill, 1967.

[10] M. Ainslie and J. G. McColm, "A simplified formula for viscous and chemical absorption in sea water," *Journal of the Acoustic Society of America,* vol. 103, no. 3, pp. 1671-1672, 1998.

[11] D. M. Pozar, Microwave and RF Design of Wireless Systems, New York: John Wiley & Sons, Inc, 2001.

[12] A. Devices, "AD8331/AD8332/AF8334," Analog Devices, Norwood, 2010.

[13] R. L. Dawe, "Detection Threshold Modelling Explained," DSTO Aeronautical and Maritime Research Laboratory, Melbourne, 1997.

[14] A. Wilkinson, "Notes on Radar/Sonar Signal Processing: Fundamentals," University of Cape Town, Cape Town, 2010.

[15] N. Levanon and E. Mozeson, Radar Signal, New Jersey: John Wiley & Sons Inc., 2004.

[16] G. L. Turin, "An Introduction to Matched Filters," Hughes Research Laboratories, Malibu, 1960.

[17] N. S. Sharma, J. R. Buck and J. A. Simmons, "Trading detection for resolution in active sonar receivers," *Acoustical Society of America,* vol. 130, no. 3, pp. 1272-1281, 2011.

[18] J. G. Hoole, *Implementation of a Low-cost FM-CW Radar,* Stellenbosch: University of Stellenbosch, 2008.

[19] H. V. Trees, Detection, Estimation and Modualtion Theory, Thrid Edition, New York: Wiley, 2001.

[20] E. Kelly and D. P. Wishner, "Matched filter theory for high-velocity targets," *IEEE Tran. Military. Electron. vol. 9 no.1,* pp. 56-59, 1965.

[21] V. Pjachev and V. Valeyev, "SONAR SIGNAL WAVEFORM IMPACT ON INTERFERENCE RESISTANCE," in *EURASIP*, Lausanne, 2008.

[22] E. A. Mayo, "Efficient Computer Decoding of Pseudorandom Radar Signal Codes," *IEEE Transactions on Information Theory,* pp. 680-681, September 1972.

[23] K. K. H. Aboulnour and O. Kawas, "Improving Ambiguity Function of Costas Signal," *IEEE,* 2009.

[24] S. P. Pecknold, W. M. Renaud, D. R. McGaughey, J. A. Theriault and R. F. Marsden, "Improved Active Sonar Performance Using Costas Waveforms," *IEEE Journal of Oceanic Engineering,* pp. 559-574, 4 October 2009.

[25] N. Levanon and E. Mozenson, "Modified Costas Signal," *IEEE Transactions on Aerospace and Electronic Systems, Vol. 40, No. 3,* pp. 946-953, July 2004.

[26] J. v. Jaarsveld, Interviewee, *Research Group Leader: Ultrasonics.* [Interview]. 23 09 2009.

[27] C. Logic, "APEX-PA107DPUREVD," 2010. [Online]. Available: http://www.cirrus.com/en/pubs/proDatasheet/PA107U_E.pdf. [Accessed 07 October 2010].

[28] D. C. Fourie, *Electronics 315 Class Notes: Basic Filter Theory,* Stellenbosch: University of Stellenbosch, Departement of Electrical and Electronic Engineering Engineering, 2008.

[29] A. Devices, "AD9959 Rev.B," 2008. [Online]. Available: http://www.analog.com/static/imported-files/data_sheets/AD9959.pdf. [Accessed 10 2010].

[30] A. Devices, "AD8332-Evalz," 2007. [Online]. Available: http://www.analog.com/static/imported-files/eval_boards/375015993AD8332_EVALZ.pdf. [Accessed 15 Feburary 2011].

[31] N. L. Scott, R. D. White and R. G. Vaughan, "The Theory of Bandpass Sampling," *IEEE Transactions on Signal Processing, Vol 39,* p. 12, 9 September 1991.

[32] Microchip, "Microchip dsPIC30F Family Reference Manual," 2006. [Online]. Available: http://ww1.microchip.com/downloads/en/devicedoc/70116e.pdf. [Accessed 04 March 2001].

[33] I. T. Corp., "Sonar Theory and Applications," [Online]. Available: http://www.imagenex.com/sonar_theory.pdf. [Accessed 07 October 2010].

[34] K. Johannesson and R. Mitson, Fisheries acoustics. A practical manual for aquatic biomass estimation, Rome: Food and Agriculture Organization of the United Nations, 1983.

[35] J. P. Costas, "A Study of a Class of Detection Waveforms Having Nearly Ideal Range-Doppler Ambiguity Properties," *Proc. IEEE 72,* pp. 996-1009, 25 April 1984.

Appendix A

CSIR TOWING TANK FACILITIES

A.1 Trolley Speed vs. Motor EMF

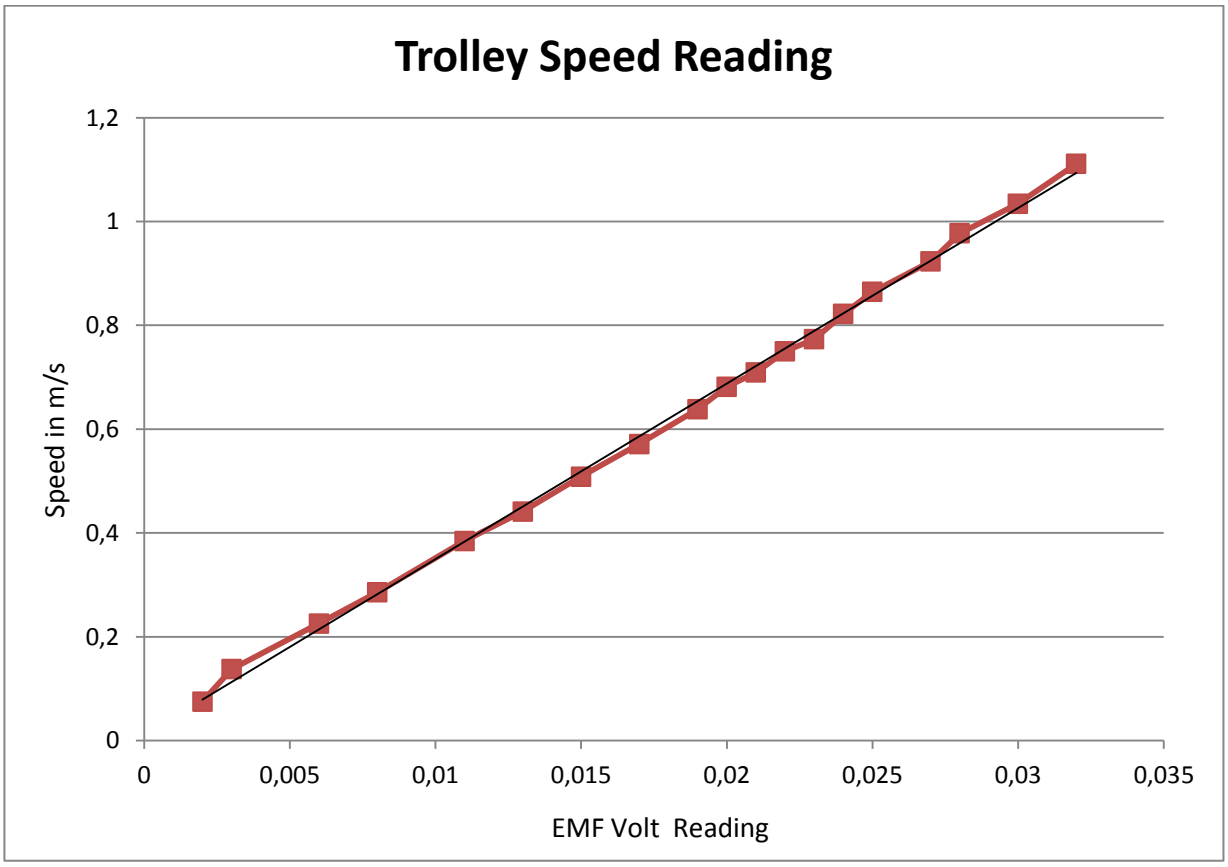

Figure A.1 – Trolley Speed vs. Motor EMF

Appendix B

USER MANUAL

This user manual explains how to set up the SONAR platform regarding both hardware and software.

B.1 Hardware Setup

An image of the complete SONAR platform, excluding the transducers is shown below.

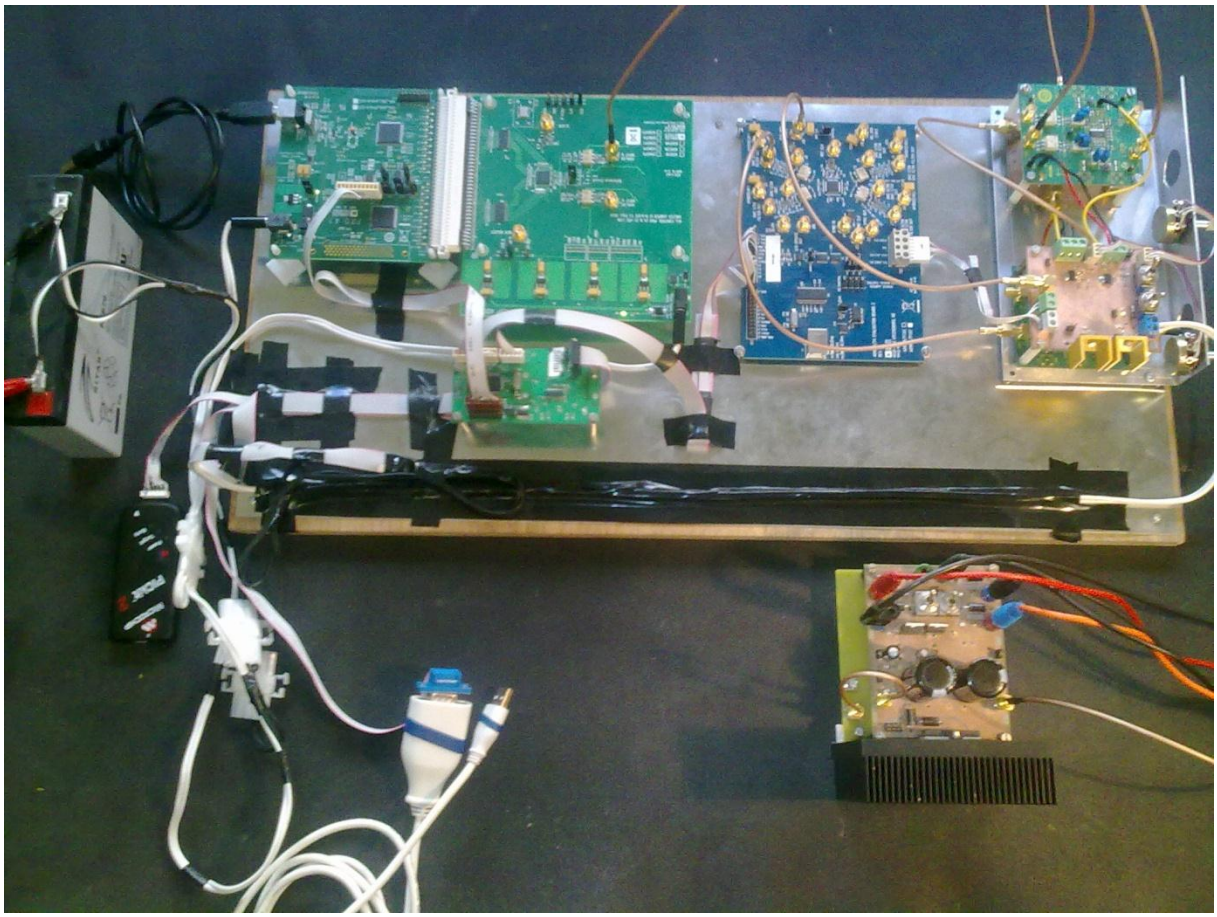

Figure B.1 – SONAR platform

B.1.1 Power Supply

Three dual rail lab bench power supplies are required for the operation of the platform. Two of the supplies power the primary amplifier.

- $+/-\ V_x$
- $+/-\ V_s$

The amplifier PCB is labelled accordingly. The PCB is protected against reverse voltage supply. Four green LEDs indicate the correct voltage application to the amplifier PCB, after the lab bench power supplies have been switched on. An image of the amplifier PCB is shown in Figure 4.13.

The third lab bench power supply is for charging, or simultaneously powering the electronics of the platform. A battery is used for powering the electronics of the platform to prevent noise from the bench power supply from entering the processing system.

B.1.2 Programmer

A PICkit 2 or 3 programmer may be used for programming the CU. The programmer should be connected with the triangle of the programmer and the triangle of the platform's connection jack, facing each other. The correct set up is shown below:

Figure B.2 – PIC programmer connection

B.1.3 USB to Serial Converter

A USB to RS232 serial converter is required for communication between a personal computer and the CU.

Figure B.3 – USB to serial converter

B.1.4 Transducer Connection

The transmitting transducer must be connected to the output of the transducer compensation circuit. The compensation circuit PCB is mounted face down underneath the main amplifier, with the open SMA connector in Figure B.4 being the transducer compensation circuit output. The output and input to both amplifier and compensation circuit is labelled on the relevant PCB.

Figure B.4 – Transducer output connector

The receiver transducer must be connected to its compensation circuit as well. The receiver transducer compensation circuit is merged on to one PCB with the band pass filter. The PCB is stacked underneath a pre-amplifier as shown below.

Figure B.5 – Compensation and filter PCB stacked underneath pre-amplifier

The input and output of the transducer compensation circuit is labelled as $T\ Comp\ In$ and $T\ Comp\ Out$ respectively.

B.2 Software Setup

The following software must be installed on a personal computer or laptop for controlling the CU, reading data from the FIFO board, and processing the received data:

- $Terminal\ v1.9b$
- $ADC\ Analyzer\ from\ Analog\ Devices$
- $Matlab$

B.2.1 Terminal

The first step for initializing the platform is to program the DDS. The terminal software is applied for sending user commands from a personal computer to the CU via the USB to serial converter. The CU, in turn, programs the DDS according to the received commands. The following steps are required for the CU to program the DDS for transmitting:

CW pulse:

1. Send: C
2. Receive: !c
3. Send: a
4. Receive: !

LFM up-chirp:

1. Send: L
2. Receive: !c
3. Send: b
4. Receive: !

LFM up-chirp & down-chirp:

1. Send: L
2. Receive: !c
3. Send: c
4. Receive: !

Other available commands are:

- To reset the DDS send: r
- To power down the DDS send: p

The CU will return a u character when receiving an unknown command. Should the DDS still be busy ramping a signal when a new command is received, the CU will return an o character.

B.2.2 ADC Analyzer

The ADC Analyzer sends a command to sample data and reads the data, once the FIFO chips of the FIFO board are full. For measurements to be correct the ADC Analyzer software needs to be configured as follows:

1. Start ADC Analyzer
2. Choose the Configuration option
3. Select the AD9248 configuration file
4. Under the Config menu select FFT
    1. Set the number of samples to 262144
    2. Set the Encode Frequency to 1 MSPS
    3. Select Output Data Format as Two's Complement
    4. Select OK
5. Under the Config menu select Windowing
    1. Select None
        - Select Analog Input Frequency (MHz)
        - Enter 0.28 as frequency
        - Select OK

To send, receive and sample a pulse, click on the receive time data button. Right click on the data window and select the export data option. Save the data in a file.

B.2.3 Matlab

Matlab is applied to process the received signal. To process the received signal, start Matlab and open Target.Processing.Code in the working dictionary. Various settings are available to simulate the required SONAR setup and environment.

1. Set the type of pulse
2. Import the replica pulse (imported data has data as variable name as standard)
3. Define the imported data as replica pulse (data = tx)
4. Import the received pulse
5. Run the code

B.3 Trouble Shooting

The problem most commonly encountered is that no signal is being sampled. The following should be checked in that case:

1. Are all the PCB's powered
2. Is the DDS programmed
3. Is the ADC Analyzer configured correctly
4. Is a signal arriving at and leaving the main amplifier

In the event of no signal arriving at the main amplifier:

1. Trace the signal back to the DDS

If no signal is generated by the DDS:

1. Reprogram the DDS. EMC spikes, like switching on the main amplifier tend to reset the DDS.
2. Check if the CU reads the write enable of the FIFO board.

In the event of a signal leaving the main amplifier but not being received:

1. Increase the pre-amplifier's gain.
2. Re-solder the connection between the transducers and the coaxial cable.
3. Trace the signal to the ADC.

Should all of the above tests fail, test the SMA connection cables for damage with a multimeter. The cables are easily damaged if twisted during the process of tightening the SMA connector.